Investigation of the Electrostatic Atomization Method for Remote Injection and High Pressure

BY

EGEMEN LEVENT ERGENE
B.S., Middle East Technical University, 2006

THESIS

Submitted as partial fulfillment of the requirements for the degree of Doctor of Philosophy in Mechanical Engineering in the Graduate College of the University of Illinois at Chicago, 2012

Defense Committee:

Farzad Mashayek, Chairman and Advisor
Suresh K. Aggarwal
Rodica Baranescu
W.J. Minkowycz
Dimitrios C. Kyritsis, University of Illinois at Urbana-Champaign

Chicago, Illinois

This thesis is dedicated to my family.

ACKNOWLEDGMENTS

I would like to express my profound appreciation to my advisor, Professor Farzad Mashayek, for his supervision and encouragement that contributed to the completion of this thesis. His guidance, patience and support helped me achieve an advanced level of research productivity.

Sincere appreciations are also prolonged to my thesis defense committee members, Professor Suresh K. Aggarwal, Professor Rodica Baranescu, Professor Dimitrios C. Kyritsis and Professor W. J. Minkowycz for revising the thesis and providing helpful comments.

I would like to thank my labmates that helped during my PhD, especially, Ghazi Malkawi, for his help with the experiments and technical discussions. Special thanks to Dr. John Shrimpton and Agissilaos Kourmatzis for providing beneficial information while also being available for brainstorming. Also to Eric Schmidt and David Mecha from the UIC Machine Shop for their valuable help in the design and manufacturing of various components for atomizers and experimental rigs.

I wish to express my utmost gratefulness to my family for their encouragement, companionship, and sacrifices. I would have never made it this far without their endless support.

Egemen Levent Ergene

TABLE OF CONTENTS

CHAPTER PAGE

TABLE OF CONTENTS (continued)

CHAPTER PAGE

LIST OF TABLES

LIST OF FIGURES

LIST OF FIGURES

LIST OF FIGURES (Continued)

FIGURE PAGE

LIST OF FIGURES (Continued)

Nomenclature

A	a constant	
B	magnetic field	Vs/m^2
D	droplet diameter	μm
d	orifice diameter	M
E	electric field	V/m
f	electric force	N
g	gravitational acceleration	m/s^2
H	magnetic field intensity	T
I	current	A
J	current density	A/m^2
k_B	Boltzmann constant	
κ	ion mobility	m^2/Vs
ℓ	jet breakup length	mm
L	needle tip distance from orifice	μm
m	a constant	
n	a constant	
Q	volumetric flow rate	mL/min
q	spray specific charge	C/m^3
r	needle tip radius	M
u	jet average injection velocity	m/s
u_i	ion velocity	m/s
u_l	liquid velocity field	m/s
V	applied voltage	V
V_{th}	threshold voltage	V

Greek

ε	electric permittivity	F/m
κ	ionic mobility	$ms^{-1}(Vm^{-1})^{-1}$
μ	dynamic viscosity	Ns/m^2
ρ	density	kg/m^3
σ	electrical conductivity	S/m
σ_T	surface tension	N/m
τ	charge relaxation time	s

Subscripts

0	reference value
C	critical
L	leakage
max	maximum
S	spray
T	total

Non-dimensional numbers

C	injection strength
Oh	Ohnesorge number
Ra	Rayleigh number
Re	Reynolds number
T	instability parameter
We	Weber number

SUMMARY

Extensive studies were undertaken in order to better understand the operation of electrostatic atomizers used in conjunction with dielectric liquids. Electrical and spray characterization studies were conducted for steady-voltage charge injection atomizers. The experimental work was complemented by further investigations concentrating on the analysis of spray breakup mechanisms and droplet size measurements.

First, a blade-plane charge injector was designed, machined and tested to better understand the operation of electrostatic charge injection method of two electrically insulating fuels of mineral and biological origins. The aim was to investigate methods to dramatically increase the total injected current. In blade-plane configuration, the fuel was quiescent and only the injected current was measured. Current flux - electrode surface electric field (*J-E*) characteristics at different blade-electrode gaps were presented. The physics of the swirl motion caused by the coulomb forces was discussed. The size of the induced flow was correlated to the performance of the multiple blade design. A new experimental rig was built and several changes were made to the atomizer to observe the electrical performance at high flow rate conditions.

A further stage was undertaken by considering electrostatic charge injection method to be a part of a different type of charge injection atomizer. In this system, the charge injection process was separated from the liquid atomization process. With this design, the charge injection system could be retrofitted to a range of existing atomization systems. This makes the electrostatic atomization method more universal. Through the initial experiments with a commercially available nozzle, it was demonstrated that the charged liquid was successfully carried to a different location and sprayed under certain conditions. The causes

for the possible charge losses during the transfer of the charged liquid to the segregated nozzle were discussed. Imaging studies proved the improvement in finer drop size and wider spray plume coverage.

Electrostatic charge injection method was applied at high hydrodynamic pressures, up to 40 bar, to evaluate the electrical and atomization performance at elevated Reynolds number. The main focus was to investigate the effect of electrostatic charging on higher pressure injection systems in order to form finer sprays. Laser Diffraction Spectrometry measurements and imaging studies were performed to investigate the effect of the electrostatic charge injection technique on drop size distribution as a function of orifice size, emitter electrode voltage, inter-electrode positioning, hydraulic pressure and corresponding average axial tip velocity. It was observed that spray dispersion was enhanced and drop size could be reduced with the increase in specific charge. The various stages experienced by the electrostatic spray as the electrode voltage was increased from zero were described in detail on the basis of an imaging study.

1. INTRODUCTION

1.1 Motivations and Objectives

The first motivation for this study is the concerns over the global economy and energy security with the increase in the crude oil prices and its limited resources, which are growing the energy market instability and as a result effecting the world economy. This has created an interest in the adaption of different liquid fuels and atomization techniques.

Second motivation is the consciousness of the environmental pollutants related with the use of hydrocarbon oils. The environmental issues led to find alternative solutions to reduce the environmental pollution and hazardous gases. Nitrogen and carbon based oxides emissions became a major point of concern after the Kyoto Protocol that was imposed in 1997. As a result, extensive efforts were made to use bio-mass oils as substitute for hydrocarbon fuels [1, 2].

The final motivation is to minimize the energy need to generate spray which has been increasing in the conventional combustion systems such as those used in larger automotive engines requiring 500+ bar in order to achieve good spray break-up and such a pressure is not available to the smaller engine variants. Small engines (20-150cc) with low power prime-movers cannot afford to waste energy towards the atomization of fuel.

The objectives for this study are, first to better understand the function of steady-voltage charge injection electrostatic atomizers (EA) used in conjunction with

highly-insulating (dielectric) Diesel fuel with the electrostatic atomization technique by using an atomizer modified from the atomizer that was designed by Shrimpton and Rigit et. al. [3-5].

Second objective is to make this method of atomization more universal application-wise by introducing a remote charge injection system developed to facilitate the implementation of the electrostatic atomization technology in existing nozzles.

Third objective is to extend the experimental database in an area where not much emphasis has been given to the method of enhancing the performance of the electrostatic atomization method at high pressures in an attempt to extend the application of the method to more practical situations.

In order to build knowledge in the area of atomization of dielectric liquids by introducing a remote charge injector and a high pressure atomizer, a more efficient electrostatic atomization system has to be built successfully while simultaneously understanding its operation. To achieve these objectives, the project is divided into these steps:

1. Study the electrical performance of the blade-plane charge injector using Diesel fuel as a function of the charge injector geometry to observe the experimental charge injection regimes.
2. Test the electrical performance of a different type of charge injection atomizer where the charge injection system is separated from the liquid atomization process.

3. Carry a major portion of the injected charge to the separated nozzle site to have flexibility on the spray pattern, flow rate and spray angle. Identify the causes of possible charge losses during the transfer of the charged fuel.

4. Improve the previous point-plane atomizer to handle higher hydrodynamic pressure and test the electrical performance of the new atomizer at elevated Reynolds numbers.

5. Analyze the results for physical understanding and improvement of the process by studying the spray breakup mechanisms and droplet size distributions as a function of the specific charge present in the Diesel fuel.

1.2 Structure of the Dissertation

The thesis briefly introduces how electrically charged sprays are beneficial in a research framework by means of several charge injection atomizer designs.

The second chapter discusses the fundamentals and relative literature regarding electrostatic atomization. The concepts of dielectric liquids and related timescales are introduced. The electrical equations for charge injection systems are discussed. Moreover, some discussion regarding the basic processes specific to electrically charged droplets is presented with the classical Rayleigh Limit, maximum amount of charge a drop may hold.

Chapter 3 defines the design process and the testing methods. Moreover, it shows the experimental setup components and their associated errors.

Chapter 4 discusses the electrical performance results of the blade-plane charge injector using Diesel fuel, as a function of electrode position, number of blades

and blade spacing to understand the fundamentals of charge injection before moving onto the segregated approach.

Chapter 5 covers the design and electrical performance of the segregated remote charge injection system. This chapter discusses electrical performance comparison with the introduction of the new parts into the system and the reasons for the possible charge losses within the system. The emphasis of this chapter is to recognize the principles of how the separated atomizer operates to achieve a wide range of spray patterns.

Chapter 6 discusses the 3rd generation atomizer, which was machined in UIC machine shop, for Diesel fuel at high hydrodynamic pressures. The data are compared with earlier results from low pressure studies as a function of average injection velocity. The spray breakup mechanisms for Diesel fuel are shown at below and above the critical velocity defined as the condition where spray forms pure hydrodynamically at zero charge. Finally, droplet size measurements as a function of spray charge density distribution are presented.

The final chapter evaluates the main conclusions in this work and delivers some recommendations for future studies.

2. LITERATURE REVIEW

2.1 Introduction

This section focuses on explaining the fundamentals of the electrostatic charge injection technique. Non-dimensional parameters and electrical timescales are presented to describe the electric charge present within the charged liquid flowing outside the atomizer body. The review delivered here is related to two different charge injection atomizers, blade and needle type charging electrodes. A good understanding of this is essential to have a brief idea about how charge is transported within a dielectric liquid with a very high electrical resistivity through which very small magnitude of conduction current flows. As a last note, some subjects related to the creation of charge are not discussed in sufficient detail expecting that provided references will lead to the corresponding subject.

The mechanism through which the electric charge is transmitted into the liquid from the injecting electrode has still been the subject of an ongoing discussion. There are two common theories to explain the mechanism of charge transport. The first one is the field emission mechanism, where an applied external electric field emits electrons into a liquid surface at very high electric field intensities (~10^8 V/m) which depend on the electrical resistivity of the fluid. The high magnitude of the electric field on the charging electrode surface permits the electrons to transport. In several experiments including this study with blade-plane geometry using dielectric liquids, the observed surface electric field was computed less than the required theoretical emission field strength. For this reason, this theory is no longer universally recognized as a standard mechanism for transporting electric charges into dielectric

liquids.

Instead, further research has pointed to a second approach, which suggests that charge enters into the bulk fluid with a series of electro-chemical reactions. This approach indicates that charge transport does not occur by the charge carriers present at the liquid-electrode metal interface. Instead, the charge transport is governed by the contained dissolved ions due to non-uniformities on the surface of the charging electrode metal. It is still not determined which of these mechanisms is dominant on the electric charge transport from the charging electrode into the dielectric liquid. However, comprehensive discussion of charge transfer mechanisms is beyond the scope of this thesis. This thesis mainly covers the optimization of the charge contained in the liquid and the observations of the charged spray.

The earliest studies of the liquid instabilities due to electric charge were conducted by Lord Rayleigh more than a century ago [6]. Lord Rayleigh indicated that the stability of a liquid jet or a drop is greatly reliant on the relation between the electrical stresses that are tending to disturb the liquid and the surface tension forces that are trying to keep the liquid stable. Ever since, a great amount of experimental studies have been undertaken on liquid jets breakup based on Lord Rayleigh's results [7-8]. Rayleigh Limit is defined as the maximum quantity of charge a spherical droplet can carry and is shown as:

$$q_{\max} = \pi\sqrt{\left(8\varepsilon\sigma\ D^3\right)} \qquad (2.1)$$

The limit is driven by comparing the electrostatic repulsion forces to the restoring surface tension forces on the surface of the droplet. Using this relation, one can conclude that a droplet or a liquid jet is stable only when its radius is larger than

the radius computed with the “Rayleigh limit”. Moreover, Rayleigh included that when a highly charged droplet gets in unstable state by evaporation, it transforms into an ellipsoidal form from its original spherical shape. Consecutive formation of significantly smaller but electrically stable drops occurs with the breakup at the end corners of the ellipsoidal form.

The electrostatic atomization method of electrically insulating liquids is one of the innovative approaches that has been studied in the past three decades. Electrostatic atomization method is based on electrostatic forces instead of the traditional pressure driven injectors where a large hydrodynamic pressure difference has been applied. The electrostatic atomization technique uses electric charge assisted atomization and spray dispersion. The most common method of applying electrostatic atomization technique is having the working liquid flowing between two electrodes a distance L apart, where the emitter electrode is at high negative voltage, and the receiver electrode is grounded. When some amount of electric charge is present in the liquid jet, the surface tension force is reduced by Coulombic repulsion. Jet breakup is observed when the charge density exceeds a threshold value and as a result, the electrostatic force dominates the surface tension.

Many experiments have been undertaken with this charge injection method [3-8], the purpose being the development of an energy-efficient method to atomize electrically insulating hydrocarbon liquids [9] and to understand the effect of nozzle geometry, electrode location, orifice size and liquid viscosity on the specific charge of the resulting spray. This method has several advantages such as formation of smaller droplets, narrow droplet size distribution and a lower power requirement to generate the spray. To obtain the same spray pattern using dielectric hydrocarbon fuels such as

Diesel fuel or kerosene, a pure hydraulic nozzle will require in the order of 10^2 W whereas it just needs a small fraction of one watt with electrostatic atomization technique. Moreover, highly viscous liquids can be sprayed by effectively lowering the surface tension with the addition of charge into the jet. Some of the other advantages can be summarized as the ability to control the droplet movement by an external electric field and more uniform coating with less over-spray. Applications now range from spray combustion, ink-jet printers, electrostatically charged oil based paint sprays to more uniform coating by charged sprays in turbine fuel injectors [10] and lubrication.

A perfect insulator with infinite resistivity resists the electric charge flow. On the other hand, a perfect conductor with no resistivity allows the space-charge flow. Dielectric liquids can still be polarized by means of an external electric field however, the motion of the electric charges contained in dielectrics do not initiate with the same mechanism as in conductors. In dielectric liquids, the movement of electric charges is limited with small shifts from the initial stable locations resulting in an internal electric field. This is known as dielectric polarization [11].

2.1.1 **Electrospray**

The conducted method here is different from the commonly known 'Electrospray' technique [12]. Electrospray is applied by doping the liquid usually with a chemical additive to make the working fluid more electrically conductivity. In some cases, the breakup is further enhanced by the utilization of additional atomization methods. The common apparatus of this technique is shown in Figure 2.1. Especially for conductors and semi-conducting liquids such as ethanol, most of the

studies conducted so far has been concentrated on the utilization of the electrospray technique as these liquids cannot be sprayed with the method used in this thesis. The main reason is the limitation in the electrostatic charge injection atomizer geometry where electrodes are rather close to each other. As a result, with the use of such semi-conducting liquids, all charge injected to the liquid will leak through the atomizer body before leaving the orifice passage and therefore, injected charge will have no effect on the resulting liquid stream. More explanations will be provided with the introduction of related timescales.

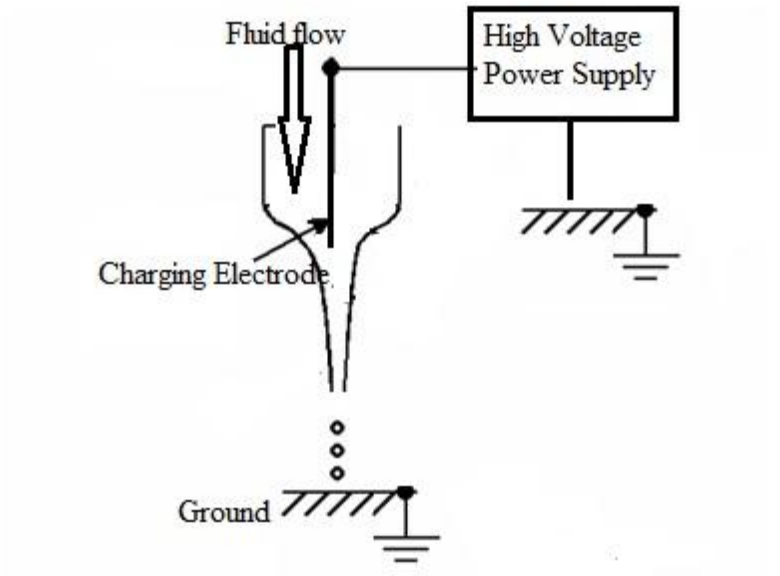

Figure 2.1 Electrospray setup

Zeleny [12] investigated the droplets formed at the end of glass capillaries and reported the electrospray technique operating regimes that can be listed as dripping, burst and cone-jet. Taylor [13] produced the theoretical underpinning of electrosprays by modeling the cone shape formed by the fluid droplet when an electric field was created by applied voltages above a threshold value which is widely known as the Taylor cone. He theoretically derived the requirements to form the perfect cone with the full angle of 98.6° (half angle of 49.3°) and confirmed that the form of the

cone approached to this theoretical angle just before the jet formation. Based on Taylor's findings, several experimental relations were derived to associate independent variables such as physical properties of the working fluid, applied voltage on the charging electrode and fluid flow rate to the charge flux and number or volumetric averaged spray droplet sizes [14-15] . Gomez and Tang [16] investigated cone-jet heptane electrosprays and observed coulombic fission, up to 80% of the Rayleigh limit. Fenn [17] extended this technique to large macromolecules of molecular weights around 10^5 that led to Fenn's Nobel Prize in Chemistry in 2002. Luther [18] sprayed Diesel fuel at very low flow rates, due to the atomization method, but still succeeded in combustion. Moreover, it was proposed that the existence of electric charge on the drops enhances the evaporation rate which may have reduced the amount of soot formed [19]. Kyritsis et al. [20-21] studied electrospray fuel dispersion to build and improve the performance of an elecrospray-based micro-burner to be used as a portable power source for mesoscale applications using kerosene fuel.

2.1.2 **Electrostatic Atomization**

The application of this electrostatic atomization method initiated with the innovative work of Kim et. al. [22] who used a chemically treated needle as a charging electrode that has an electrode tip radius of smaller than 1 μm. They sprayed Freon 113 which was placed inside a glass tube. Due to the small magnitude of flow rate and currents (~10^{-3} ml/s and ~10^{-9} A, respectively), the usefulness of their atomizer was rather limited. Additionally, atomization performance was not reliable because the needle tip melted as a result of the high current flux. The same geometry

was then revisited by Robinson et al. [23] who extended the work to highly insulating liquids and utilized both negative and positive polarity voltage, yielding the important result that ionization (positive voltage) required an order of magnitude higher field emission than (negative voltage) applied electric field of $5x10^9$ V/m .

Kelly [24] significantly improved on the problems of low-flow rate and the low levels of spray current by developing his patented spray triode design that involves inserting a grounded orifice very near the charger electrode. With this design, atomizer electrical performance and spray flow rate were improved significantly. Based on the spray triode design, new electrostatic charge-injection atomizers have been developed [25-26]. There are two paths for the current in this type of atomization system. The total charge injected into the liquid per time is denoted as the total current, I_T. I_T is composed of the current that leaked into the grounded orifice plate, termed the leakage current I_L and I_S, which is the current carried out of the atomizer with the exiting liquid stream or spray. Increasing the charge contained in the liquid exiting the orifice and also reducing the charge leakage to the atomizer ground is necessary for enhancing the atomizer efficiency and the quality of the spray. Several atomizers were built and tested extensively to understand the relation of the specific charge on the flow rate, internal geometry, electrode gap, orifice diameter and viscosity of the working fluid [24-27].

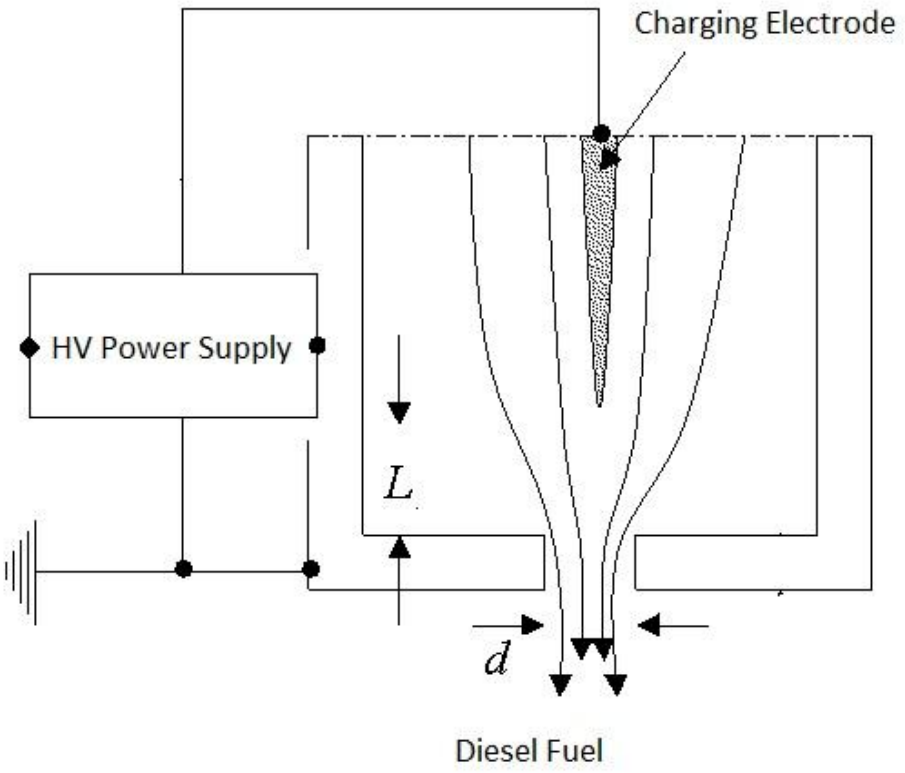

Figure 2.2 Schematic of charge injection atomizer spray triode design

Although the first generation atomizer designed by Shrimpton [26] was able to inject charge enough to create charged fuel sprays, the electrode tip was too far behind the orifice plane to allow small orifice diameters to be used efficiently. The first generation atomizer that used the point-plane atomizer concept achieved spray specific charge levels of typically 0.5 C/m^3 using Diesel fuel and a minimum orifice diameter of 500 μm and L/d=6.6.

Further improvements were achieved with the second generation electrostatic atomizer such as lower values of electrode gap distances, which allowed for larger electric field regions between the charger and receiver electrodes. The improved design in the charge injection process of the second generation atomizer entailed smaller orifice diameters that resulted in a greater level of specific charge, 2 C/m^3 with the utilization of diameters as small as 150 μm and L/d=1. Preheating tests were also performed on second generation atomizer and it was found that the liquid fuel temperature did not significantly affect the maximum specific charge over the considered temperature range of T = 20 – 60 °C but it was noted as a possible way to enhance the quality of atomization for fuels.

A third generation atomizer was designed and fabricated by Rigit [24] using the first two generations designed by Jido [27] and Shrimpton [26], respectively. A 26% increase in spray specific charge was obtained compared to the second generation atomizer. Moreover, the alignment between the electrodes was further improved. This design alteration permitted successful atomizer operation with orifice diameters around 100 μm. A discussion will be provided in the following sections explaining how using smaller diameter orifice is extremely crucial on the performance of the electrostatic atomizer imposing a limit on the spray specific charge levels.

Malkawi [28] had the third generation atomizer manufactured in the UIC machine shop to study a wider range of liquid viscosities and used a blunt electrode to allow multiple orifices. The author of this thesis assisted him with his studies on spraying vegetable oils. Malkawi [28] showed the differences in the break-up mechanisms of Diesel fuel and more viscous vegetable oils. Moreover, for the higher viscosity soybean oil experiments, he noted that the jet starts to spin like a whip that

can also be defined as electrospinning effect as observed from the image in Figure 2.3(b) with the permission of Malkawi.

The spray specific charge is strongly dependent on the orifice size. The surface electric field of the exiting fluid stream can be approximated as follows:

$$E_0 = \frac{qd}{4\kappa} \qquad (2.2)$$

The amount of the surface electric field is restricted by the initiation value of corona discharge in the surrounding environment. As *d* gets smaller, the increase in volume to surface area ratio inside the orifice channel allows for larger values of specific charges before the corona discharge into the surrounding air. The value of the *qd* is roughly constant and is the restrictive quantity which moderately governs the atomizer performance. Therefore, in order to further increase the *q* limit, smaller orifice disks should be used.

In order to increase the flow rate to which an acceptable *q* could be transferred, multiple orifice atomizers were introduced with blunt electrodes. With the use of blunt electrodes, uniform electric fields could be obtained on a larger surface. As a result, equal amount of electric charge could be obtained among the multiple orifices yielding uniform spray plumes from all orifices [28]. Another advantage of using blunt electrode plane-plane atomizer is that it does not have the electrode alignment issue with the needle type atomizers where the position of the charge injection electrode with the orifice is very important [29].

(a) Diesel fuel (b) Soybean oil

Figure 2.3 Images at u = 10 m/s for (a) Diesel fuel at V=-7 kV, (b) soybean oil at V=-9 kV (courtesy of Malkawi [28]).

Multiple orifice studies started with Allen et al. [30] who investigated the multiple orifices with a blunt emitter electrode using gasoline to investigate multiple arrangements and sizes of orifices. Their experiments showed a decrease in droplet diameter with a decrease in orifice size and an increase in applied hydrodynamic pressure. Moreover, their setup managed to produce uniform mono sized droplets by controlling the use of the electrostatic atomization method.

Kelly [29] further studied the multiple-injection concept with an electrode which consisted of a material that contained numerous pin emitters on the surface, used to inject charge from multiple locations and thus improve atomization performance. The findings indicated similar current-voltage trends with traditional point-plane charge injection atomizer systems. Both electrical current and spray droplet size measurements revealed that the multi-orifice atomizer was able to provide finely atomized jets with a slight degradation in spray performance with the introduction of more orifice holes.

Recently, Malkawi [31] conducted electrical measurements and spray characterization studies of the multiple orifices in plane-to-plane atomizer for several orifice sizes and geometries using Diesel fuel to have a comparison with the previous studies using the point-to-plane electrostatic atomizer [31]. The author of this thesis took active part in his experimental studies. Higher specific charge levels were attained with the use of blunt electrodes compared to the needle ones. However, the electrical efficiency was significantly lower due to the considerably larger amount of leakage current.

2.2 **Theoretical background**

The aim of this section is to provide a brief overview of the research carried out thus far in charge conduction in quiescent liquid, electrohydrodynamics and other fields of study directly relevant to these subjects. The fundamental equations governing electrostatics are presented and the physics for dielectric liquids. In addition, basic physics of the electric charge effects on the electrical forces are introduced. The majority of the review shall be restricted to that area of insulating

liquids as this study focuses on dielectric liquids, however, in order to cover some basic concepts, the discussion at some points also cover the conducting and semi-conducting liquids. Electrohydrodynamic system related timescales and non-dimensional numbers have been provided by introducing the extensively studied T, C and M parameters. The effect of independent variables governing charged jet break-up, such as liquid flow rate and viscosity is introduced. In addition, information on estimates of droplet charge and qualitative and quantitative research on charged spray characterization are reviewed.

2.2.1 **Electrohydrodynamic fundamentals and electrical equations**

Electrohydrodynamics (EHD), also known as electro-convection, is the study of electrically charged fluid dynamics. It is the study of the motions of ionized particles or molecules and the interaction dealing with the interaction between electrical and hydrodynamic forces.

Maxwell equations were simplified by Castellanos [32] using suitable scales and non-dimensionalized with electroquasistatic assumption which states that the electrical energy is greater than the magnetic energy and the system is electrically dominated. Therefore, all electromagnetic wave phenomena related terms and the effect of radiation may be neglected. The electrical energy is defined as $(1/2)\varepsilon E^2$ and the magnetic energy as $B^2/(2\psi)$ where ε, ψ, c, E and B are permittivity, permeability, speed of light in the system, electric field and magnetic field, respectively. Then the main criterion to validate electroquasistatic assumption becomes:

$$\frac{(\varepsilon \, \mathrm{E}^2)/2}{\mathrm{B}^2/(2\psi)} = \frac{\mathrm{E}^2}{\mathrm{c}^2\mathrm{B}^2} \gg 1 \qquad (2.3)$$

Permittivity, ε is a material property that can be envisioned as a capacitance that is normalized to the geometry of the continuum under consideration making it a property completely independent of shape. All contained charges act free on each another without any external interfering in free vacuum. However, the permittivity is known to be strongly linked to the intermolecular configuration and the specific charge in the region. Insulating materials, such as the liquids used in this project have low electric permittivities while conducting liquids such as water have significantly higher values. The value of permittivity is usually stated in terms of the permittivity of free space and is thus presented non-dimensionally. A typical value for insulating dielectric oil such as Diesel oil is approximately 2.2 while ,for air, it is approximately 1.

The magnetic field is negligibly small for charge injection in dielectric liquids. As a result, Maxwell equations reduce to:

$$\nabla \times \boldsymbol{E} = 0 \qquad (2.4)$$

$$\nabla \cdot \boldsymbol{E} = \frac{q}{\varepsilon} \qquad (2.5)$$

$$\frac{\partial q}{\partial t} + \nabla \cdot \boldsymbol{J} = 0 \qquad (2.6)$$

The complete steps of the Maxwell equations derivation can be found in Castellanos' book [32].

The instantaneous continuity equation for a constant-density fluid remains the same regardless of electrical charge presence. Navier-Stokes equations for the conservation of mass and momentum becomes:

$$\nabla \cdot \boldsymbol{u} = 0 \qquad (2.7)$$

$$\rho\left[\frac{\partial \boldsymbol{u}}{\partial t} + \boldsymbol{u}\cdot\nabla\boldsymbol{u}\right] = -\nabla p + \mu\nabla^2\boldsymbol{u} + \rho\boldsymbol{g} + \boldsymbol{f} \qquad (2.8)$$

where ***u, p, g, f*** are the injection velocity, pressure, gravity and the body forces. Using the suitable substitutions of Lorentz force [33], the electric force term is given by:

$$\boldsymbol{f} = q\boldsymbol{E} - \frac{E^2}{2}\nabla\boldsymbol{\varepsilon} + \nabla\left[\frac{E^2}{2}\rho\frac{\partial\boldsymbol{\varepsilon}}{\partial\rho}\right] \qquad (2.9)$$

where $q\boldsymbol{E}$ is known as the Coulomb force. Second term is the force through the electric field as a result of the emissivity gradient which is known to be dominant only when the system is under AC electric field. The third term is a modification to the fluid pressure accounting for the density variations [34]. With the assumption that permittivity is constant in all directions, $\nabla\varepsilon = 0$, the equation simplifies to:

$$\rho\left[\frac{\partial \boldsymbol{u}}{\partial t} + \boldsymbol{u}\cdot\nabla\boldsymbol{u}\right] = -\nabla p + \mu\nabla^2\boldsymbol{u} + \rho\boldsymbol{g} + q\boldsymbol{E} \qquad (2.10)$$

The appropriate boundary conditions for the case of a dielectric material enclosed between two parallel plates, containing a uniform charge density q can be listed as $V=V_0$, $q=q_0$ and $u=0$ on the emitter electrode and $V=0$ on the collector.

The non-linear relation between the electric force and liquid motion is rather complex, which make electrohydrodynamics rather complicated. However, with the free flow case assumption, $\boldsymbol{u}=\kappa\boldsymbol{E}$, and using this substitution will bring to the surface some important non-dimensional parameters in order to characterize EHD convection between two parallel plates. The mobility, κ, of a fluid is usually assumed to be

constant for simplicity although it is known to vary as a function of the physical properties in the flow region.

There is an analogy between the charge injection in parallel plane electrodes geometry and the Rayleigh-Benard problem [35] of a liquid layer given heat from underneath. In the Rayleigh-Benard case, the gradient of the charge density initiates fluid motion as the temperature change is above a critical value. At this point, buoyancy overcomes the effects of viscous forces. In the charge injection case, charge density distribution is potentially not stable. As a result, the convection begins due to the Coulomb force perturbation which surpasses the viscous forces.

2.2.2 **Non-dimensional parameters**

At this point, the first non-dimensional parameter, *T*, is derived from an analogy to the Rayleigh-Benard problem, by comparing the viscous effects with the Coulombic forces and provides an insight into the stability of the system. The *T* parameter, also represented as the electrical Rayleigh number, is shown as:

$$T = \frac{\varepsilon V}{\kappa \mu} \qquad (2.11)$$

where V and μ are the applied emitter electrode voltage and dynamic viscosity, respectively. The transition from stable to unstable state is denoted by the critical stability parameter, T_C. It has been shown [36] that for the quiescent fluid case, electroconvection starts at a value of $T_c \approx 100$.

The second non-dimensional parameter, *M*, is defined as the ratio of hydrodynamic mobility to ion mobility,

$$M = \frac{\left(\frac{\varepsilon}{\rho}\right)^{1/2}}{\kappa} \qquad (2.12)$$

M is known [36] to have values in the range of $4 \le M \le 400$. According to the Walden's rule for highly insulating liquids ($\kappa\mu$ is constant for hydrocarbon fuels) and the permittivity of these experimental fluids are of the same order of magnitude; therefore, one can conclude that M is directly proportional to the viscosity of the fluid. Moreover, the higher the non-dimensional number M is, the higher is the resistance on the space charge and, hence, the lower is the drift velocity.

The last non-dimensional parameter, C, is the measure of the injection strength. It is given as the time ratio of the ionic drift to the coulombic charge relaxation,

$$C = \frac{ql^2}{\varepsilon V} \qquad (2.13)$$

where l is the electrode length. For $C \ll 1$, the charge injection is regarded as weak injection. In this case, the electric field is determined by high voltage power supply connected to the charge injector electrode. On the other hand, for high values of C (>1), the injection regime is strong and the electric field mainly depends on the charges inside the liquid. Tobazéon [37] improves the description for the regimes of C number that can be briefly listed as: strong injection: $5 < C < 8$, medium injection: $0.2 < C < 5$ and weak injection: $0 < C < 0.2$.

An electrical Reynolds number defined [38] as the fraction of inertial forces with respect to viscous forces, Re_E, analogous to a conventional Reynolds number, is

defined as $\mathrm{Re}_E = \frac{\rho \kappa V}{\mu}$. A term due to the inertia associated with ionic drift is present instead of an inertial term in the numerator.

There are various ways a jet can break up into droplets and in order to classify these mechanisms some further non-dimensional numbers must be presented and discussed. Primary breakup is the initiation of the atomization process due to inherent perturbations that cause the liquid jet to form individual droplets. In secondary breakup, air resistance is sufficient to further reduce droplet diameter with the inviscid effects of the surrounding air. The non-dimensional numbers that define the beakup regimes are the Reynolds number (Re), the Weber number (We) and the Ohnesorge number (Oh) are given by:

$$Re = \frac{\rho u d}{\mu},\ We = \frac{\rho u^2 d}{\sigma_T}\ ,\ Oh = \frac{\mu}{\sqrt{\rho \sigma_T d}} \qquad (2.14)$$

The Weber number is a measure of the liquid's momentum relative to its surface tension and the Ohnesorge number is the ratio of viscous force to surface tension force. For low *Oh*, an increase in the *We* will increase the contribution of the secondary breakup to form a finer spray to increase the surface area to liquid volume ratio [39].

2.2.3 **Timescales**

In order to help in defining the various processes that occur within an EHD flow system within a charge injection atomizer, several timescales were defined. In the ohmic regime (at low amount of electrical fields), the charge density distribution reduces to:

$$\boldsymbol{J} = \sigma \boldsymbol{E} + q\boldsymbol{u} \qquad (2.15)$$

Thus equation (2.6) can be written as

$$\frac{Dq}{Dt} + \frac{\sigma}{\varepsilon} q = 0, \text{ where, } \frac{D}{Dt} = \frac{\partial}{\partial t} + u.\nabla \qquad (2.16)$$

In a Lagrangian framework, the solution for this equation set can be written as: $q(t) = q(0)e^{-t/\tau_e}$, here $\tau = \varepsilon / \sigma$ is the Ohmic-charge relaxation timescale (τ_{oc}) that characterizes the time elapsed for electric charge contained within the working fluid to be neutralized by opposite polarity or neutral charge carriers. Ohmic-charge relaxation timescale is the ratio of permittivity (ε) over conductivity (σ).

$$\tau_{oc} = \frac{\varepsilon}{\sigma} \qquad (2.17)$$

The relative permittivity (ε_r) for Diesel fuel is in the range of $2.0 \leq \varepsilon_r \leq 2.2$. The relative permittivity value for corn oil is around 3.0. The electrical properties for all of the tested liquids are listed in Table 2.1.

	Diesel fuel	Corn oil
Resistivity (Ω.m)	10^{10}	$2x10^{10}$
Relative permittivity	2.2	3.1
Charge relaxation time (ms)	1.9	4.5

Table 2.1 Electrical properties of Diesel fuel and corn oil

Naturally, Ohmic-charge timescale is taken into account when working with conducting liquids. However, dielectric fluids used in this study are highly insulating and as a result, Ohmic-charge relaxation timescale is not relevant. For this reason, space charge relaxation timescale (τ_{sc}) is defined to show how fast a charge will decay in a dielectric liquid. These timescales are derived as follows:

In unipolar charge injection, the current flux can be shown as [40]:

$$\boldsymbol{J} = q\kappa\boldsymbol{E} - D\nabla q + q\boldsymbol{u} \qquad 2.18)$$

The terms; $q\kappa\boldsymbol{E}$, $D\nabla q$ and $q\boldsymbol{u}$ are the drift, diffusion, and convection expressions, respectively. The diffusion term is negligible for highly insulating liquid. Then, the charge conservation equation reduces to:

$$\frac{\partial q}{\partial t} + (\boldsymbol{u} + \kappa\boldsymbol{E}).\nabla q + \frac{k}{\varepsilon}q^2 = 0 \qquad (2.19)$$

with the solution:

$$q = q_0(1 + t/\tau_{sc}) \qquad (2.20)$$

$$\tau_{\mathrm{sc}} = \frac{\varepsilon}{q\kappa} \qquad (2.21)$$

When molecular diffusive processes are of interest, the ionic diffusion timescale is relevant in the vicinity of the metal high voltage emitter electrode in the charge injection atomizer, and can be thought of as the timescale which characterizes electro-chemical reactions. At this point, Debye length (λ_d) is defined [43] as:

$$\tau_{\mathrm{d}} = \frac{D_d}{\lambda_d^2} \ , \ \ \lambda_d = \frac{\varepsilon\ \mathrm{k_B T}}{\mathrm{ne}^2} \qquad (2.22)$$

The mechanical timescale (τ_m) is defined as the flow channel length (x) over the average orifice channel velocity (u). The breakup timescale (τ_l) is the ratio of the breakup tip length (l) to the injection velocity. These timescales are shown as:

$$\tau_m = \frac{x}{u} \ , \ \tau_l = \frac{l}{u} \qquad (2.23)$$

It will be beneficial to talk about the internal combustion engine timescale as one of the most popular applications of this method is related to automotive industry, fuel injection systems of Diesel engines. There is a wide range of timescales defined for internal combustion engines but in this study, we will define the internal combustion engine timescale (τ_e) as the time interval between the injection of fuel and ignition as a function of the engine speed neglecting the other effects resulting from temperature increase and loss of mass due to evaporation. This timescale can be shown as:

$$\tau_e = \frac{\pi\theta}{180w} \qquad (2.24)$$

where w is the angular velocity of the crankshaft and Θ is the crank angle.

During this period, the processes of fuel atomization, heat up, evaporation and air/fuel mixing should be completed in order to produce a combustible mixture. Therefore, the electrostatic atomizer should from the charged fuel spray at this short timescale on the order of a few milliseconds. In order to achieve this, the charge injected into the liquid should decay to the boundary of the drops within this period to enhance the dispersion. The creation of smaller droplets will decrease the mass transfer timescale. This will leave more time for evaporation and mixing to form a better air-fuel mixture.

2.2.4 **Electrical observations of charge injection atomizers**

The most common approach to quantify the electrical performance of an electrostatic atomizer is to observe the total injected current (I_T) as a function of electrode voltage. This approach has been followed by many researchers and several

injection laws were obtained based on I_T-V data. Initially, a simple, two regimes of charge injection developments were defined as 'low' and 'high' values for quiescent dielectric liquids [44]. According to the field emission mechanism, the regime transition is by continuous transmissions of electrons into the liquid around the charge emitter tip as the electrons surpass the emitter-fluid boundary. This transition initiates at a voltage defined as threshold voltage V_{th}, . The amount of the threshold electric field E_{th} at charger electrode surface is determined as:

$$E_{th} = \frac{2V_{th}}{r \ln[4L/r]} \qquad (2.25)$$

It is considered for the electrode to have a very small tip radius to assure the existence of a very high electric field which would increase the level of charge injection.

Atten [46] confirmed the three regimes of current-voltage characteristics, I_T *(V).* ohmic part, quasi-ohmic and rapid increase regimes were observed using insulating dielectric liquids. The proportionality of I_T to V^2 for voltages above the threshold value was first observed by Bonifaci [45] and later on confirmed by Atten [46] for needle-to-plane configurations. Atten further analyzed the quadratic relation for quiescent liquid between two parallel plates and suggested an empirical injection law of the form:

$$\sqrt{I_T} = A(V\text{-}V_{th}) \qquad (2.26)$$

where Atten determined that A was dependent on the fluid properties and inter-electrode distance (L), with an $A^2 = L^{-m}$ variation law, where m was found to vary between 0.7 and 1.0 for dielectric transformer oil.

The other important parameter in quantifying the electrical performance is the distribution of spray current with respect to voltage. From these distributions, using

the liquid flow rate, spray specific charge, q may be derived. Studies [45-46] have been conducted based on the maximum value of q that can be attained with the corresponding electrostatic atomizer device used. It's known that the specific charge should be at least on the order of 1 C/m^3 to form a fully developed Diesel fuel spray [47].

Shrimpton and Rigit [48] studied the jet breakup length, defined as the continuous jet liquid length downward from the orifice before break-up of the liquid column. A model was determined by Shrimpton and Yule [49] as:

$$\ell = ut_\ell \qquad , \qquad t_\ell = \frac{\varepsilon_r \varepsilon_o}{\kappa q} \tag{2.27}$$

where, t_ℓ is the duration elapsed for a charge to transport from the core to the surface of the jet [41]. As seen from the relation, breakup tip length is strongly related to the q. Shrimpton et al. [49] indicated longer breakup tip length was generally observed with sprays produced with larger orifice diameters. This conclusion was indicating the governing effect of axial component of spray momentum with respect to the radial component. The axial components of droplet velocity are the liquid jet and the radial deflections are triggered by electrical forces on the droplet paths repelling each other.

As mentioned, semi-conducting liquids cannot be sprayed with the method conducted here due to the limitations in the electrostatic charge injection atomizer geometry where electrodes are rather close to each other. If such semi-conducting liquids are used, all charge injected to the liquid will leak through the atomizer body and will have no effect on the resulting spray. At this point, a threshold conductivity value can be computed for the electrostatic atomizer used in this study based on the

flow and Ohmic-charge relaxation timescale. To see the effect of the charge, it is expected to have the Ohmic-charge relaxation timescale should be less or equal to the flow timescale till the break-up occurs.

$$\sigma \leq \frac{\varepsilon_r \varepsilon_o u}{x_b} \qquad (2.28)$$

Assuming typical operating values of 10 m/s injection velocity at a break-up tip length of 5 cm, threshold conductivity is found as $\sigma \leq 4x10^{-8} S/m$.

The charge injection technique discussed here allows a range of hydrocarbon fuels to be atomized with no need for doping, unlike the electrospray technique. The application efficiency of the charged sprays in combustion systems is quantified with the behavior of the charged droplets inside the combustion chamber. The movement of the charged droplets near the grounded electrode is as a result of the applied electric field created by spray space charge and specific charge density [50]. Therefore, droplet diameter measurements as a function of specific charge density is crucial in order to predict the spray plume pattern and its combustion performance. As expected, larger values of specific charge results in sprays of smaller and better dispersed droplets. The existence of electric charge on the spray droplets enhances the droplet break-up and hence the evaporation rates. These charges contained in the mixture also increase the possibility of residual charges in the combustion products which may increase the emissions control systems performance to reduce the amount of soot produced.

More detailed spray characterization was carried out using phase Doppler anemometry (PDA) and Fraunhofer diffraction that is also known as laser diffraction

spectrometry (LDS). In PDA systems, the variation in droplet diameter along with droplet axial and radial velocities vs. radial displacement was investigated at an individual point. Whereas, LDS systems measure the variation in droplet diameter through a plume cross section.

The common result of these droplet size measurements was that the smaller droplets were predominantly deflected away from the spray axis, as they, on average, contained higher specific charge [48] as a result of the larger electrical force existent on the smaller droplets and thus these droplets exhibit a more dominant radial force compared to larger droplets. $D = 0.4d$ for high injection velocities and $D=d$ for low injection velocities were observed [48].

3. EXPERIMENTAL SETUP

3.1 Introduction

This chapter describes the test rig and the experimental techniques presented in the following three chapters of this thesis. It also summarizes the atomizer design and calculations, the electrodes, calibration and quantification of errors for the experimental work. A more detailed analysis of the atomizer design construction, calibration and quantification of errors may be found in appendices.

3.2 Atomizer electrode configurations

Two different configurations, namely blade-plane and point-plane, were considered in our experiments. Below, we describe the experimental setup for these experiments.

The first test rig was constructed and tested with the objective to produce a continuous charged liquid fuel spray, and to examine qualitatively and quantitatively its physical and electrical characteristics. Figure 3.1(a) illustrates a schematic of the experimental layout and electrical connections for the first part of the experimental work, i.e. the electrical evaluation of the blade-plane charge injector. This test rig was designed for quiescent liquid, i.e. no liquid flow. The initial concern was about the sharp edge effect of charge injection from the corners of the razor blades resulting in premature breakdowns; therefore, we investigated a set of collector electrodes with several different radii of curvature, including infinite (flat). The experiments used collector radius (R) values of 75 mm, 100 mm, and 125 mm for performance comparisons, as illustrated in Figure 3.1(a). A cylindrical collector surface is chosen

over the spherical surface to maintain the assumption of two-dimensional charge injection in blade-plane system. Extra sharp blades with a tip radius of 100 µm and projected thickness of 65 µm were used for optimum charge injection as shown in Figure 3.2. To reduce corner injection, the blades had a 1.7 mm radius ground out the blade edge, parallel to the plane of the blade at the corner. Figure 3.3 shows the assembled blade-plane type charge injector.

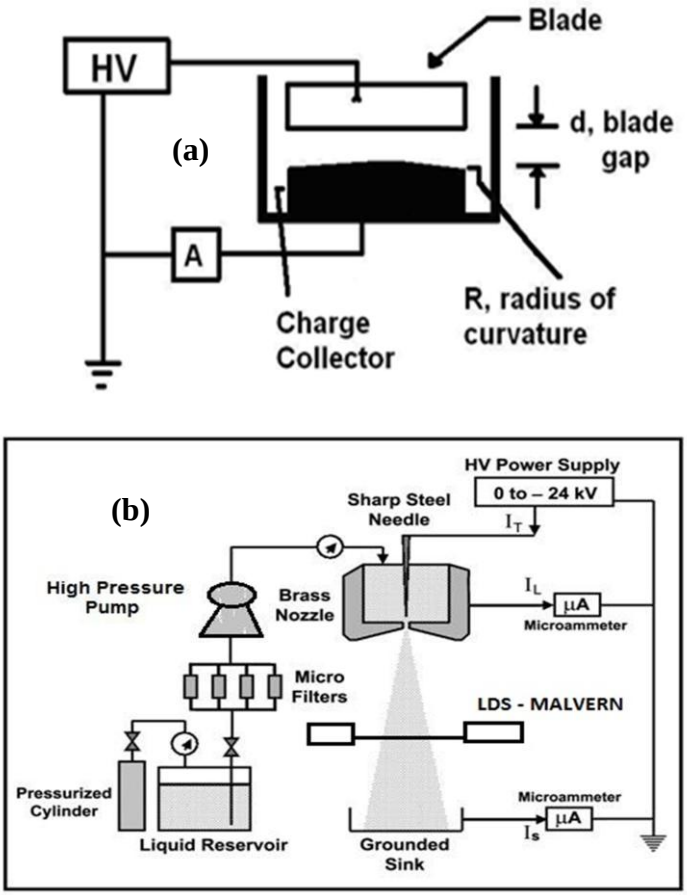

Figure 3.1 Experimental layout and connections (a) blade-plane charge injector (b) point-plane atomizer rig

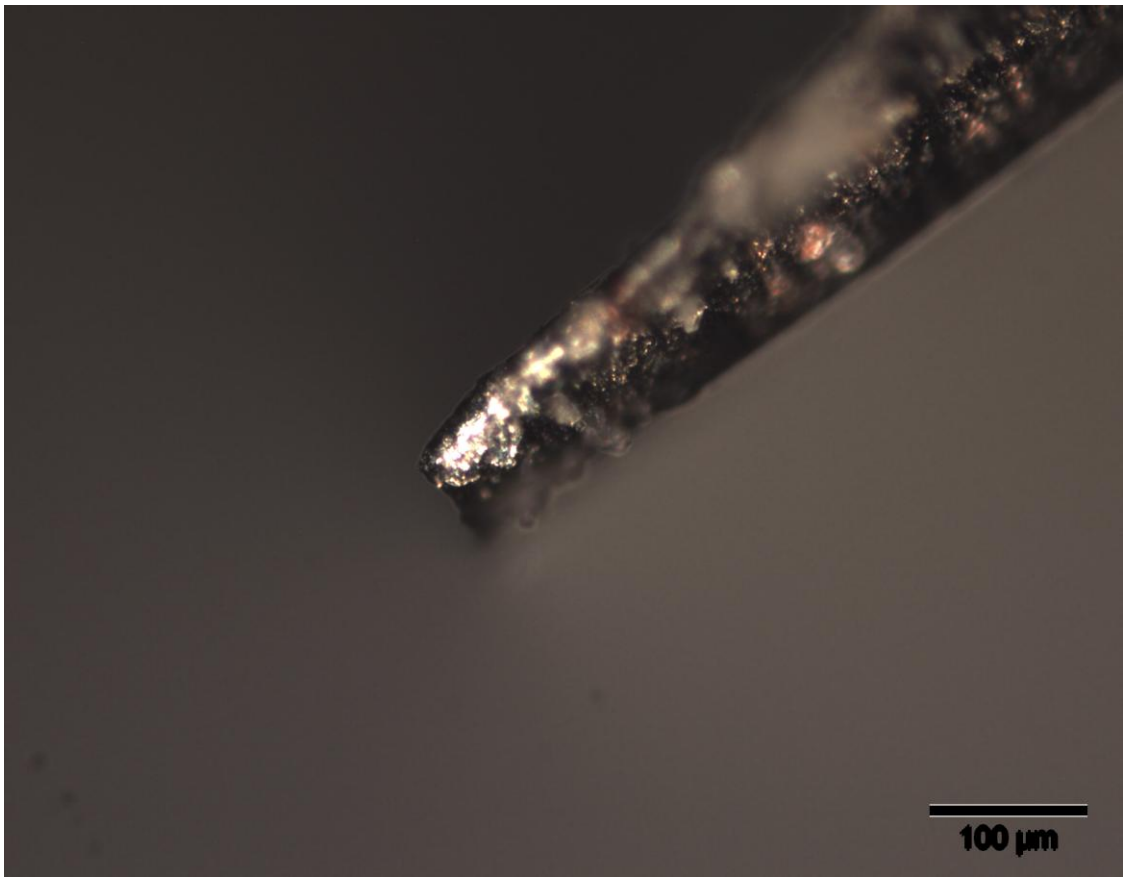

Figure 3.2 Hi-mag photo of the blade tip

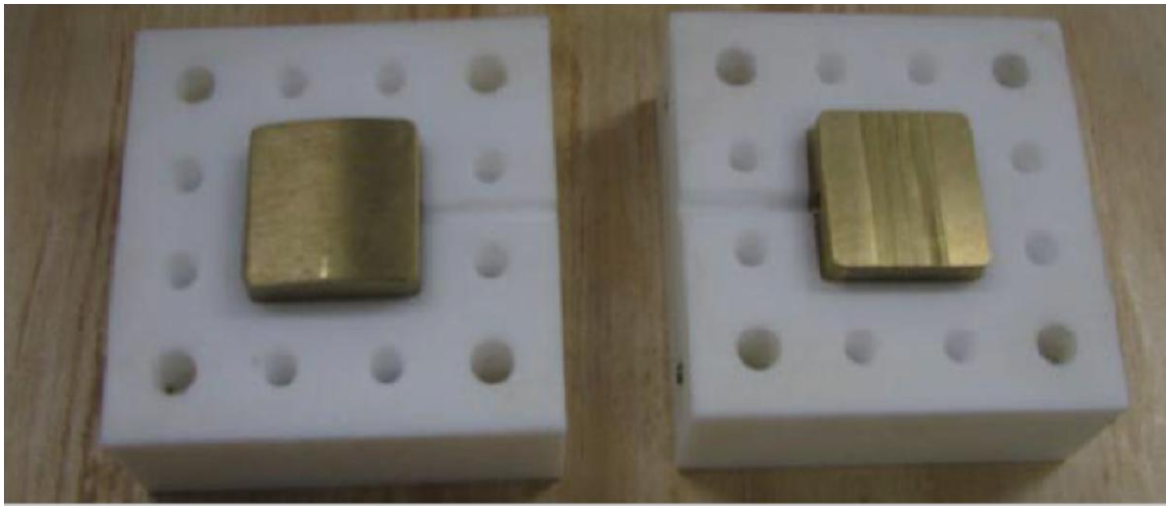

Figure 3.3 Blade-plane charge injector

The purpose of the point-plane atomizer, shown in Figure 3.1(b), is to introduce an electric charge into the liquid while flowing through the nozzle orifice producing a charged spray. An improved version of the third generation electrostatic charge injection atomizer was redesigned and machined at UIC machine shop. All metal parts were made from brass for its resistance to wear and machinability. PTFE spacer and nylon bolts are used to insulate the interior of the atomizer body from electrical breakdown. The charging needle position was easily controlled coaxially in both directions by a micrometer..

A 10 MΩ resistor was attached in series among the nozzle body and earth to reduce the influence of electrical transients on atomizer operation. A 10 kΩ resistor was also connected between the electrode rings and the electrometer to minimize errors, which was due to the capacitance effect from the accumulation of residue charge.

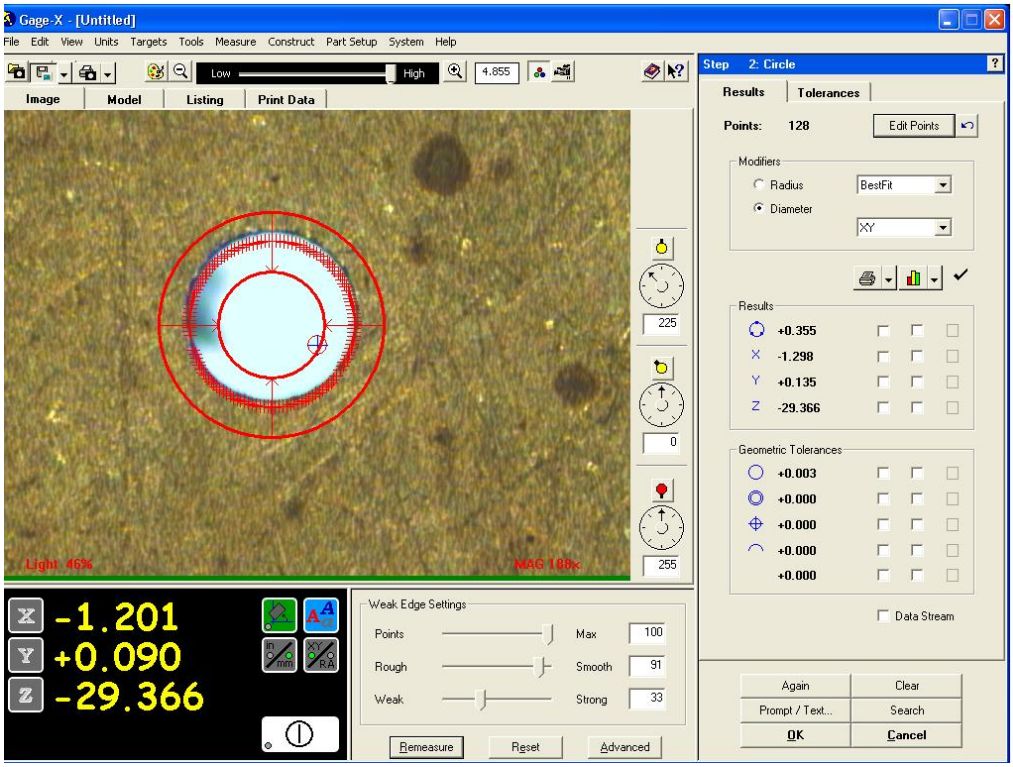

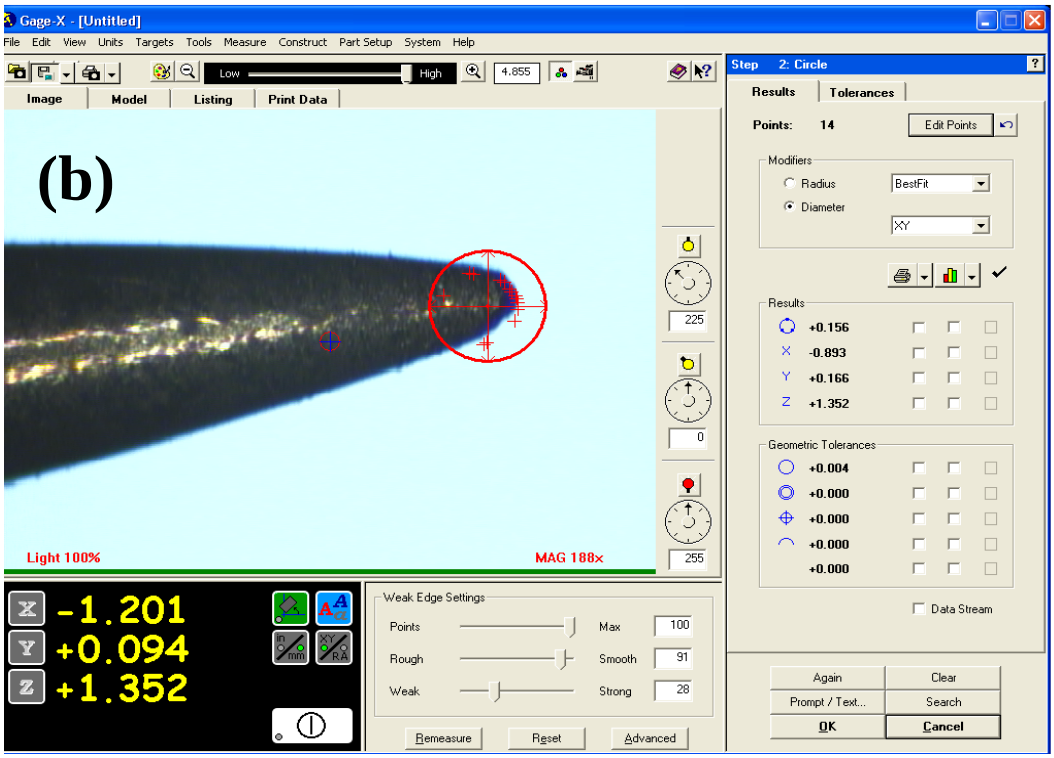

Figure 3.4 Hi-mag photos of (a) 350 µm orifice disk (b) charger needle tip

A stainless steel needle with a tip radius of 100 μm was used as the charging electrode. The needle tip radius and orifice size were measured using 200x magnification on GageX software system within 0.1 μm as shown in Figure 3.4.

Figure 3.5 Needle type atomizer

A micrometer was mounted as seen from Figure 3.5 on the atomizer body to adjust the charging electrode distance from the grounded nozzle orifice inlet within 5% accuracy. The electrode gap is non-dimensionalized (*L/d*) by taking the ratio of

the electrode gap (L) to the orifice size (d). The dielectric liquid flows through the PTFE insulated passage and gets in contact with the charging needle electrode connected to high voltage power source and sprays through the nozzle orifice tip.

3.3 **Testing fluid and properties**

As explained before, commercially available Diesel fuel was used mostly for the experiments. The working liquid, Diesel fuel was not recycled during testing as its electrical properties were observed to have changed once used, which were evidenced with lower threshold V_{th} and breakdown voltage values obtained with the reuse. The lower values of voltage may also be due to molecular degradation of the liquid, which reduces the electrical resistivity indicating that the injection mechanism is electrochemical.

For the blade type high flow rate setup, Diesel fuel was recycled in a closed loop system. Low specific charge levels in the fuel prevented major changes in the electrical properties of the fuel. Also, it would be costly to run such a high flow rate system by spraying the fuel only once.

The other test liquid used in the experiment was the regular commercial raw (unused) corn oil. Three important physical parameters of liquids, density (ρ) was measured by using a 10 mL beaker measured the fluid sample weight with a digital scale, ProScale 600 Luxe, with $\pm 0.1\,\mathrm{g}$ reading accuracy. Weight measurements were repeated several times and the average of the repetitive runs was taken.

The liquid electrical conductivity was measured with a rubber tube filled with liquid free of bubbles, high-voltage power supply and a HP 3458A picoammeter that

has a built in protection from the probable high-voltage surges. These measurements are verified with EMCEE 1152 that meets the ASTM standards [53].

3.4 **Experimental Rig**

The experimental rig consisted of these components: pressure vessel, filters, flow-meter and pressure gauge. A 7-gallon pressure tank was used to pressurize the fuel up to 6 bar. Transparent tubing with 3 mm inner diameter was connected to check the tank fuel level. A ball type regulator was connected to control the flow outlet from the tank.

A 7 μm particle size filter made by Swagelok was used to filter the solid particles from the Diesel fuel. For the high pressure runs on 75 μm orifice size, 2 μm filter was installed just before the atomizer inlet. The aim of the filters was not only to clean the fuel from particles but also to avoid air bubble formation.

For high flow rate studies, a digital gauge made by GPI was used. This gauge was already calibrated for Diesel fuel and mostly used by gas stations to calibrate their fuel pump gauges. This digital pressure gauge was placed at the atomizer inlet. The gauge can measure up to 15 bar within %0.1 error.

A Zenith HPB series gear pump is used to achieve a steady, pulseless, repeatable high pressure flow to assure better quality control for experiments conducted above 6 bar as shown in Figure 3.7. Although this system could deliver much higher pressures, measurements were done at a maximum 40 bar due to limitations of the atomizer design.

Figure 3.7 High pressure pump connections and frequency controller

The leakage current (I_L) meter was measured via HP 3458A Multimeter that offers long-standing performance of speed and accuracy in lab testing. This device can make a measurement reading rate at 100,000 readings per second within ±1%. An Agilent 82357B USB/GPIB (General Purpose Interface Bus) was used to provide a connection to the laboratory computer. To read, record, and process data a Labview code was written.

The possibility of collecting a significant number of data and performing an accurate statistical analysis on them provides a better understanding of the process in act. A LabView code could be also an advantageous tool for future transient analysis on spray characteristics or general studies based on the time dependency. Spray current data were collected with a frequency of 150 samples per minute. The values reported in the results are averages of data recorded in each measurement run. The interface of the LabView code is seen on Appendices section.

The high voltage power supply used in this study was the Spellman LS30PN operated with negative polarity, voltage range from 0 to -25 kV in 0.01 kV intervals and 30 watts of output power. The output voltage rated accuracy equals 0.5%.

Negative polarity of the high voltage supply was chosen based on the literature [49] that a more stable charge injection is possible at lower electric field. As known, the electrons have much larger ionic mobilities than the positive ions and therefore, are quickly accelerated by the applied electric field.

3.5 **Droplet Size Analyzer**

Droplet size measurements were taken with a Malvern 2600 LDS particle analyzer as shown in Figure 3.10. The Malvern analyzer is a laser diffraction instrument that measures droplet size based on the energy of the diffracted light caused by droplets passing through the analyzer's sampling area. The scattered light intensity is measured through the diodes housed in the receiver unit without creating an image of the particle on the detector. The computer software reads the detector signals over a period of time and sums this data.

Laser light scattering method has several advantages that can be listed as:

- Non-intrusive: low power laser beam to probe the particle size
- Fast: Requires typically less than a minute to take a measurement and analyze.
- Precise: Giving high resolution size discrimination.
- Wide Range: Several optical configurations that the user selects to suit the expected range of droplet sizes.

- Absolute: No calibration is required.
- Simple: Can easily be operated by unskilled staff due to the provision of the measurement mode.
- Versatile: Switching from one sample presentation to another just takes a few minutes.

The analyzer has a 2mW He-Ne laser beam with 9 mm diameter at a wavelength of 632.8 nm. The 300 mm focal length receiver lens configuration allows a measurement range of 5.8 µm to 564 µm at a maximum working distance of 400 mm from the receiver. For smaller droplet size distributions, 100 mm focal length receiver lens is used with a range of 1.5 µm to 188 µm. Due to the properties of the range lens the diffraction pattern of a particle within the analyzer beam will remain stationary and centered on the detector regardless of particle position or velocity. The scattered light is collected by the detector, which in turn emits an electronic signal proportional to the light intensity.

Over the size range 2 µm and larger, forward scattered light is related to the optical properties of the fluid. Refractive index becomes significant for particles in the 0.5 to 2 µm range. The Malvern 2600 assumes that the particles are distributed in 32 size bins. Particle size distribution can be displayed as Rosin-Rambler, or model independent where model independent allows measurements of multi-mode distributions.

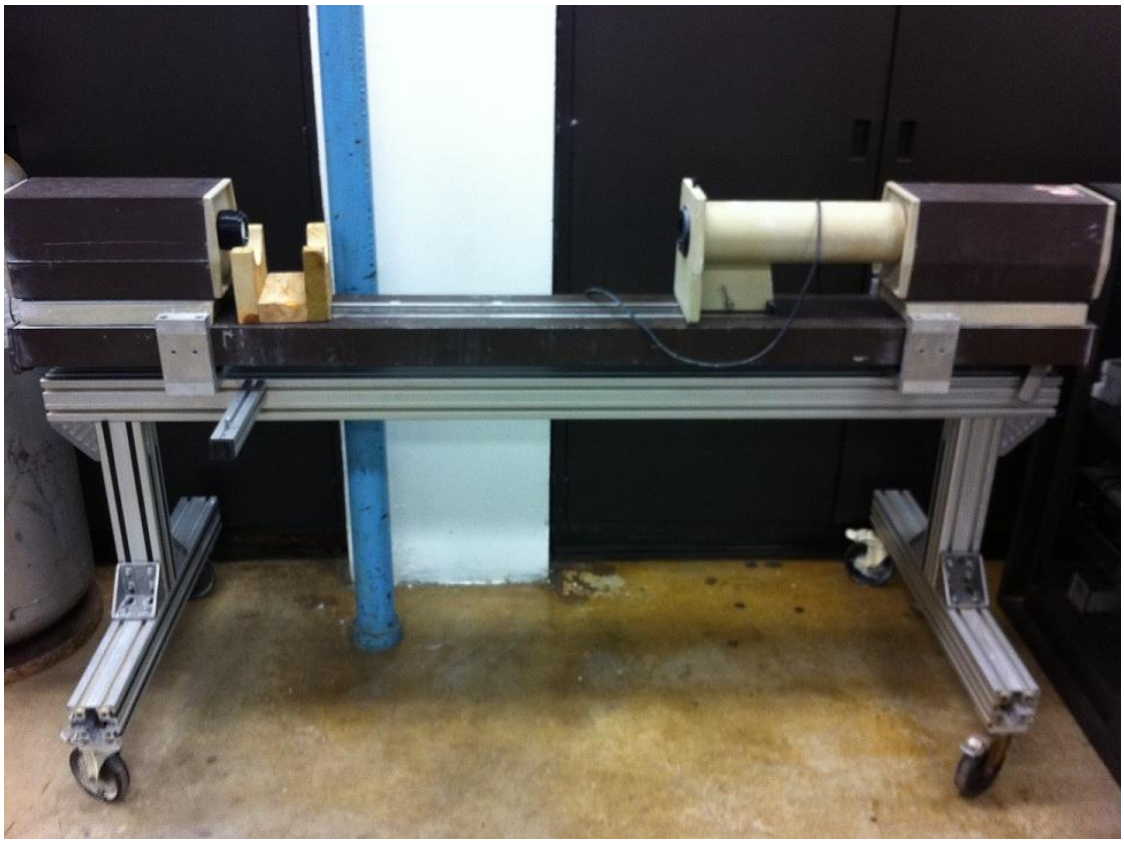

Figure 3.8 Malvern 2600 LDS particle analyzer

In addition to all the advantages of the laser diffraction technique, there are several limitations. These limitations can be listed as the lens setup range, cut-off length, multi-scattering effect, diode light sensitivity, repeatability, test procedure and misting.

- Lens setup range: Malvern 2600 Series particle analyzer has several lens configurations i.e. focal lengths of the receiver lens as shown in Table 3.1.

Focal length (mm)	Minimum Size (μm)	Maximum Size (μm)
63	1.2	118
100	1.9	188
300	5.8	564
600	11.6	1128
800	15.5	1503
1000	19.4	1880

Table 3.1 Lens setup range

- Lens cut-off length: Each lens setup has a limited aperture for the scattered light collection and a maximum scattering angle as shown in Table 3.2. If the sample spray is too far away from the measurement zone, some scattering light cannot be collected on the receiver diodes. Due to the nature of electrostatic atomizers, the spray is attracted by the droplet size analyzer body. As a result, it's hard to spray the sample within the cut-off length (133 mm) of the corresponding 100 mm focal length lens setup. To avoid this issue, a protective lens cover is built to blow air outside the lens to avoid the contamination of the lens with fuel.

Focal length (mm)	Cut-off length (mm)
63	55
100	133
300	400
600	780
800	1050
1000	1300

Table 3.2 Cut-off length

- Multiple Scattering: When the sprays are highly transient, dense, composed of very small droplets and heterogeneously distributed in space, it originates the undesirable effects of light multiple scattering. Multi-scattering term refers to the finding of scattered light at different angles. Nowadays, recent laser diffraction droplet size analyzers are equipped with self-correction formulations for multiple scattering effects. For the analyzer used in this study, a correction developed by workers at Sheffield University was applied only in Rosin-Rammler mode.
- Diode light sensitivity: If the spray is too dense and has significant number of droplets at a certain droplet size range, it might saturate the light intensity level of a diode at the receiver detector. The device will perceive it as the maximum allowable intensity level and will form a droplet size distribution accordingly. This distribution might have differences from the actual distribution. All runs in this study performed at a minimum spray distance of 100 mm to avoid the dense regions near the orifice.
- Repeatability: Results within 6% can be regarded as identical with the Malvern 2600 analyzer. To have more dependable results, three runs for each case was performed and the numerical average results were tabulated.
- Test Procedure: Tests were conducted when the spray was steady. However the beginning and end of the testing was set manually. Although it was tried to be consistent within each runs, there might be

some inevitable differences in the test ending location within the spray. This might lead to some of the data on the outer radius to be disregarded. It is known that smaller droplets exist in the outer radius, therefore actual results might be lower in those cases.

- Misting: As explained earlier, it was sprayed into a bucket to protect the lenses operating within the cut-off length. This caused some misting to be enclosed inside the bucket and especially at high operating pressures; some of the mist created was emerged in the measurement zone.

Spray is considered here as the collection of droplets. Most atomizers in practical use generate droplets in the size range from a few microns to around 500 microns. The droplet sizes within a spray vary due to the heterogeneous atomization process. As a result, practical nozzles generate sprays that can be considered as a collection of droplet sizes distributed around an average value instead of a spray of unique uniform droplet size value.

At this point, the $D_{V0.5}$, D_{32}, $D_{V0.1}$ and $D_{V0.9}$ diameters were used to evaluate the droplet sizes that can be found in ASTM standard E1620-97 [51]. The following lists the most popular mean and characteristic diameters used in this study. $D_{V0.5,}$ volume median diameter (VMD), is the value where half of the total liquid volume is in droplets with smaller (or larger) diameter. This diameter is used to compare the change in droplet size on average between test conditions. D_{32}**,** Sauter mean diameter (SMD) is the diameter of the whole spray volume-surface area fraction. This diameter is best suited to calculate the chemical reactions during the combustion process. D_{32} is for stating the spray fineness in terms of the area whereas VMD correlated the size to

the volume of the liquid sprayed. $D_{V0.1}$ and $D_{V0.9}$ are the values where respectively 10% and 90% of the volume of sprayed droplets with diameters smaller or equal to these values. $D_{V0.1}$ is used to have an insight of the minimum size range and $D_{V0.9}$ is used to approximate the maximum droplet size.

Several mathematical expressions are derived to provide a satisfactory fit to the droplet size data and to allow extrapolation to droplet sizes outside the measurement range where measurements are least precise. Moreover, these distributions make it easy to calculate mean and other representative diameters of interest without dealing with large amount of data. The most popular distributions can be listed as the log-normal, upper-limit and Rosin-Rammler. As the mechanisms of spray break-up are not well understood, there is no single distribution function to cover all data. Therefore, a comparison testing should be conducted to find the best fit to the collected data. In this study, a well-known expression for droplet size distribution developed by Rosin and Rammler [52] is used. This distribution function is presented as:

$$F(D) = 1 - \exp\left[-\left(\frac{D}{D_{v0.632}}\right)\right]^{\psi} \qquad (3.1)$$

where F(D) is the ratio of the volume in droplets of diameter less than D. ψ is the constant that gives the width of droplet size distribution. A higher value of ψ indicates a more uniform distribution. All droplets will be equal size when the value of ψ is infinite. For a spray having ψ =3, $D_{V0.9}$ is about 50% larger than VMD.

4. QUIESCENT DIELECTRIC LIQUID

4.1 Introduction

The overall motivation for the quiescent dielectric liquid study is to build fundamental information to understand charge injection process and to investigate the development of energy-efficient solutions for the atomization of high-viscosity liquids such as vegetable oils. However, due to the high viscosity of such bio-mass oils, there is some difficulty during injection and atomization [55]. Biological fuels reduce the environmental pollution and emission of hazardous oxides of sulfur and carbon. These emissions became a major point of concern after the Kyoto Protocol was imposed in 1997 [56].

A practical limitation of the common single-point atomization method is that the spray specific charge is a function of the orifice diameter [57]. The practical consequence is that, for a single orifice, highly charged sprays are only possible at low flow rates. A more fundamental issue with the point-plane charge injection method, as identified by Rigit [58] and Al-Ahmad et al. [59], is that damage can occur to the high voltage electrode sharp point due to strong current flux emitted from the high voltage point.

Here, we evaluate a linear, rather than a point charge injector, in this case single and multiple razor blades. This linear geometry is essentially a series of points on a line [60]. This greatly increases the surface area of charge injection and should, in theory, increase the total emitted current, while simultaneously reducing the current flux. Single blade atomizers have been studied in the last two decades, computationally or experimentally by investigators using various fluids. Takashima et

al. [61] used transformer oil on both needle-plane and blade-plane rigs and compared the I-V characteristics. Atten et al. [62] studied vortex formation around the blade and determined the velocity profile. The present study extends the previous research into more viscous liquids and multi-blade systems. Moreover, we also investigate a charge injection process using rounded charge collectors, which increase the stability of the charge injection, but at a loss of efficiency.

We consider this charge injection method to be a part of a different type of charge injection atomizer than that proposed previously [63]. In these cases, the charge injection process and the atomization process are inextricably linked, due to the manner in which the charge injection site is positioned directly above the atomizer orifice. In the proposed system, the charge injection system is separated from the liquid atomization process. Because of this, the charge injection system should be able to be retrofitted to a range of existing atomization systems. The flow rate should be optimized to keep the charge density high enough to obtain a finely atomized liquid spray.

The injected current is the primary variable to quantify the performance of a charge injection device. In the following study, the independent parameters are the applied voltage (V), the working fluid type, the gap between the blade and the charge collector (L), the radius of the collector (R), the number of blades (n) and the spacing between the blades (S). In the presentation of the results, the variation of the injected current with these independent parameters is discussed. There is a transient period for the injected current to reach steady state and typically the time constant for the system was 5 minutes. All the data discussed hereafter pertains to this steady state regime.

The formations of vapor bubbles at the emitter electrode tip were observed to cause current pulses.. Through the investigations, it was found for negative polarity charging that the density and magnitude of the pulses raise with applied voltage. A discussion on the formation of these bubbles is included at the end of the section.

4.2 **Design**

Several calculations were computed to determine the dimensions of the charge injector necessary for insulation from high voltage emitter blades to avoid any possible charging breakdowns. Figure 4.1 shows the assembly of the blade type charge injector. Design stages can be reviewed in more detail in Appendix D.

–

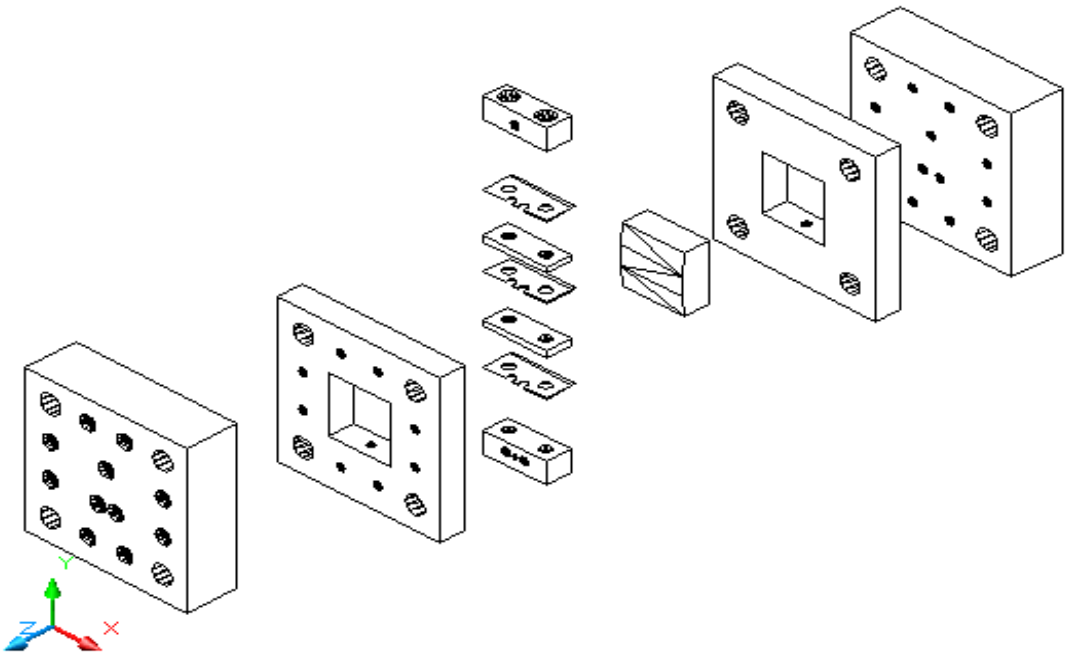

Figure 4.1 Blade type charge injector – assembly

4.3 **Electrical Performance**

4.3.1 **Single blade charge injector**

There are various experimental *I-V* relations to explain charge extraction mechanisms at the electrode. Denat et al. [65] presented an *I-V* model assuming that the ion dissociation is not affected by the electric field. Castellanos et al. [66] improved this model by including the field enhanced dissociation and the Onsager effect [67]. Recently, Neagu et al. [68] confirmed their own model for the electron injection experimentally. In this study, we consider a modification of the model suggested in [69] that focuses on the electrical characteristics above the threshold surface electric field, the dependence of blade-plane electrode gap with the current flux. This model is expressed as:

$$J = A(E - E_{th})^n \qquad (4.10)$$

The current flux (J) is obtained by dividing the measured injected current (I) by the projected cross-sectional area of the blade tip where the major charge injection occurs. The current flux is related to the surface electric field (E), which is calculated by assuming that the tip of the blade has a cylindrical surface. In this study, the surface electric field is found by dividing the voltage (V) to the blade tip radius [70]. This modification is performed to leave the size and the number of the blades out of discussion and hence, to enable a better comparison with literature.

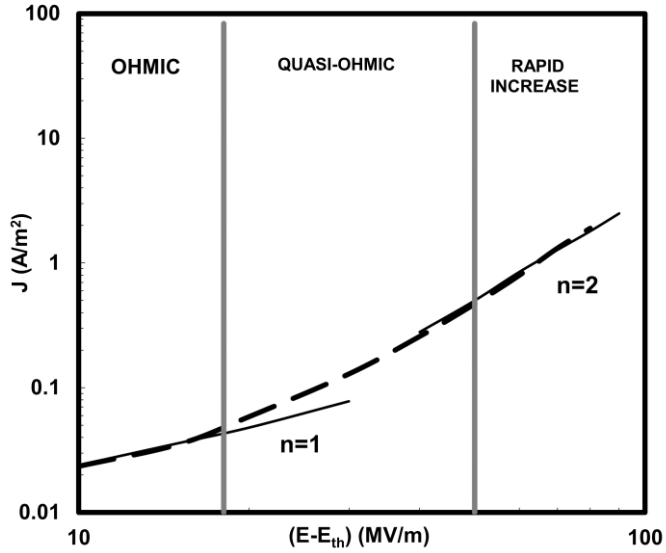

Figure 4.2 Regimes shown on the selected diesel fuel data for single blade case with straight collector and L=1.25 mm.

Surface electric field is a significant parameter in the initiation and development of the charge injection. The conducted experiments show that the threshold voltage is dependent on the inner electrode gap and the type of the fluid. Planar charge receiver electrodes yield lower threshold voltages. Corresponding threshold voltages are found as $V_{th} = 2.5 \pm 0.5$ kV for Diesel fuel and $V_{th} = 6.0 \pm 0.5$ kV for corn oil.

The charge transport in the quiescent fluid is generally presented in three regimes: ohmic regime, quasi-ohmic regime, and rapid increase regime [69]. In our model (4.10), the value of parameter n determines the charging regime. In the ohmic charging regime, a linear *J-E* curve is observed and $n \cong 1$. However, in the rapid increase regime, *J-E* curve is no longer linear. In this regime, the curve is parabolic with the value of n=2 as shown in Figure 4.2. The transition region between these two phases is called the quasi-ohmic regime.

Work carried out in this section focuses on characteristics for voltages above the threshold voltage. The experiments were initially conducted with one blade for three different gaps, which are measured from the center of the blade to the charge collector: L=0.75 mm, 1.00 mm and 1.25 mm. These blade gap values are found from the literature [71] to lead to stable charge injection.

Diesel fuel data for all electrodes at different blade gaps are given in Figure 4.3. There is a similarity between the current injection regimes of our charge injector and those in the charge injector used by Atten et al. [69] for benzyle neocaprate (BNC). They achieved lower injected currents due to the differences in the physical properties of the fluids, blades and the blade gap. Moreover, the charge injection stability for high viscosity corn oil is investigated and shown in Figure 4.3(c). Corn oil is over 20 times more viscous than the Diesel fuel. This difference in viscosity results in lower injected current as mentioned earlier in the discussion of the non-dimensional number M. Smaller gap between the electrodes results in higher flux; however, the stability of the injector imposes a limit on this gap value. Furthermore, the more planar the receiver electrode is, the higher the current flux is at a constant number of blades, and surface electric field.

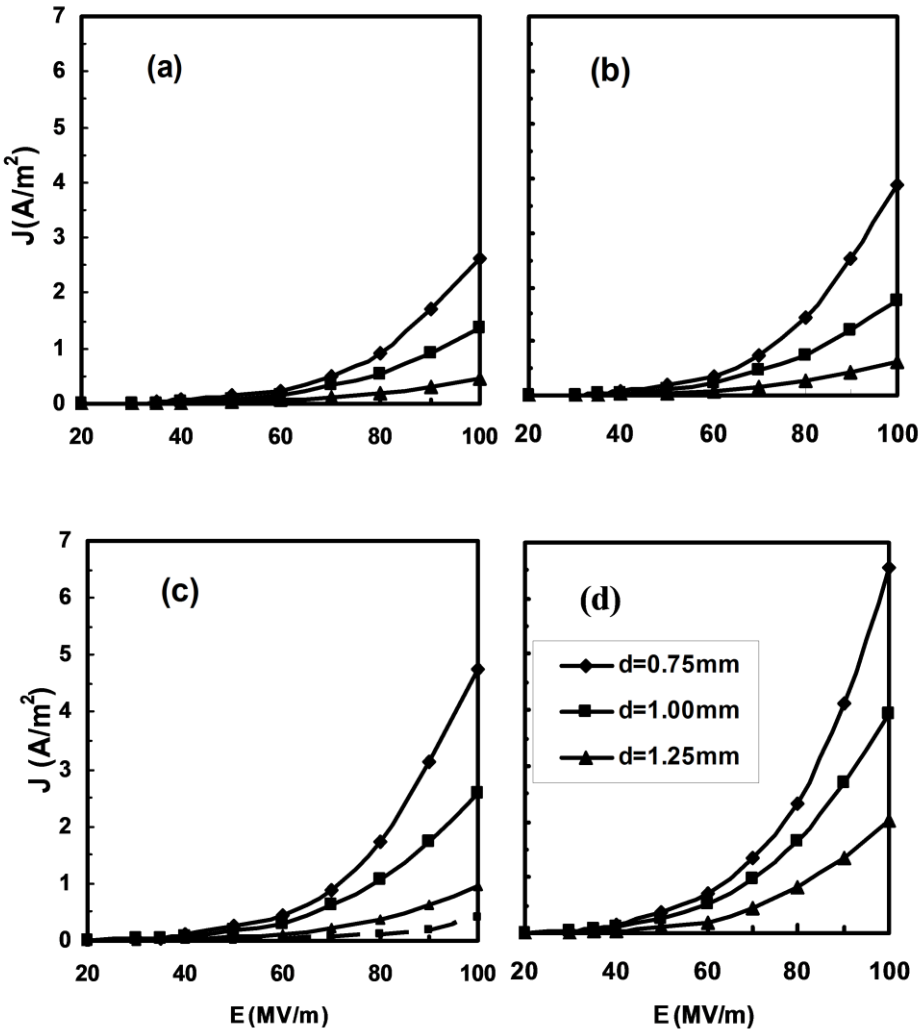

Figure 4.3 Comparison of the current flux in (a) *R*= 75 mm, (b) *R*= 100 mm, (c) *R*= 125 mm, and (d) straight collector, at three different gaps *L*= 0.75 mm (♦), 1.00 mm (■) and 1.25 mm (▲) for diesel fuel with a single blade. Dashed line in (c) is for corn oil at *L*= 0.75 mm.

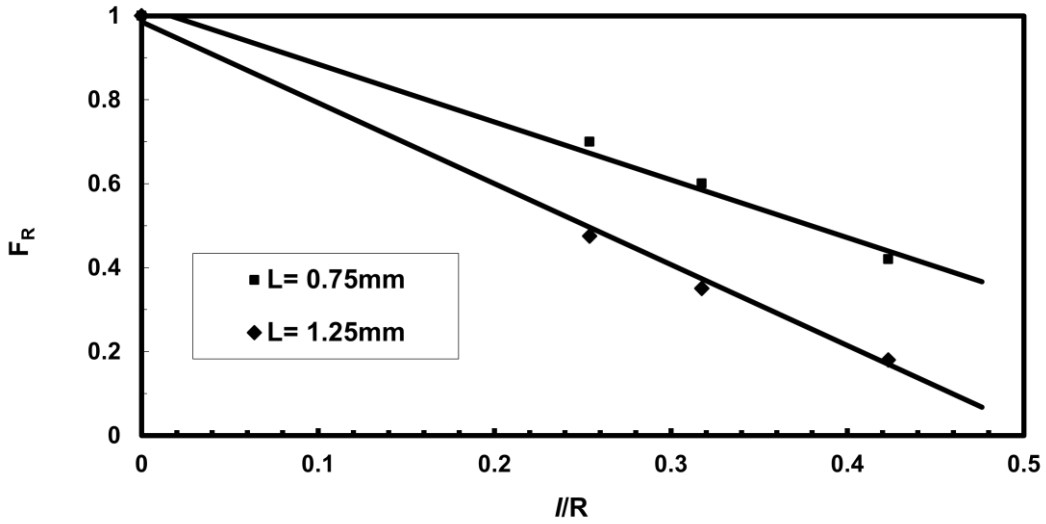

Figure 4.4 Variation of the radius efficiency factor (F_R) with the non-dimensionalized radius, l/R at blade gaps L= 0.75 mm (■) and 1.25 mm (♦) in single-blade setup with diesel fuel. Lines indicate the linear regression fittings.

At constant voltage, the term A in equation (4.10) scales as;

$$A \propto L^{-m} \qquad (4.11)$$

the term A is inversely proportional to the gap distance (L) and the exponent m in equation (4.11) is a function of the geometry and the working fluid. Using the straight electrode with Diesel fuel, the exponent m of equation (4.11) is found to be $m = 2.0 \pm 0.2$. The value of m is found to be larger for rounded electrodes. For the most rounded electrode used in the experiments, $R = 75$ mm, m increases to 4 for $6 \text{ kV} < V < 10 \text{ kV}$.

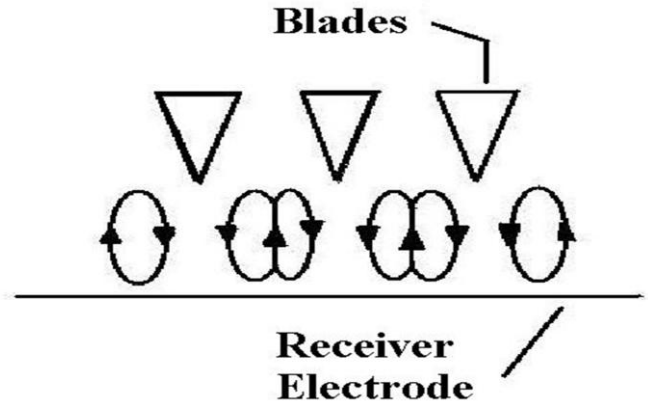

Figure 4.5 Schematic representation of space charge induced flow between the blades and the receiver electrode.

Table 4.1 Units and Properties.

Properties	Diesel	Corn oil
Density [kg/m^3]	840	870
Viscosity [mPa.s]	2.4	54
Surface tension [N/m]	0.025	0.031
Electrical conductivity [1/(Ohm.m)]	$1.0\text{x}10^{-10}$	$0.6\text{x}10^{-10}$
Electrical Permittivity [F/m]	$3.54\text{x}10^{-11}$	$3.10\text{x}10^{-11}$
Electron mobility [m^2/(V.s)]	$1.3\text{x}10^{-8}$	$5.6\text{x}10^{-10}$

The magnitude of the injected current increases as the receiver becomes more planar; however, it was observed that the rounded collector electrodes provide a more stable charge injection process by increasing the robustness at higher operating voltages. At this point, a radius efficiency factor (F_R) is defined to indicate the injected current of the rounded charge collector relative to that of the flat collector in the rapid increase regime. Figure 3.4 shows the efficiency factor as a function of the

non-dimensionalized radius, *l/R*, at $L = 0.75$ mm and 1.25 mm. From this data, linear regression fittings are obtained using the model:

$$F_R = f_1 \frac{l}{R} + f_2 \qquad (4.13)$$

It is found that $f_1 = -1.38$ for $L = 0.75$ mm and $f_1 = -1.93$ for $L = 1.25$ mm. A higher distance between the blade and the electrode results in a steeper loss of efficiency with the decrease of R.

4.3.2 **Multiple-blade charge injector**

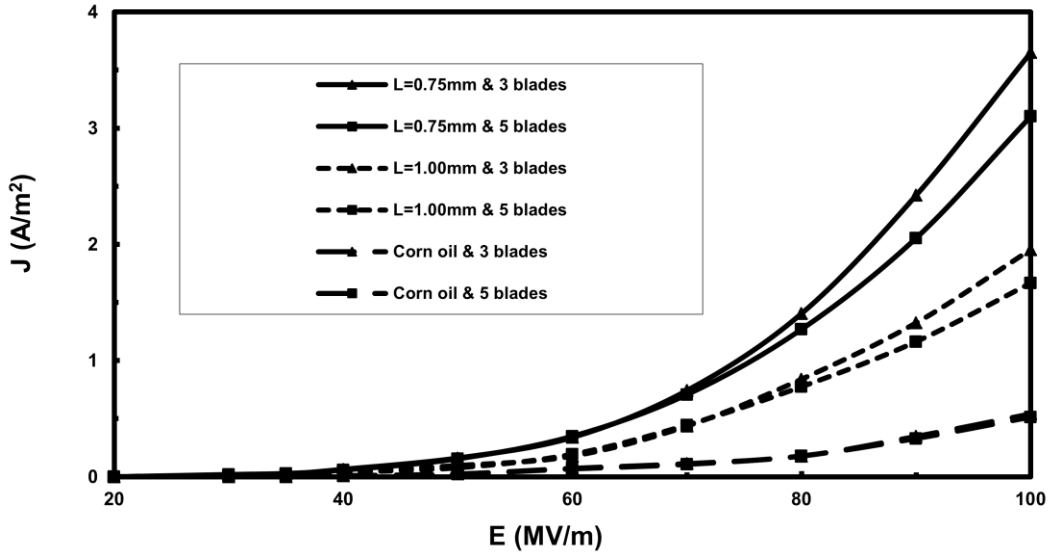

Figure 4.6 Injected current flux using multi-blade configurations for diesel fuel and corn oil with *R*= 125 mm rounded collector. Corn oil data are evaluated at L= 0.75 mm.

Several experiments have been conducted with a multi-blade charge injector. The distance between the blades (*S*) is fixed at 6.4 mm for the 3-blade and at 3.2 mm for the 5-blade configurations. These values are chosen to investigate the interaction between the blades caused by the coulomb induced flow, a theoretical EHD roll structure is shown in Figure 4.5. Roll structures have been referred to and the

structures that one is referring to are those that appear in an electrode gap, once the instability criterion has been satisfied as shown at previous section when the physics of instability (T parameter) was introduced. As already stated, the investigation of roll structures is also an area of study that appears in the more conventional Rayleigh-Benard or natural convection. Here, three dimensional roll structures are produced by the input of thermal energy as opposed to electrical energy, though many have drawn analogies between the two areas of physics. Some studies on electroconvection in insulating liquid were conducted by Watson et al. [72]. The emitted charge transports to the anode by means of ionic drift and initiating electroconvective roll structures within the system.

At this point, a critical stability parameter is defined (T_c), also known as electrical Rayleigh number, at which electroconvective roll structures begin to appear assuming that charge transport is dominated by the drift. It has been shown that electroconvection in a quiescent liquid for strong injection case, initiates at a value of T_c=100. At this critical stability parameter value is reached, electroconvective forces surpass the viscous forces and this induced occurs. This critical value corresponds to -90V for Diesel fuel in the used charge injector.

Perez et al. [71] utilized the finite volume method in a blade-plane geometry and investigated the roll structures for very high T numbers of the order $T>10^4$ which is the case we observed at around -10 kV applied voltage in the current charge injector. They observed chaotic variations of velocity with time for T numbers of the order $T>10^5$. For the blade-plane configurations, this electroconvection takes the form of a bi-dimensional charged plume while it is an axisymmetric shape in needle type charge injection atomizers. For laminar case, electroconvection exists in a narrow

core that entrains surrounding uncharged fluid. The injection surface is highly non-planar leading to non-uniform charge distributions in the bulk fluid.

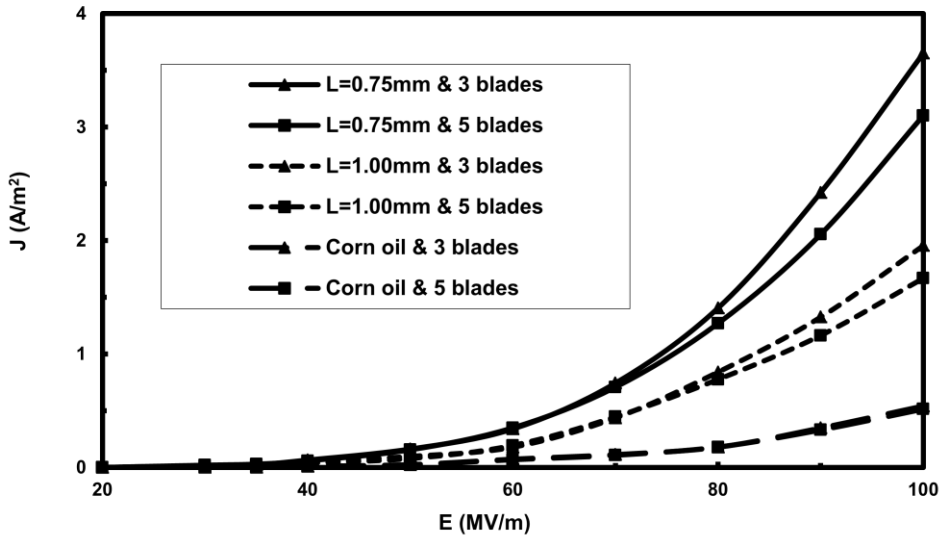

Figure 4.7 Injected current flux using multi-blade configurations for diesel fuel and corn oil with *R*= 125 mm rounded collector. Corn oil data is evaluated at L= 0.75 mm.

Experiments show that using multiple blades results in an overall increase in the conducted charge. From the *I* values, current fluxes are calculated to estimate when the induced flow interaction becomes noticeable. This interaction results in a less efficient operation of the charge injector as it causes deflections on the path of the injected charges while transporting between the electrodes. As one may expect, less efficient operation leads to lower *J* values. In Figure 4.7, for *L*=0.75 mm, 3-blade and 5-blade injectors behave very similarly up to 65 MV/m but then a deviation is observed which is more pronounced with increasing the surface electric field. The 5-blade configuration yields a lower *J* due to the smaller distance between the blades. The beginning of this deviation can be interpreted as the point where interactions start taking place. When the electrode gap (*L*) is raised to 1.00 mm, the deviation starts at a higher surface electric field value of 75 MV/m. One can conclude that the induced

flow is weaker at higher *L* and becomes comparable to the blade gap (*S*) at high values of surface electric field. These findings are in aggrement with the study conducted by Atten et al. [69] where they observed unsteady plumes having a diameter around 1mm. So far, there is no data in literature regarding the velocity profiles of such roll structures due to the limitation of the existing velocimetry techniques. However, roll structure velocity could be deriven with the thermal analogy resulting in an estimate velocity of 2 m/s [73].

Corn oil shows the same *J-E* characteristics irrespective of number of blades. The induced flow, in corn oil case, has relatively smaller magnitude due to the higher viscosity of the fluid. As a result of this, the induced flow caused by each blade is not affected at the designed blade spacing (*S*). When the size of the induced flow becomes comparable to *S*, the interaction with neighboring blade begins. At this point, a blade-number efficiency (F_B) is defined for determining the ratio of the injected current using multiple blades over the injected current with single blade. These ratios are further normalized by dividing by the number of the blades. Figure 4.8 illustrates the variation of the blade efficiency for the tested fluids with 3 and 5 blades over the operating voltages. Lower blade spacing in the 5-blade configuration leads to lower efficiencies than in the 3-blade configuration as a result of the higher interaction of the induced flow. As a final remark, multiple-blade configurations perform more efficiently for corn oil due to the lower induced turbulence around the blades as a result of the high viscosity of the oil. However, higher viscosity results in lower ion mobility, and hence, lower amount of charge can be injected to the fluid.

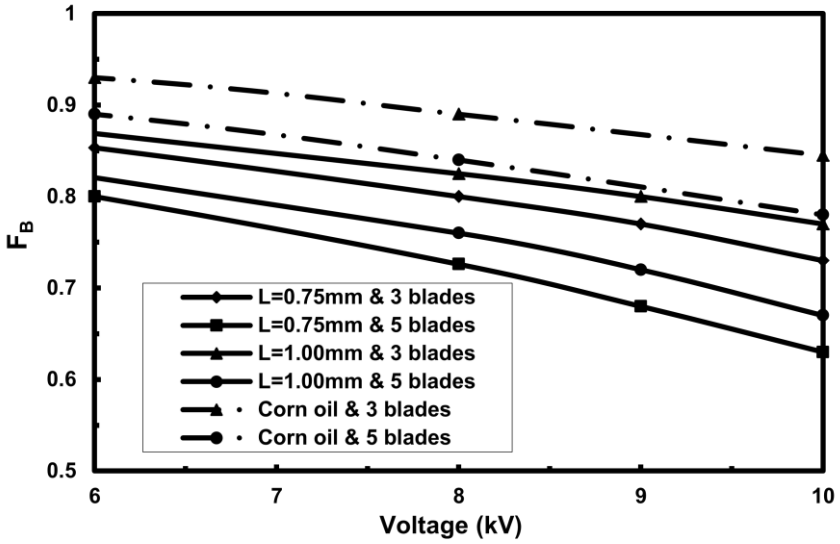

Figure 4.8 Blade-number efficiency, F_B using multi-blade for diesel fuel and corn oil with 125 mm rounded collector. Corn oil data is evaluated at L= 0.75 mm.

4.4 **High flow rate**

After validating that the blade type charge injector works reliably for no-flow case, it was proposed to build a new rig capable of high flow rates in the range of 0.1 to 0.5 l/s. This setup was recircilating the used fuel in a closed loop system, as seen in Figure 4.9. The system was composed of a 40–liter capacity stainless steel tank and a Sandpiper air-operated PTFE diaphragm pump chosen for their compatibility with Diesel fuel. A surge-protector was placed on top of the pump to ensure a steady flow. An air exhaust line was built for the pump for more stable operations. Filtration was conducted with fuel filters capable of filtering particles larger than 10 microns without any significant pressure drop. The volume of the filtered fuel was measured by a digital flow-meter calibrated for Diesel fuel. Two digital hand-held multi-meters were used to measure leakage and spray currents.

Figure 4.10 shows the variation of the liquid current at two different electrode gaps of d=0.75 mm and d=1.00 mm at constant flow rate of 3.6 gpm in the single-

blade configuration. Closer gap between the blade and the electrode results in higher injected currents, as per the zero flow work. Figure 4.11 confirmed that an increase in the (injected) liquid current was obtained with the increase in the flow rate, though the increase observed here was not significant in terms of the liquid charge density per flow rate. The low amount of specific charge levels makes this system impractical for practical situations.

Figure 4.9 The complete flow rig with blade type charge injection system

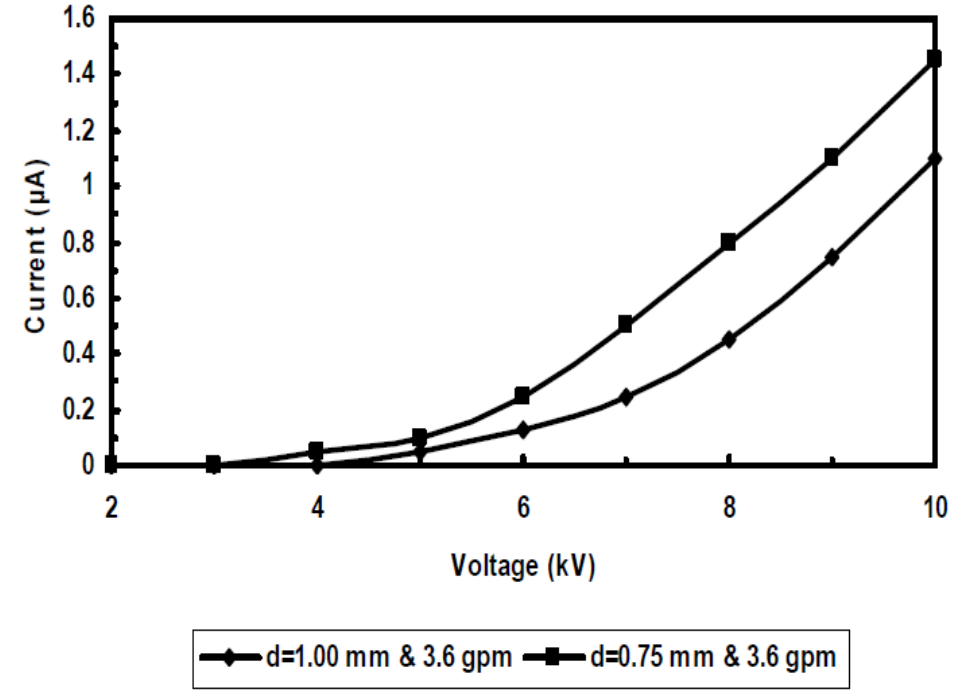

Figure 4.10 Injected current versus the blade gap at constant flow.

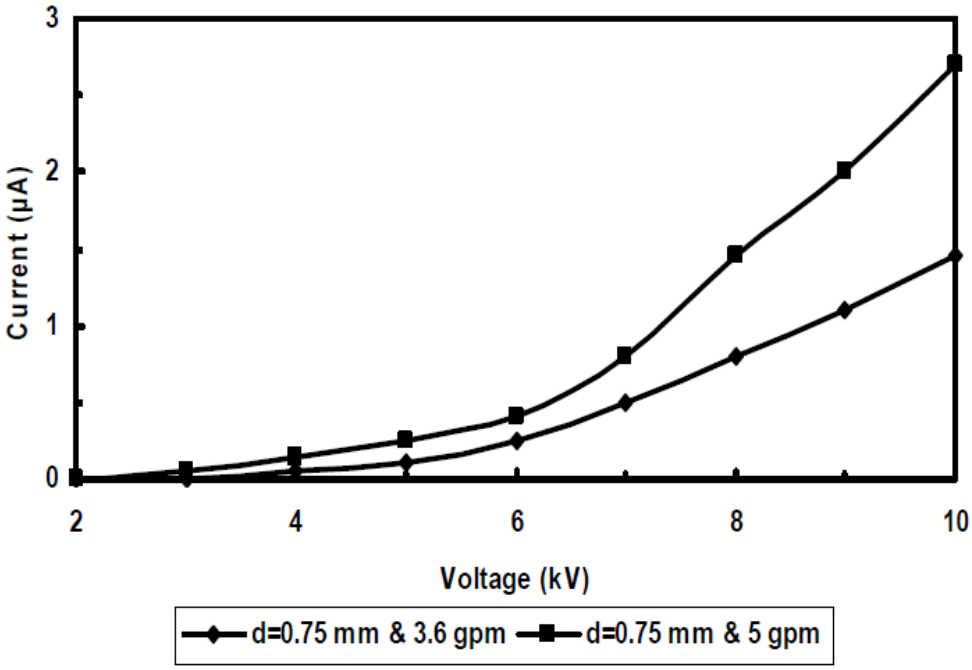

Figure 4.11 Injected current versus flow rate at constant blade gap.

4.5 **Bubble formation**

During the experiments, the formation and collection of small bubbles were observed as shown in Figure 4.12. These bubbles were greatly affected by the blade and the fluid motion around the blade. Bubbles of different sizes had different oscillation frequencies. It was observed that smaller bubbles tended to oscillate faster whereas movements of larger bubbles were not noticeable with the naked eye. There have been studies of "nucleation", which is known as the onset of a phase transformation in the form of bubbles from a liquid [74-75]. According to these studies, there are generally three phases of bubble formation as the generation of the cavity, the ionization, and the cavity expansion [76].

We could not study the dynamics of the bubble formation and propagation but it has been shown [76] that the triggering force to form the cavity and its growth is usually enabled by a current pulsation at the charger electrode. Localized injection of the current is converted into heat which causes evaporation of the liquid. Once the bubble is formed, its motion is governed by the bulk fluid swirling flow caused by the electrostatic field. When the electric field is removed, bubbles disappear and no significant change is observed in the electrical properties of the working fluid..

Several authors [77] have used excimer laser light pulses and electrical sparks to create bubbles for cavitation [78]. Kattan et al. [79] used ultra-purified cyclohexane with point-plane electrode to study the bubble formation associated with triggering current pulse as a function of ambient pressure. They created individual bubbles by a fast and restricted energy injection and the analysis of their results showed that some of the electrical energy introduced is transformed into heat that helped to the evaporation of the liquid. When the applied hydrodynamic pressure of the working

fluid surpasses the critical pressure no bubbles were observed while the current pulses still occurred. Some erosion of the charging needle electrode was observed due to cavitation erosion.

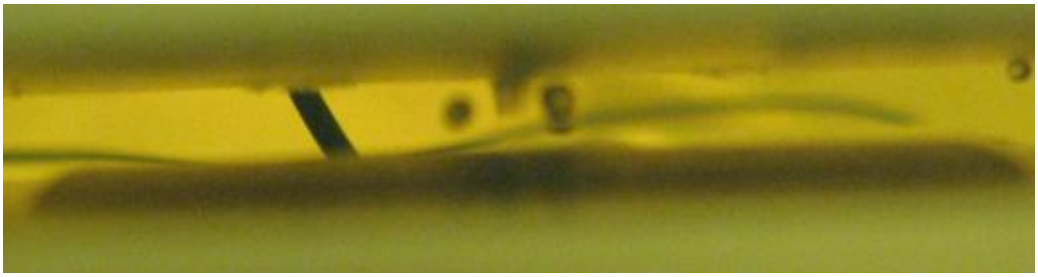

Figure 4.12 Bubble formation and oscillation

5. REMOTE CHARGE INJECTOR

5.1 Introduction

The main objective of this chapter is to make this method of atomization more universal application-wise by introducing a remote charge injection system developed to facilitate the implementation of the electrostatic atomization technology in existing nozzles. Restrictions in the current electrostatic atomizer designs, such as the size of the current electrodes and electrostatic atomizer bodies are the major obstacles to the employment of these electrostatic systems in some applications where modest dimensions and various injector geometries are required.

Studies, conducted so far, had to sacrifice the flow rate to increase the rate of specific charge density injected to the fluid [80]. For this reason, narrow spray angles are obtained at moderate voltage values. Increasing the system pressure to achieve higher flow rates resulted in even narrower spray angles. Another common concern is the lack of electrical insulation as the atomizer should be directly in contact with the target chamber. In response to these challenges of traditional electrostatic atomizers, some modifications in the design were proposed. The aim was to carry the charged liquid to a separate atomizer, which meets the demands for higher flow rate and provides better electrical insulation.

In this work, the electrostatic charge injection method is considered to be a part of a different type of charge injection atomizer. In the traditional atomizers, the charge injection process and the atomization process are inextricably linked, due to the manner in which the charge injection site is positioned directly above the atomizer orifice. In the proposed system, the charge injection system is separated from the

liquid atomization process. With the help of this design, the charge injection system could be retrofitted to a range of existing atomization systems to obtain different spray plume patterns, for instance flat or hollow cone. Flexibility in the spray pattern is of importance in several industrial processes such as coating, cooling and lubrication, all of which are potential domains for electrostatic atomization applications.

The main challenge of segregated charge injection system design is to carry a major portion of the injected charge to the separated nozzle site by minimizing the charge density losses through the grounded atomizer body and the flow channel wall of the fuel delivering device. In order to overcome this challenge, a synthesis of design and experimental analysis was deployed in order to investigate the effect of geometrical parameters of the segregated system and operating flow conditions on the spray specific charge. Moreover, research was undertaken to determine the possible causes of charge loss in the segregated system. The findings from the aforementioned studies were complemented with visual observations of the spray plume as a function of the specific charge contained in the fuel.

5.2 **Design**

Initially, the charged liquid from the atomizer was carried by nylon tubing to a segregated, commercially available nozzle manufactured by Spraying Systems Co. The separated nozzle chosen for the initial testing, TXVS-1, is a wide angle hollow cone pattern nozzle that consists of an orifice diameter of 500 μm in a poly-propylene body. This nozzle ensures stable operation at a maximum hydrodynamic pressure of 20 bar with the help of a rubber gasket present at the female-male contact point. The

testing pressures were significantly less than 20 bar due to the limitations of the additional parts that were machined on the atomizer in order to facilitate charged liquid transfer. Figure 5.1 shows the TXVS-1 nozzle with the rubber "quick connect" adaptor which makes it easy to switch to another nozzle if a different spray pattern is required while ensuring proper alignment.

A supplementary adaptor made of Delrin® was designed and then manufactured to serve as an intermediate piece to facilitate the transfer of the charged liquid to the extended nylon tubing and later to the separated nozzle. At the design stage of the Delrin® add-on piece, an adaptor having a larger passage than the atomizer orifice diameter was proposed. The dimensions of this part were determined to have the desired flow rate and velocity throughout the entire flow passage within a reasonable pressure drop. Preliminary adaptor design is shown in Figure 5.2.

Delrin®, also known as polyacetal, is used in parts that require high stiffness, low friction and excellent electrical properties [81]. This adaptor piece was attached under the atomizer orifice disk and mounted to the nozzle assembly using a stainless steel ring. This ring prevented the orifice disk from buckling and retained proper alignment with the atomizer.

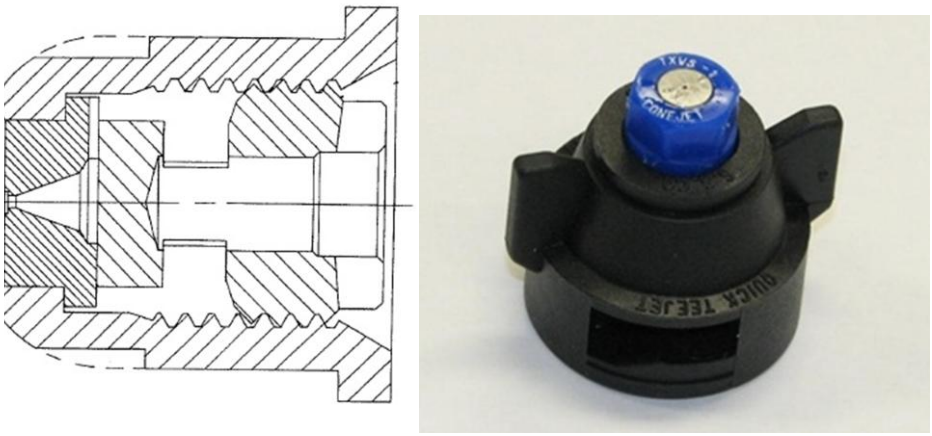

Figure 5.1 TXVS-1 nozzle

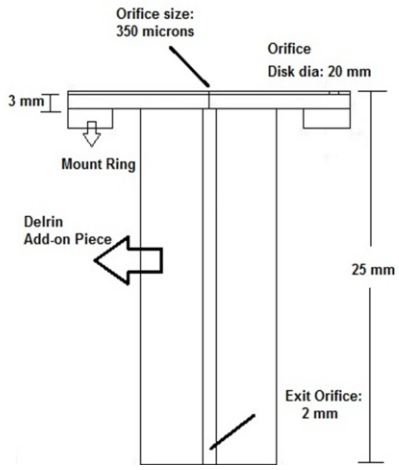

Figure 5.2 Delrin® add-on piece

5.3 Electrical Performance

5.3.1 Testing conditions

Experiments were initially conducted in three different configurations as shown in Table 5.1 using the blunt charging electrode and an add-on piece having a flow channel diameter larger than the atomizer orifice size as illustrated on Figure 5.2. These cases were chosen to make a comparison with the previous studies of direct atomization (case 1) and to analyze the causes of any possible charge losses while

transferring the charged liquid. The first case is the baseline configuration of pure spray without the nylon tubing and the separated nozzle. This configuration was extensively used with smaller orifice disks and was shown to be working for both Diesel fuel and highly viscous organic oils [82]. In the second case, the brass orifice plate is attached to the Delrin® add-on adaptor piece. The current measurements were taken at the exit of this add-on piece as shown in Figure 5.3(a). The third case is the complete setup with the connector tubing and the TXVS-1 separated nozzle. A drawing of the complete segregated atomizer system is shown in Figure 5.4.

CASE		d (µm)	V (m/s)	Q (ml/min)
1	Spray	343	10	55
2	Delrin® adaptor			
3	Separated spray			

Table 5.1 Initial testing conditions

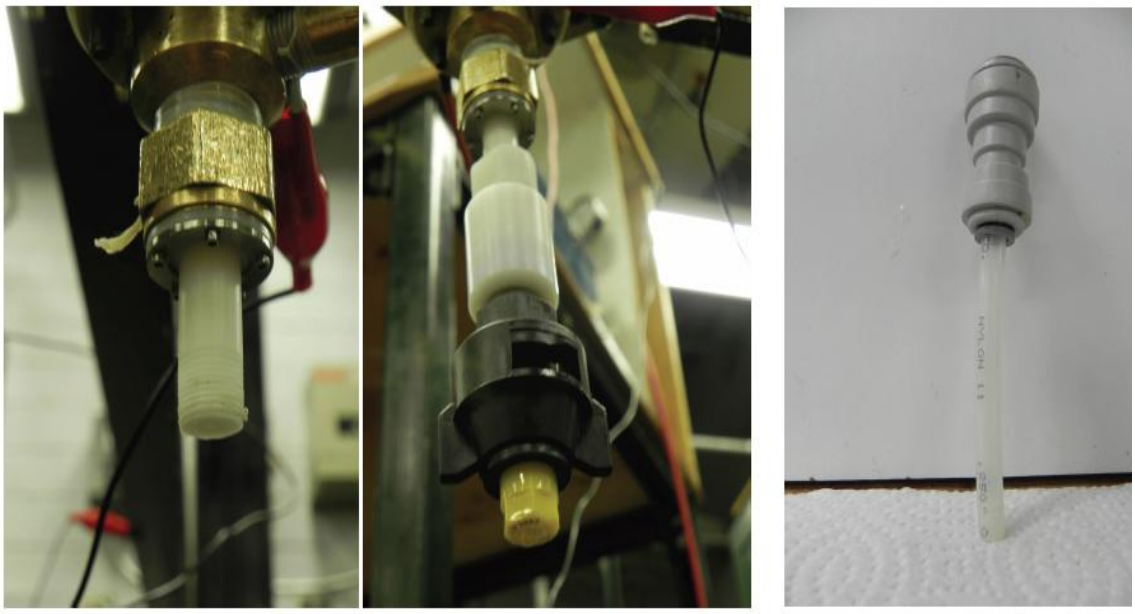

Figure 5.3 Different configurations of separated charge injection (a) case 1 (b) Delrin® adaptor and separated nozzle (c) tubing used

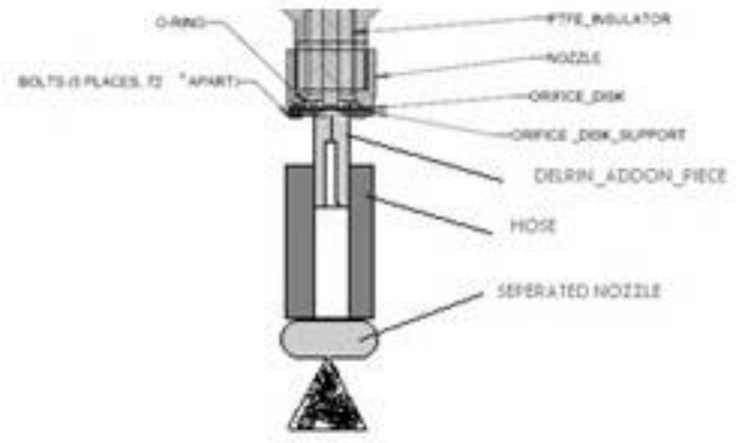

Figure 5.4 The electrostatic atomizer modified for segregated charging

The initial step undertaken in this study was to measure the spray current carried outside the atomizer with the liquid jet stream exiting the orifice as shown in Figure 5.5. The spray charge contained within the working fluid was measured from a stainless steel collector located about 20 cm away from the segregated nozzle tip. Specific charge was measured for each case using the corresponding flow rate. The specific charge curves as a function of the applied voltage for all three cases are shown in Figure 5.6. As expected, some minor charge losses were observed during the transfer of the charged liquid to the separated nozzle. A maximum specific charge (q) of about 0.4 C/m^3 was noted with the baseline pure spray configuration. With the addition of the adaptor and separated nozzle, a decrease in the specific charge level down to q=0.32 C/m^3 was measured. The possible causes of this charge loss will be analyzed in detail in the following pages.

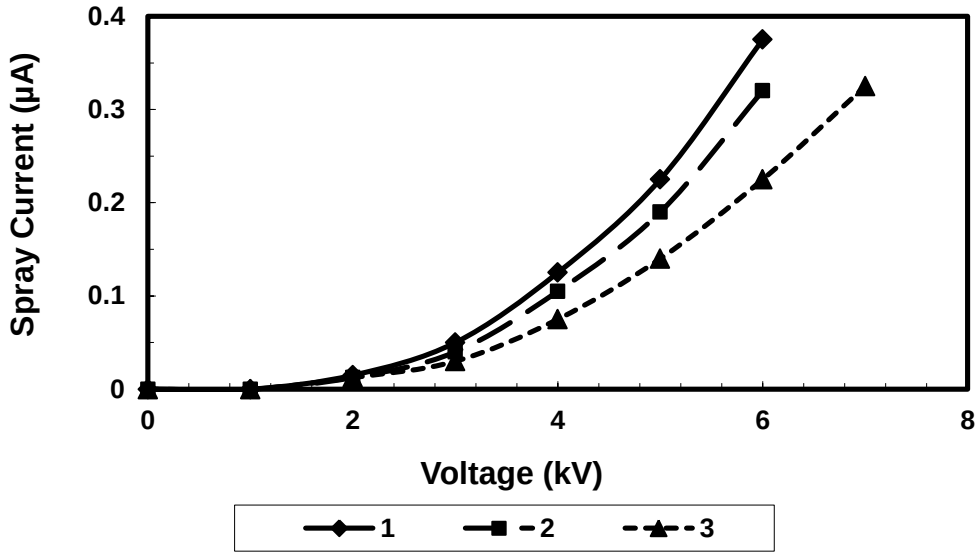

Figure 5.5 Comparison of the spray current with respect to the applied voltage for the three cases (1) pure spray (2) with Delrin® adaptor (3) separated spray

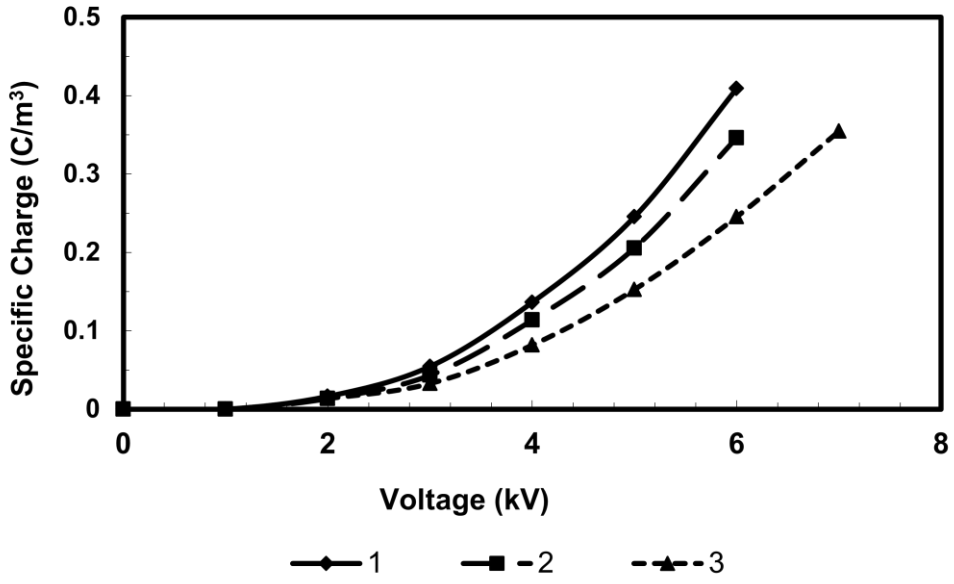

Figure 5.6 Comparison of the specific charge with respect to the applied voltage for the three cases (1) pure spray (2) with Delrin® adaptor (3) separated spray

5.3.2 **Effect of L/d on spray current**

After confirmation of the efficient use of the separated electrostatic atomizer in this adaptor configuration, further experiments were conducted with this atomizer configuration to observe the effect of blunt electrode positioning with respect to the orifice size, L/d ratio. For these experiments, an orifice size of 500 μm was used at L/d ratios of 0.5 and 3.0. The spray current values were measured as the spray formed with the segregated nozzle tip. As in agreement with the findings of the blade type charge injector study, a closer electrode gap helps to obtain spray at a relatively lower applied voltage whereas a larger gap brings extra operating stability to the system. As seen from Figure 5.7, the increase in the electrode gap resulted in an increase of the threshold voltage (V_{th}) from 2kV to 6kV. Higher amount of voltage was needed to overcome the electrical barrier as the electrodes set further away from each other. The maximum amount of charge contained in the resulting spray did not vary noticeably with the alteration of the electrode position. However, the atomizer performed more stably over a wider range of operating voltages. The effect of the injection velocity on the spray current was also studied by performing another set of runs at u=15 m/s. It was found that higher injection velocity not only resulted in carrying out higher amount of spray charge but also a small increase in the maximum operating voltage.

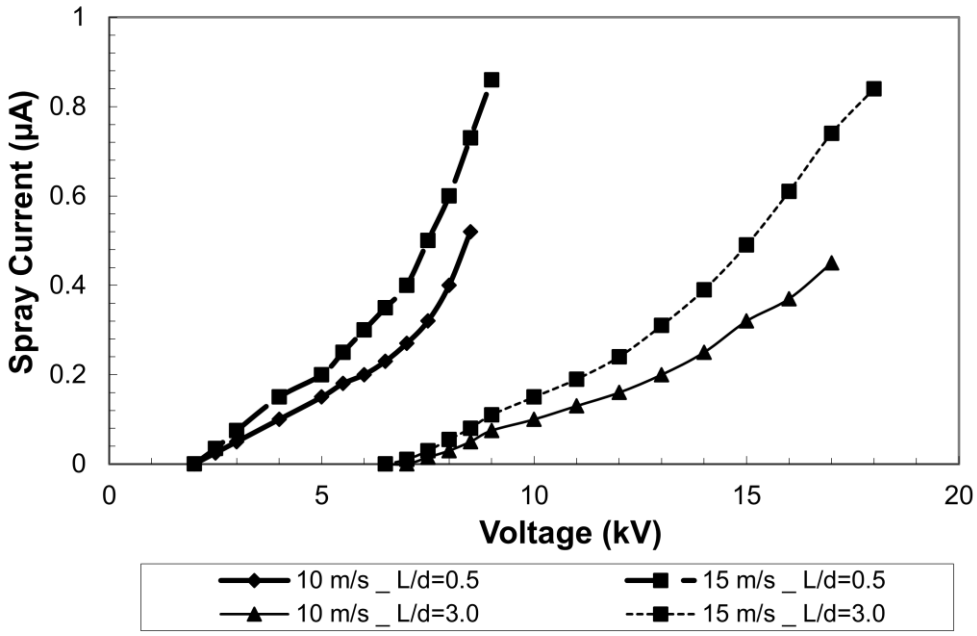

Figure 5.7 Spray current measurements at the segregated nozzle tip at d=500 μm at two different L/d ratios of 0.5 and 3.0

5.3.3 **Causes of charge losses within the atomizer**

As noted from the initial runs, some minor charge losses were observed during the transfer of the charged liquid to the segregated nozzle site. One of the reasons for the charge loss is the increase in the flow resistance inside the atomizer with the addition of the second orifice. The discharge coefficient of an atomizer is governed majorly by the pressure losses inside the nozzle flow passages but mostly by the flow through the final discharge orifice. Addition of the extra parts to the system increased the orifice channel length (x) of the discharge orifice while keeping the orifice diameter (d) constant. As x/d ratio increased, the discharge coefficient dropped noticeably in agreement with the literature [83-84]. In order to match the flow rates with previous cases, pressure of the system was raised. The changes in the

aforementioned flow parameters increase the disturbances inside the system and as a result, decrease the electrical efficiency of the atomizer.

A timescale analysis indicates that another major cause of the charge loss is inside the hose that carries the charged Diesel fuel from the charge injector orifice to the separated spray nozzle. The Ohmic charge relaxation timescale (τ_{oc}) across the hose wall is compared to the flow timescale (τ_m) through the hose. The Ohmic-charge relaxation timescale (τ_{oc}) that characterizes the time elapsed for electric charge contained within the working fluid to be neutralized by opposite or neutral polarity charge carrier by taking the ratio of permittivity (ε) over conductivity (σ).

While comparing these characteristic timescales, one may expect to see three different cases that can be listed as:

1. $\tau_m \gg \tau_{oc}$

2. $\tau_m \approx \tau_{oc}$

3. $\tau_m \ll \tau_{oc}$

In the first case, a significant amount of charge loss is highly expected as the charge has enough time to cross the radial section of the tubing wall and then be polarized on air due to electrical friction i.e. air neutralization that will be discussed further. In the second case, there is still some minor charge loss expected comparatively less than the charge loss expected at the first case. In both cases, one can improve efficiency by minimizing the loss with increased tube wall thickness or by changing the tubing material to a more electrically resistive compound. Finally, in the third case, if the Ohmic relaxation time is measured to be much larger than the mechanical flow time, the order of the loss is expected to be minimal. Flow timescales for different tubing sizes and flow velocities are tabulated in Table 5.2.

Tubing ID (mm)	Flow velocity (mm/s)	τ_m (s)
4.8	56.1	1.8
6.4	31.6	3.2
9.5	14.0	7.2

Table 5.2 Flow timescales for different tubing sizes of 10 cm in length at Q=1 mL/s

For rubber, τ_{oc} is calculated to be 0.2 s, which is significantly less than the tube length to average flow velocity ratio, τ_m=7 s. This indicates a possible loss of charge as the charge has enough time to cross the radial section of the hose wall and then be polarized in air due to electrical friction. Polyurethane (τ_{oc}=265 s) and PTFE (τ_{oc}=1860 s) are known to have excellent electrical resistivity properties; however, these materials have a very poor flexibility that does not satisfy the goal of creating a mobile atomizer. Ohmic charge relaxation timescales and some related electrical properties of the tubing materials used in this study are tabulated in Table 5.3.

Material	Electrical Resistivity [Ωm]	Dielectric Constant	τ_{oc} [s]
Rubber	10^{10}	2.5	0.2
Nylon	10^{12}	3.0	37
Polyurethane	10^{13}	3.3	295
Teflon	10^{14}	2.1	1860
FEP	10^{16}	2.1	186,000

Table 5.3 Ohmic charge relaxation timescales for different tubing materials

Another critical location where charge losses might occur is the contact point of the brass atomizer orifice disk to the adaptor piece due to the lack of isolation of

the charged fuel from the grounded atomizer body. As mentioned earlier, preliminary studies had an adaptor piece with a larger orifice channel diameter than the atomizer orifice disk. While operating at low injection velocities (<5 m/s) using this configuration, the charged liquid has more time being exposed to the atomizer body and probably loses some of the contained charge to the ground.

In order to observe any possible charge losses at the contact point, a different adaptor was designed and then manufactured where the flow channel diameter was equal to the atomizer orifice diameter and kept constant all the way to the separated nozzle. With this design, it was hard to align the adaptor piece with the atomizer orifice. For this reason, stainless steel wires were used to ensure the proper alignment. Moreover, machining this design was significantly harder as drilling a precise channel at such small diameters on a plastic based material was a big challenge. Another concern was the long orifice passage making the system more susceptible to clogging and the atomizer required significantly higher operating pressure to achieve the desired injection velocity range. However, it was initially estimated that the charge losses at the atomizer-adaptor contact point would be minimized with this design as the charged liquid would no longer be in touch with the grounded atomizer body during the transportation process to the segregated nozzle.

Tubing made of fluorinated ethylene propylene (FEP) was ordered with an inner diameter of 500 μm to match the diameter of the atomizer orifice. FEP differs from the PTFE in that it can achieve small inner diameters with precision. FEP shares PTFE's useful properties of great electrical resistivity as seen in Table 5.3, low friction and non-reactivity with Diesel fuel, but also is more easily formable, softer and highly transparent [85]. FEP could not be glued to Delrin® surface strong enough

to seal at the operating pressure ranges. For this reason, same adaptor design was machined from nylon. The outer surface of the FEP tubing was roughened using a fine sandpaper to increase the grip on the inner wall of the adaptor. The preliminary testing with this adaptor resulted in very low injection velocities (< 2 m/s). Therefore, the tubing was replaced with larger tubing having an inner diameter of 2 mm to get closer to desirable velocity range.

All injection velocities were measured at the atomizer orifice. As expected, velocities drop inside the tubing due to the larger inner diameter. Therefore, the operating injection velocity ranges are lower with this supplementary piece due to the higher pressure drop with the increase in the length of the orifice channel. Velocity variation as a function of the system hydrodynamic pressure with the new adaptor-tubing design is shown in Figure 5.8.

Several measurements were conducted using the needle type electrode instead of a blunt electrode to lower the pressure drop inside the atomizer. Initially, runs were conducted without the tubing at the range of 2 m/s to 7 m/s to observe the effectiveness of the adaptor piece as a function of the injection velocity, lower in magnitude compared to the initial setup.

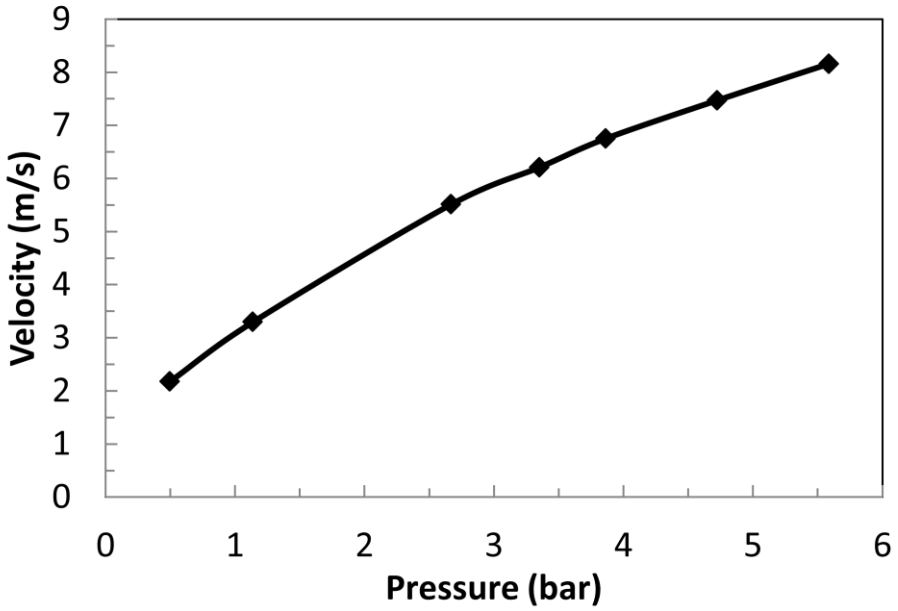

Figure 5.8 Velocity variation as a function of hydrodynamic pressure

The I-V characteristics, without the tubing, are shown in Figure 5.9. As seen from Figure 5.9, leakage current was significantly more than the spray current for the lower injection velocity of 2 m/s at $V > 11$ kV, yielding an inefficient operation of the atomizer. On the other side, for 7 m/s injection velocity case, larger amount of spray currents were noted as desired. At around u=3.5 m/s, leakage and spray currents became comparable to each other in terms of the magnitude as the applied voltage was raised. From these findings, it can be concluded that at higher injection velocities, higher amount of charge could be carried out with the fuel jet before it leaks to the ground from the atomizer body. In order to have a better observation of the charging efficiency, the ratio of the spray charge compared to the leakage current is also shown in Figure 5.9 for the three injection velocities as a function of the applied voltage. The ratio was decreasing with the decrease in injection velocity. A further decrease was noted with the increase in the applied voltage for all three cases. As the voltage was

raised, smaller droplets located away from the spray axis were attracted to the atomizer body and lost their charge by grounding. This resulted in electrically less efficient operation of the atomizer.

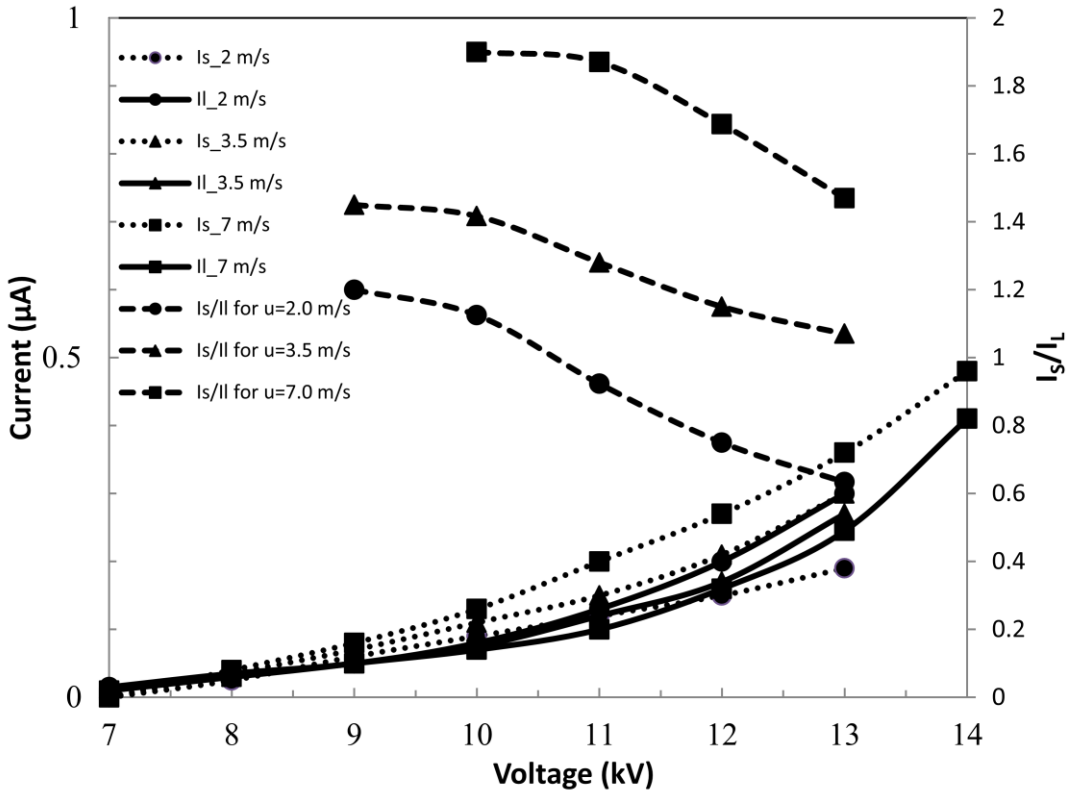

Figure 5.9 I-V Characteristics with no tubing

Next set of runs were conducted with the tubing glued to the inner wall of the adaptor piece. The tubing extended about 3 cm from the tip of the nylon adapter piece. Figure 5.10 illustrates a comparison of the spray and leakage current of the tubing and no-tubing configuration at the atomizer orifice average injection velocity of 7 m/s. As seen from the Figure 5.10, with the addition of the tubing, a decrease was noted in the amount of spray charge while a noticeable increase was observed in the leakage current.

In order to determine the causes of the charge loss in the system with the tubing, total currents were compared between the tube and tubeless system. Total current was computed by adding the leakage current to the spray current. A small decline was observed in the summation of spray and leakage current readings (I_T= 0.85 µA without tubing) with the addition of the tubing to the system (I_T=0.75 µA with tube) at 14 kV. In order to investigate the differences in the total current values, the potential for "Static Discharge" [86] should be considered to increase the knowledge and understanding of this phenomenon. Static Discharge is the neutralization of the excess charge that is built up on a surface to surrounding medium.

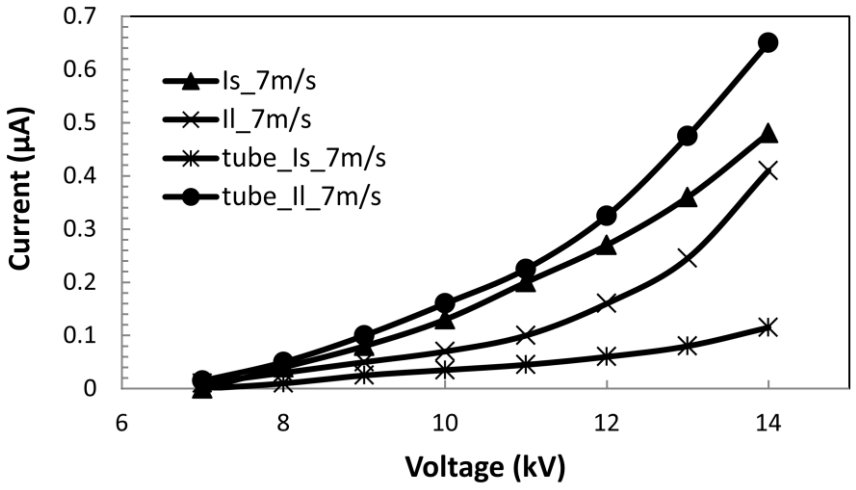

Figure 5.10 I-V characteristics comparison of the *u*=7 m/s cases with and without tubing

5.3.4 **Air neutralization of static charge accumulation**

When different substances are in touch, electrons from one of the materials may transport to the other in several ways depending on the electrical properties. In this study, both media, fuel and tubing are good insulators and the charge transport occurs in a different manner than charge transfer in conductors. Although Diesel fuel flowing in the system is known to be a poor conductor of electricity, there are some non-uniformities present in the fluid due to friction and charging resulting in an electrical instability among electrons and positive ions. As the non-polar Diesel fuel flows through a tubing that is also not a good conductor, nylon or FEP in this case, accumulation of electric charges that are contained in the flowing fuel, is observed on the surface of the tubing innerwall due to viscous wall friction. Static charge accumulation results in an audible clicking sound as the discharge of the electrostatic charge results in sparks which is an indication of hazardous operation occuring within the atomizer system [87].

The amount of static charge accumulation and fluid flow rate are linearly dependent. For this reason, in order to avoid hazards, hydrocarbon fuels are commonly transferred at moderately low flow velocities below 1 m/s in gas station pumps or gas transmission pipelines. However, some electrostatic discharge risk may still be present as a result of several ambient environmental conditions such as temperature, wind and moisture [88]. Generally, these parameters are carefully monitored to observe their effects on fuel phase separation and static charging by means of sensors. For this reason, most commercially available tubing products are altered to enhance their conductivity by adding some amount of carbon to the tubing inner wall during the manufacturing process, which makes it hard to find pure

insulator virgin Teflon tubing. The carbon permits the electrostatic charges to be conducted down the inner wall of the tubing to the conductive end fittings, thereby preventing the static charge accumulation on the tubing inner wall. Military Specification MIL-H-25579E states that hoses used for hydrocarbon fuel transfer should be capable of conducting a static current greater than 6 μA at a potential difference of 1,000 V DC applied between the hose inner wall and the conductive end fitting [89].

The next step was the process analysis of how the static electricity charges are neutralized or grounded. For charge neutralization to occur, the electric charges should be in interaction with opposite polarity charge carriers. With the help of applied electrical field, charges will move towards opposite polarity charge carriers and may be neutralized. Moreover, the neutralization can also be possible by the free air ions, the lifetime of which is in the order of minutes.

Military Standard-3010B-2008 [90] contains information regarding the electrostatic properties of materials including the measurement method of static decay time. This method covers monolayer homogenous materials such as the adaptor and tubing materials used in this study. As a general rule, a homogenous monolayer material with a surface resistivity of approximately 10^{12} Ohms will have a static decay time of 2 seconds. Experiments show that static decay times between 0.6 to 9 seconds are possible for this resistivity range.

In the pure spray case #1, the injection velocity is around 10 m/s with the grounded bucket located about 20 cm away from the atomizer. This yields approximately 0.02 second travel time which is much shorter than the decay time and

therefore, the pure spray case is not affected from air neutralization. However, the flow velocity drops down significantly below 1 m/s inside the add-on piece and the tubing which brings the travel time around 1 second. As a result, the charge collected on the tubing surface has enough time to be neutralized by the free air ions.

5.4 **Spray visualization**

Figure 5.11 shows the spray development at the laboratory light conditions with the adaptor part only. Observing Figure 5.11 from (a) to (c), it is hard to comment on the size of the droplets formed but some general observations can be made. Firstly, as the voltage rises, the spray angle becomes wider as seen in previous studies [91] as a result of the increase in the repulsive Coulomb force. An increase in the spray angle from 0 degree solid stream to 20 degrees is observed with the increase in specific charge present in the liquid. Secondly, the break-up tip length drops with the existence of charge present on the jet as the voltage increases.

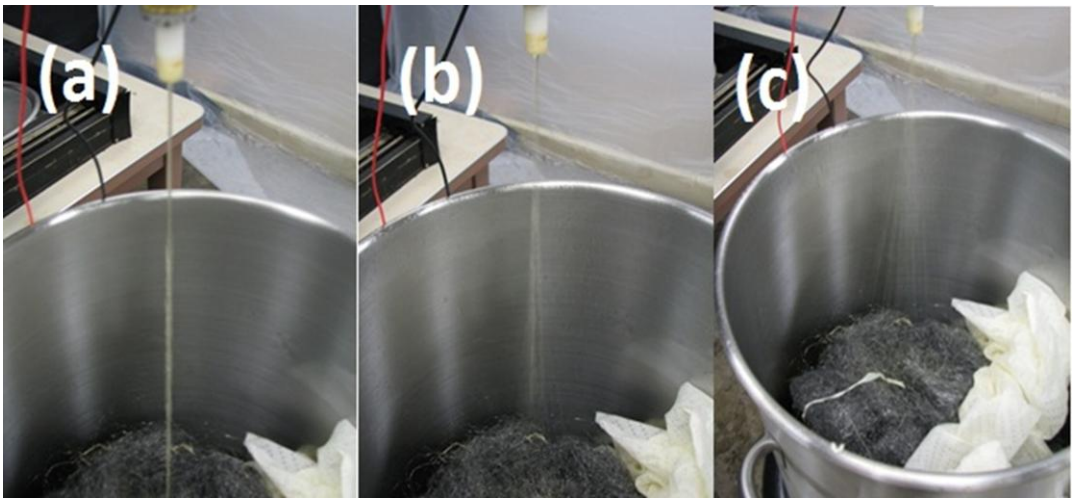

Figure 5.11 Spray patterns at the adaptor outlet (a) q= 0 C/m^3 (b) 0.2 C/m^3 (c) 0.5 C/m^3

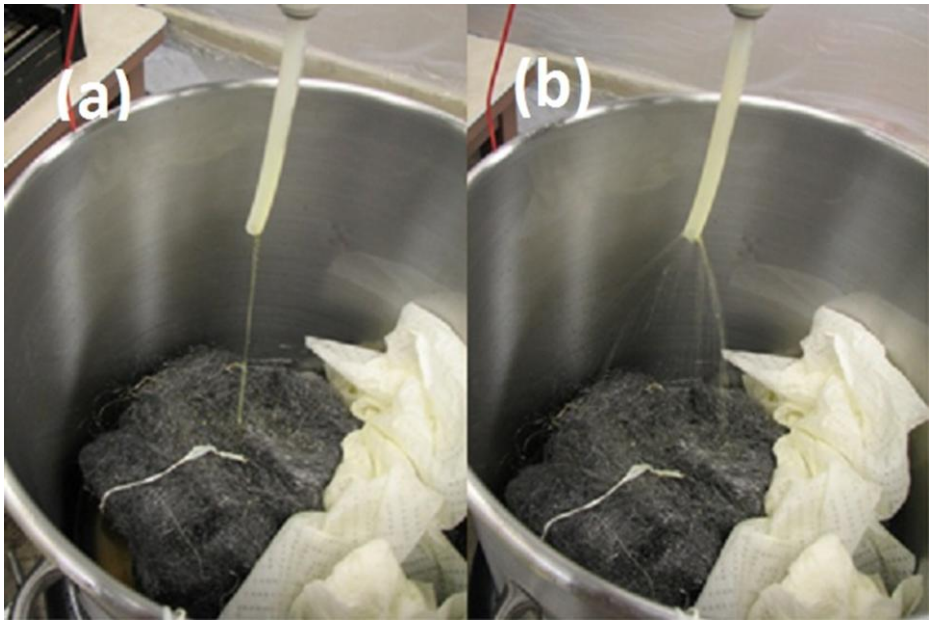

Figure 5.12 Spray patterns with tubing (a) q= 0 C/m^3 (b) 0.3 C/m^3

In the next step, a 10 cm long tubing has been connected to the system and the effect of the tubing on the jet is observed. Figure 5.12(a) shows the uncharged case and Figure 5.12(b) shows the optimum charging case at this configuration. The contribution of the charges contained in the stream on the jet break-up is clearly seen as the jet is moving from solid stream to a hollow cone pattern.

After the visual confirmation of the electrical performance using the adaptor part, an imaging study was performed with the full setup including the separated nozzle as a function of the contained charge in the fuel jet in order to investigate the formation and the development of the spray plume. The development of the spray passes through several stages as the voltage is being applied. These commonly observed stages can be listed such as: solid stream, distorted cylindrical stream, fine atomization and collapsation. These stages are presented in Figure 5.13.

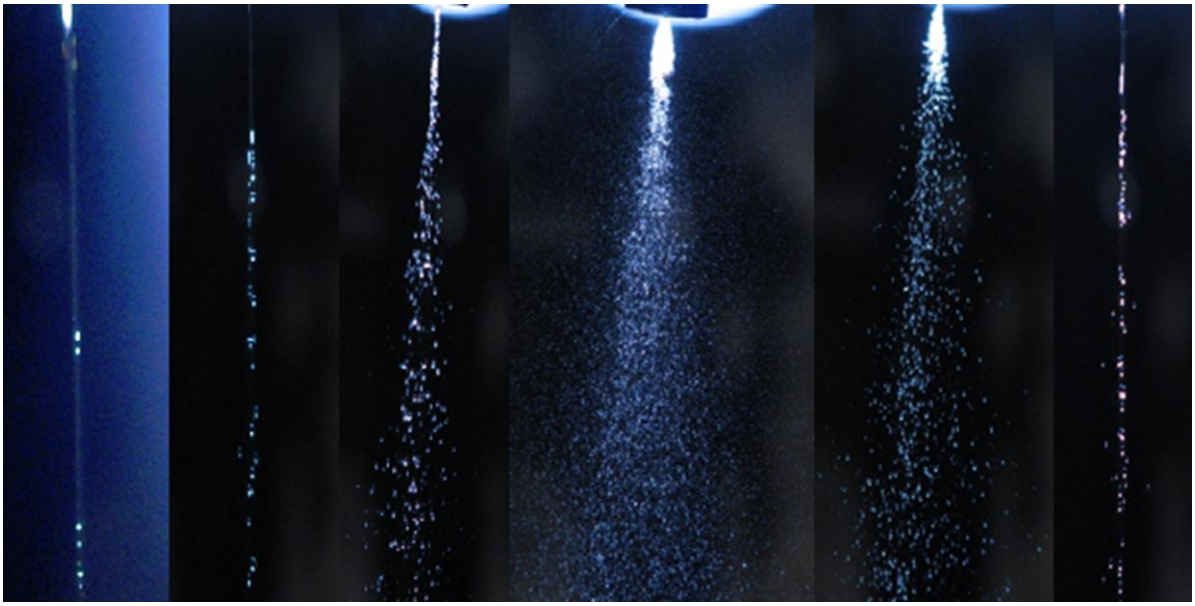

Figure 5.13 Stages of spray development with increasing voltage (a) 0 kV (b) 2 kV (c) 3 kV (d) 6 kV (e) 7 kV (f) 0 kV (right after the voltage source was turned off)

Figure 5.13(a) shows the solid stream and dribble stage when there is no applied voltage to the atomizer. It can be concluded that the nozzle cannot form a spray at this flow rate hydrodynamically. Stream is getting narrower as it moves along the tip due to surface tension effects. At a relatively further distance, dribbling is observed. Figure 5.13(b) above shows the initiation of the breakup at 2 kV. The initiation starts at a certain downstream distance called breakup tip length (l). Large droplets are observed at a narrow spray angle. This stage is also known as distorted pencil due to the distorted centerline of the liquid stream. As the applied voltage is raised to 3 kV, the break-up tip length gets noticeably shorter as seen from Figure 5.13(c). The spray angle is noticeably wider with the help of the increase in spray current; however, large drops still exist. Comparatively smaller droplets are observed at the outer edges as the smaller drops are deflected further away from the plume center. Figure 5.13(d) illustrates the fully developed spray at 6 kV. As seen from the figure, spray pattern is significantly wider with finer drops. Although TXVS-1 is

designed as an anti-drift nozzle, some minor circulations are observed at the outer edges of the plume. The major reason of the wakes observed with drops having zero or minus axial velocity, is that the spray could be formed far below the nozzle operating pressure range using electrostatic atomization technique. Therefore, the liquid has less momentum compared to the inevitable disturbances present in the gaseous medium. Also, the charged small drops are attracted to the atomizer body. After a certain magnitude of applied voltage, the atomizer cannot inject more charge into the liquid and the spray starts collapsing. Figure 5.13(e) shows the spray at around 7 kV, where the spray has collapsed. Figure 5.13(f) shows the spray right after turning off the applied voltage. Although the voltage is off, it goes on spraying as there is still charged liquid existing in the supply hose. The existing charge inside the transfer line is still able to form jet dispersion. Afterwards, the solid stream is observed as the whole charged liquid has been sprayed.

6. HIGH PRESSURE DIELECTRIC LIQUID FLOW

6.1 Introduction

The potentially beneficial effects of spray atomization on the combustion of Diesel fuel have long been known. Better atomized fuel will result in less production of soot, which is formed in the fuel-rich regions of the spray. Higher hydrodynamic pressure is being applied in modern injection systems (>1000 bar) to enable lower emission combustion.

The main objective of this study is to show that the electrostatic charge injection technique is a viable method of producing fine sprays at hydrodynamic pressures of up to 40 bar with the 3rd generation charge injection electrostatic atomizer design. Moreover, this chapter seeks to describe jet break-up dynamics, jet break-up length, spray cone angles, effects of externally applied electric fields on charged spray plumes, and general spray characteristics. The effects of orifice diameter d, injection velocity u, spray specific charge q and liquid physical properties on the jet break-up length will be described and discussed. An enhancement in the atomization performance is expected as compared to the previous results [92-93] at lower pressures. In order to analyze the high-pressure effects on spray dispersion, the general spray characteristics are quantitatively described and the break-up mechanisms are evaluated by means of a Malvern Laser Diffraction Spectrometry (LDS) droplet size measurement system, digital camera imaging techniques and electrical measurements. Using the results of these measurements, it is investigated how electric charge improves the aerodynamically driven atomization of the dielectric

liquid jet. A further objective of this work is the observation of the stages of the spray development at increasing electrode voltage.

6.2 **Electrical Performance**

Experiments were performed using 3 different orifice sizes of 100 μm, 200 μm and 250 μm. The range of the operating system pressure at the atomizer inlet was between 7 to 40 bar to maintain the same velocity range for different size orifice disks. The electrode gap ratio (*L/d*) was set at 3 for 100 μm and 200 μm and 2 for 250 μm orifice disks as these gap ratios were observed to be the optimum point to provide a more uniform spray pattern within our high voltage power supply limit. Testing conditions are summarized in Table 6.1.

d (μm)	*Q* (ml/min)	*u* (m/s)	*We*	*Oh*	*Re*	q_{max} (C/m^3)
100	14 24	30 50	3024 8400	0.052	1250 2083	4.9 4.0
200	57 94	30 50	6048 16800	0.037	2500 4167	2.2 2.1
250	88 147	30 50	7560 21000	0.033	3125 5208	1.5 1.3

Table 6.1 Variables and relevant non-dimensional numbers for all experimental cases.

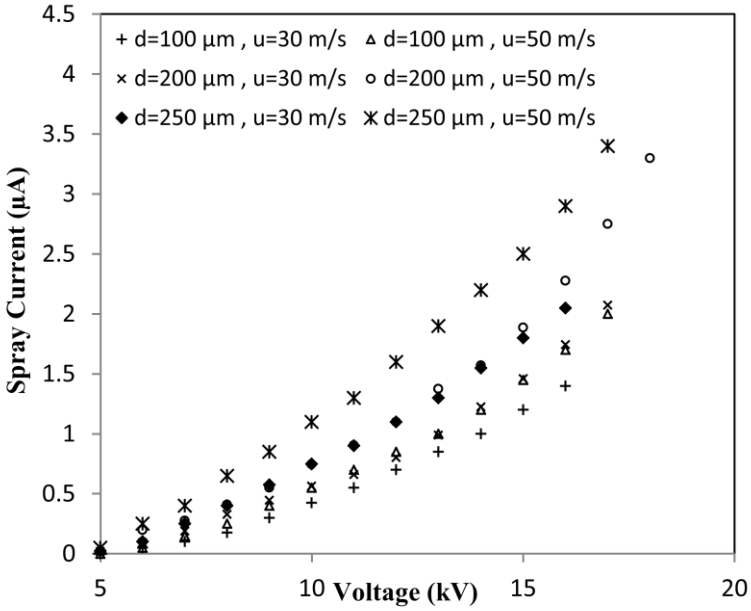

Figure 6.1 Spray current as a function of orifice size (*d*), applied voltage (V) and average axial orifice velocity (*u*).

The variation of I_s as a function of the applied electrode voltage is shown in Figure 6.1 for different testing conditions up to the partial breakdown point where spray current starts to decline as the applied voltage is increased. As seen from Figure 6.1, a greater amount of electric charge could be injected into the liquid at a higher axial orifice velocity, as observed in literature [92]. This may be explained due to higher injection velocity allowing for charge to be carried away from the inter-electrode gap prior to leaking to the ground through the atomizer body. In addition to injection velocity, electrode voltage is an important parameter in the initiation and development of charge injection. Injection of the charge starts around 5 kV at these testing conditions.

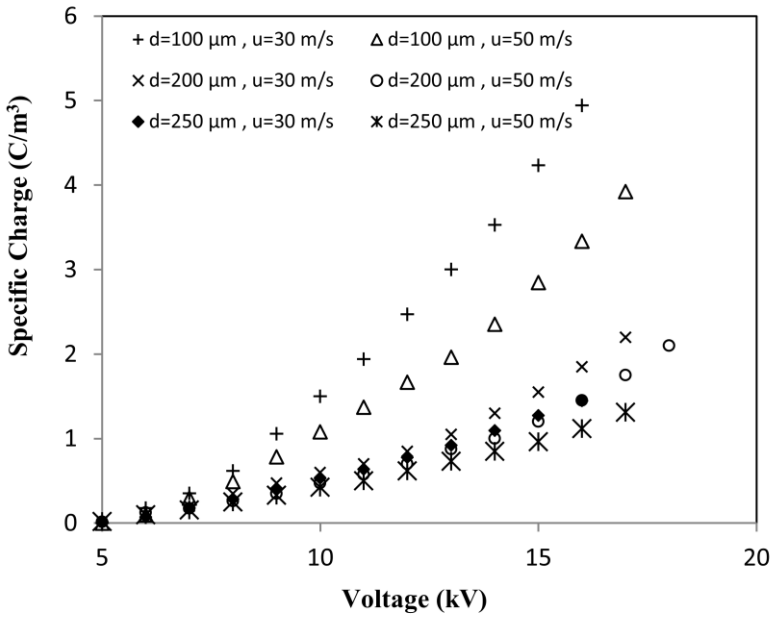

Figure 6.2 Specific charge profiles as a function of orifice size (*d*), applied voltage (*V*) and average axial orifice velocity (*u*).

One of the main challenges in electrostatic atomization is to maximize the spray charge per unit volume to maintain spray quality defined as the uniformity across the spray plume radius. Figure 6.2 shows the corresponding specific charge for various orifice diameters at two testing velocities. A slight decrease in *q* is observed at elevated injection velocities. As seen from Figure 6.2, the maximum level of specific charge with a 100 µm orifice disk equating to 5 C/m^3 is significantly larger than the specific charge obtained in low pressure studies [93], showing the potential of high pressure electrostatic charge injection systems.

6.3 **Spray visualization**

After establishing that the high pressure system can achieve high amounts of spray specific charge (*q*) for a good spray pattern, an imaging study was carried out to identify the stages of atomization. The development of the spray pattern has several

stages as the applied voltage is increased. These stages show similarities with the remote atomization study and can be summarized here as solid stream, distorted stream, deflection of smaller droplets from the core, and fine atomization.

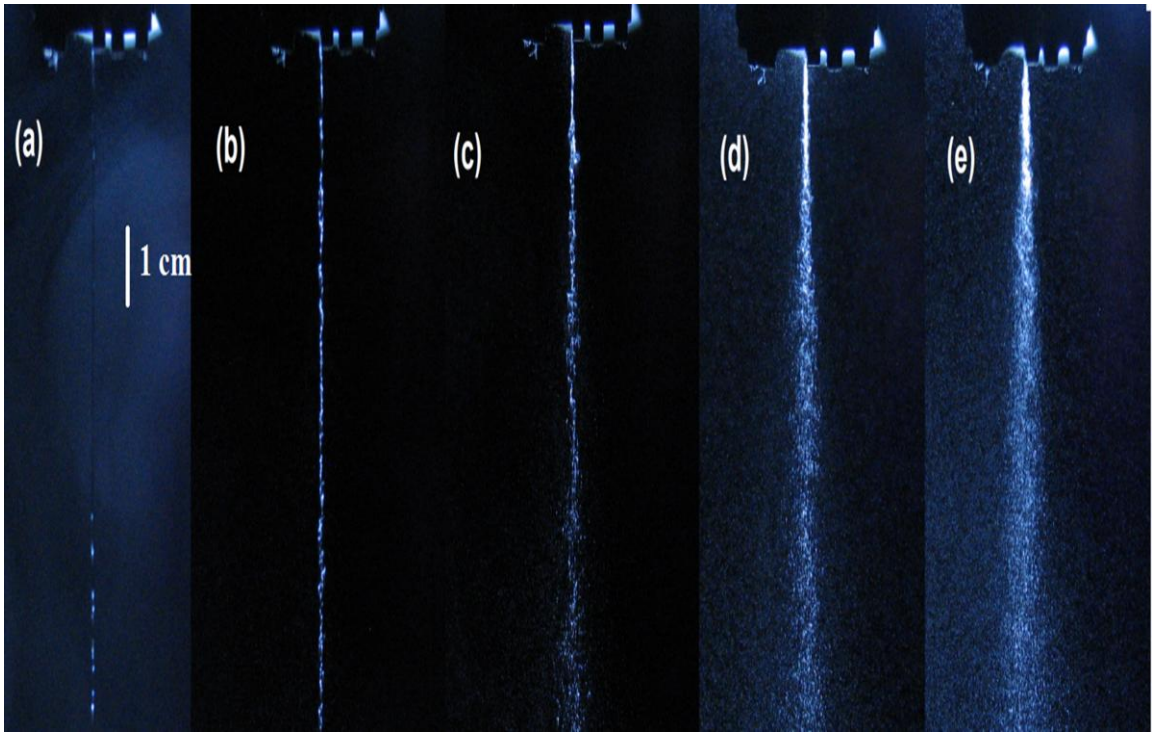

Figure 6.3 Stages of spray with increasing voltage at 250 micron disk and u=30 m/s (a) V=0 kV (b) V=-6 kV, q=0.15 C/m^3 (c) V=-9 kV, q=0.45 C/m^3 (d) V=-12 kV, q=0.8 C/m^3 (e) V=-16 kV, q=1.5 C/m^3

Figure 6.3 shows the spray development with increasing voltage. The solid stream stage is the uniform integrity of the working fluid observed between zero and the threshold voltage as shown in Figure 6.3(a). The stream narrows while moving away from the orifice due to the effects of the surface tension force which causes a fluid to tend to minimize its surface area. At a certain distance from the orifice, the emerging stream of liquid breaks up into droplets. This breakup can be explained with the inevitable small perturbations present. Above the threshold voltage, jet instability

is observed as a distorted cylindrical stream as the jet is pinched into smaller segments with the effective decrease in liquid surface tension. This instability is shown in Figure 6.3(b) and (c). Seemingly, as the specific charge increases proportionally with voltage, finer droplets are formed and deflected away from the core of the spray, as if they repel each other. Smaller droplets carry more specific charge and so they are repelled further from the center. At this stage, a heavier centerline pattern is observed as in Figure 6.3(d). As the applied voltage is increased further the radial droplet size distribution becomes more uniform. Figure 6.3(e) shows the maximum specific charge case at this condition at around -16 kV. This pattern continues until the spray collapses at higher applied voltages.

Figure 6.4 is the spray development of the same orifice disk but at a higher axial orifice velocity. The images are brighter than the lower velocity case due to the higher strobe light intensity perceived by the digital camera. This may be explained by the development of mist around the spray which causes light from the strobe to be deflected into the camera lens, thereby increasing perceived intensity. As seen in Figure 6.4(a), there was no spray at zero voltage, indicative that this test condition was still under the critical velocity, defined as the case where the spray forms hydrodynamically without charge in the spray. At voltages just above the threshold voltage, the distorted stream stage was observed with a noticeably heavier core (Figure 6.4(b) and (c)) as a result of the higher flow rate. When a larger specific charge is reached by further increasing the voltage, lateral electric forces stretch the liquid jet as shown in Figure 6.4(d). The main difference with the aforementioned case (Figure 6.3(d)) is the noticeably wider angle of the spray resulting from the increase in flow rate. Figure 6.4(e) shows the condition of the widest spray angle

achieved at the maximum specific charge level when applied voltage was approximately -17 kV. In this regime, the atomized spray appears to be almost perfectly mixing with the surrounding air as it moves a short distance from the orifice, resulting in a fairly uniform spray pattern.

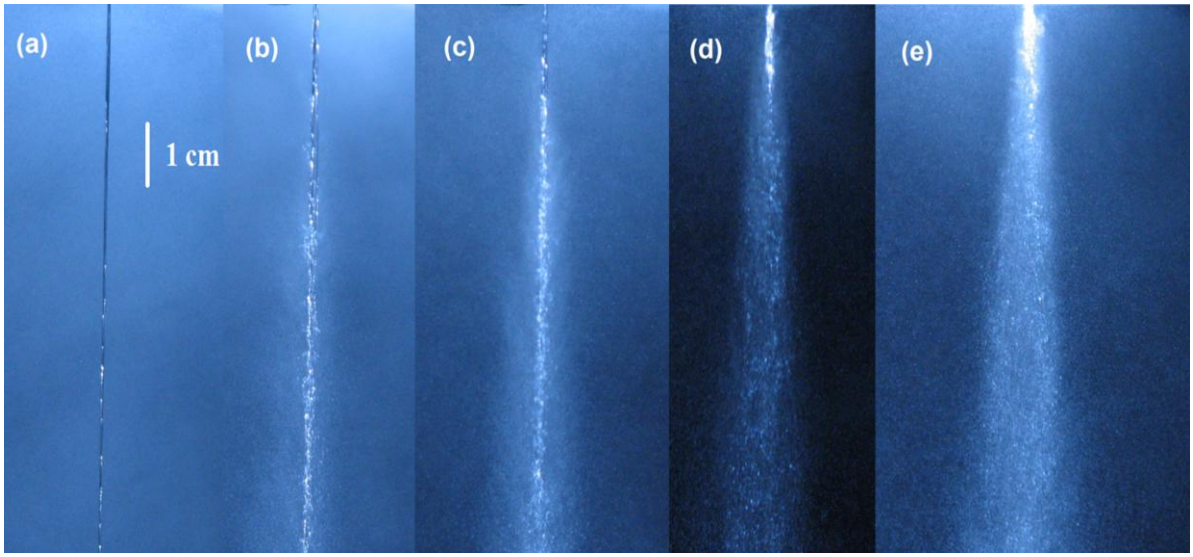

Figure 6.4 Stages of spray with increasing voltage at 250 micron disk and u=50 m/s, (a) V=0 kV (b) V=-6 kV, q=0.1 C/m^3 (c) V=-9 kV, q=0.35 C/m^3 (d) V=-13 kV, q=0.75 C/m^3 (e) V=-17 kV, q=1.3 C/m^3

It is clear that jet breakup and dispersion are strongly affected by specific charge (q) and to some extent, by injection velocity (u). These relations may be discussed in terms of a length and time-scale analysis comparing the space-charge relaxation timescale to the breakup timescale. As described earlier, space-charge relaxation time scale represents the time elapsed from when a charge travels from the center of the jet to the surface of the jet. In order to observe the effect of the electrostatic charging technique on the jet dispersion, the charge should have travelled to the boundary before the breakup occurs. For a case where hydrodynamic effects are negligible, both timescales should be equal or very close in magnitude. If the breakup timescale is significantly less, it will be in agreement with the experimental findings

that the hydrodynamic effects have a significant contribution in jet dispersion.

A typical value of ionic mobility of Diesel fuel can be computed as $1.3x10^{-8} m^2 / V.s$ according to the Walden's rule for highly insulating liquids ($\kappa\mu$ is constant for hydrocarbon fuels). Using the values of L/d = 2.0 with 250 μm orifice size and average jet velocity of u = 30 m/s, τ_{sc} is calculated to be 1.1 ms. From the imaging study, a breakup length of approximately 8 mm is seen which yields a breakup time (τ_l) of 0.25 ms. As the applied pressure is raised until an average jet velocity of u = 50 m/s is reached, the τ_l drops down to 0.1 ms whereas τ_{sc} stays close to the previous value, 1.2 ms. The increase in the ratio between these two timescales (τ_{sc} / τ_l) from 4.4 to 12 indicates the increase in hydrodynamic effects leading the jet to breakup at a shorter downstream distance from the orifice tip.

6.4 **Drop size measurements**

Volume median diameter (VMD) comparison for different testing conditions obtained via LDS droplet size analysis is presented in Figure 6.5. Note that the measurements could not be conducted at very low specific charge levels (q<0.3 C/m^3) due to the drop size analyzer's range limit of the corresponding receiver lens. In addition, multi scattering issues are commonly observed with LDS for very dense sprays. Furthermore, no fluid breakup was observed at zero applied voltage as shown in the imaging section. Measurements were conducted at a spray distance of 15 cm (x=15 cm) downstream from the orifice. All data presented were measured at sustainable, stable operating conditions.

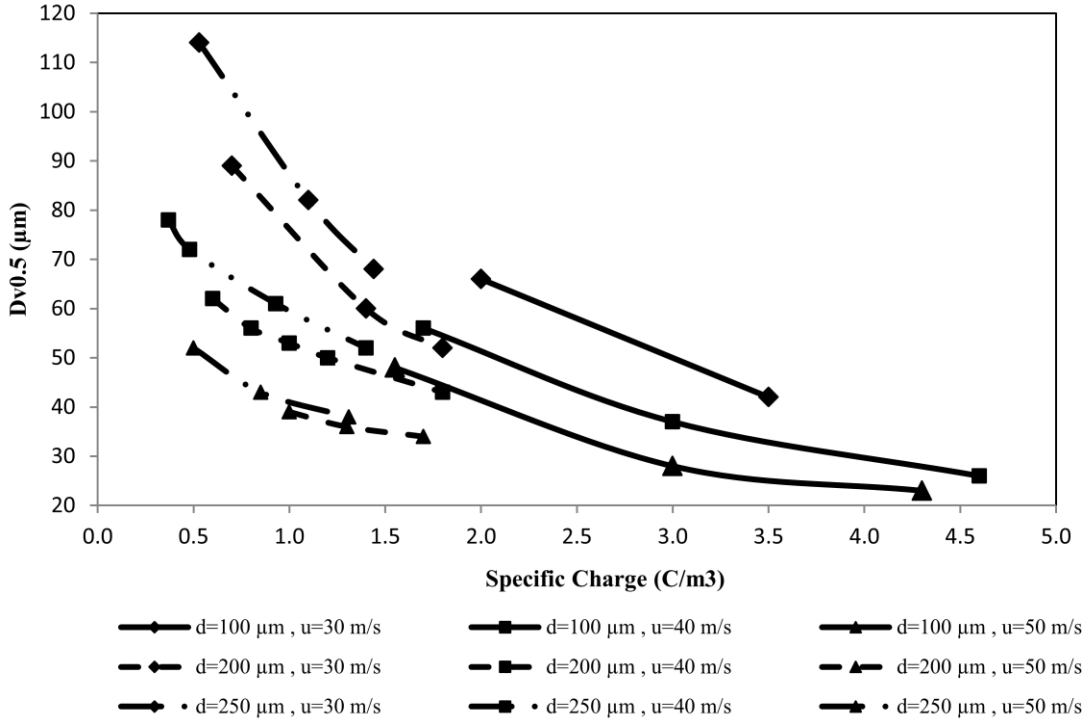

Figure 6.5 VMD Profiles as a function of orifice size (*d*), specific charge (*q*) and average axial orifice velocity (*u*).

Major factors in the fuel spray dispersion are known to be aerodynamic forces and disruptive electric forces [94]. From Figure 6.5, VMD decreases with the increase of specific charge for all cases. Spray dispersion, the spreading of the dielectric liquid, increases proportionally to electric potential applied especially at the low specific charge levels and hence drop size reduces in agreement with the images of the previous section. For large values of *q*, the dependence of specific charge on dispersion is observed to be minor. It may be expected that the higher injected amount of fuel tends to increase the fuel-rich heavy spray core region. In contrast, in this study, smaller VMD values can be achieved with the same orifice size at higher Reynolds number with the help of the hydrodynamic pressure effects. Therefore, it can be concluded that the combination of both higher aerodynamic and electric forces improves atomization and spray performance at higher flow rates.

For the smallest orifice size tested, d=100 µm, the value of the VMD was slightly smaller than the orifice diameter measured (D=0.70d) at the lowest testing pressure and the lowest measured specific charge setting. For this configuration, the VMD value decreased down to approximately one half of the orifice diameter as the specific charge was raised until a uniform radial spray plume was formed. For larger orifice sizes, the largest VMD values that could be measured within the acceptable obscuration rates were approximately 90-120 µm (~0.4d-0.5d). A wider spray pattern was observed indicating greater dispersion of smaller drops. Increasing the injection velocity further led to lower VMD values of 0.22d for 100 µm and 0.16d for larger orifice disks.

The spray pattern radius is smaller and thus less dispersed than lower pressure cases that offer significantly wider angles; however, high hydrodynamic pressure technology allows for fairly small droplet diameters over a smaller area at a higher flow rate.

Larger orifice diameters lead to larger droplets for the same system pressure in pure hydraulic nozzles that are not electrostatically assisted. However, in electrostatic atomizers, atomization rate at the corresponding specific charge level becomes the major factor in drop size profiles at constant system pressure. In the tested electrostatic atomizer, the 250 µm orifice disk produced a fully developed spray in the range of ~1.5 C/m^3 with VMD of 65 µm at the lowest pressure setting. At these q levels, for the d=100 µm orifice diameter, irregular large drops were still observed to persist in the spray central core region. These large drops skew the VMD and $D_{v0.9}$ volumetric curves towards the larger drop size range, as large drops contain a proportion of the spray volume that is substantially higher than the numerical

percentage of these droplets.

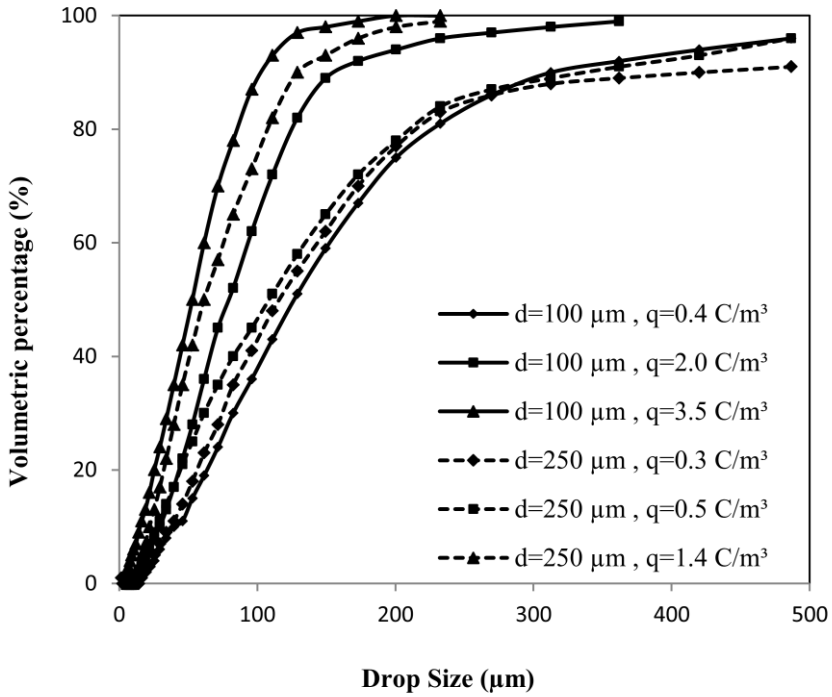

Figure 6.6 Volumetric percentages as a function of specific charge (q) for d=100 µm and d=250 µm at u=30 m/s

Figure 6.6 illustrates the shift in the volumetric percentage distribution curves versus the droplet size for 100 µm and 250 µm orifices at the lowest testing pressure setting corresponding to an average axial nozzle tip velocity of u=30 m/s. The increase in specific charge results in hundreds of microns shift in $D_{v0.9}$ whereas the change in $D_{v0.1}$ is negligibly small comparatively. Therefore, it can be concluded that primary breakup of larger drops into several small drops occurs significantly more often than the secondary breakup of small drops into further smaller droplets. Note that some drops for low specific charge cases were beyond the drop size measuring

range limit (1.2 µm < D < 530 µm) of the analyzer lens setup as seen from Figure 6.6.

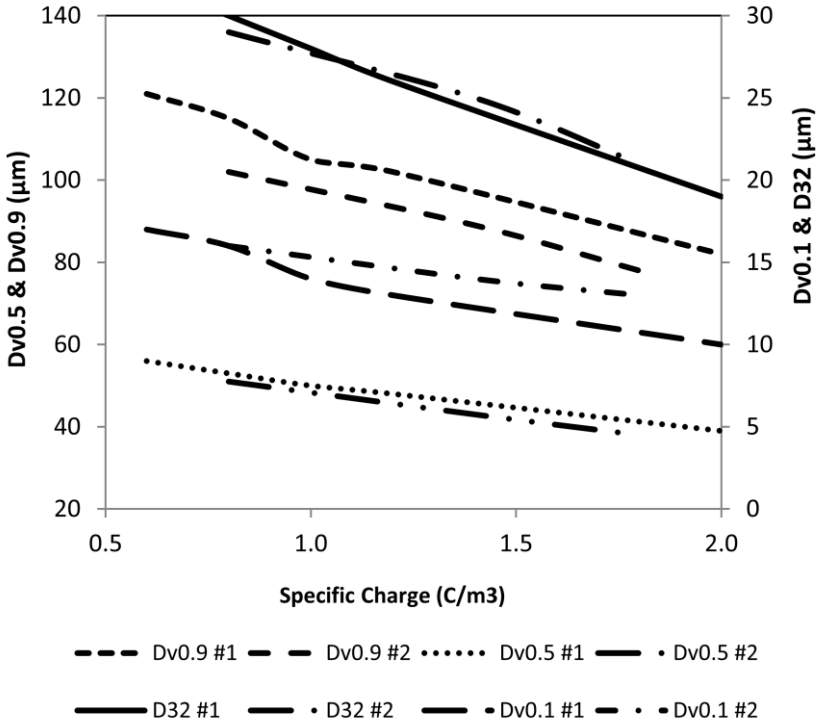

Figure 6.7 Drop size distribution data as a function of specific charge (q) for d=200 µm, u=40 m/s at x= 15 cm (case #1) and x=25 cm (case #2)

Figure 6.7 shows the drop size distribution at two different downstream positions from the nozzle tip using d=200 µm orifice disk at u=40 m/s. As seen from Figure 6.7, there is a small variation between drop size profile curves moving from x=15 cm to x=25 cm downstream. This can be explained with the decrease in breakup tip length and as a result, a uniform spray pattern is already formed at the measured downstream positions. The decrease in $D_{v0.9}$ curves further downstream indicates the decrease in maximum drop size with more air entrainment to the fuel spray. In contrast, the $D_{v0.1}$ curve shows a slight increase which can be a result of evaporation while moving downstream. In addition, smaller droplets that have small momentum

can easily drift away from the measurement volume because of the turbulence created inside the charge collector cage. The VMD and SMD curves show minimal variation which implies an identical combustion performance for both cases.

6.5 Critical velocity conditions

6.5.1 Testing conditions

In this section, high pressure assisted electrostatic atomization technique is further investigated by analyzing the effect of critical jet velocity defined as the injection velocity at which pure hydrodynamic atomization starts to occur without any electrostatic voltage applied to the atomizer. To achieve this end, smaller orifice size of d=75 μm was used to achieve the critical velocity condition at a lower hydrodynamic pressure. As explained in the experimental setup section, the atomizer could handle up to 40 bar with this configuration and the other orifice sizes used in this study (d>125 μm) could not spray hydrodynamically at this pressure.

The aim of this step is to investigate the effect of electrostatic atomization method at conditions where the hydrodynamic force dominates the electrical force. It will be crucial to see if electrostatic atomization method is still a viable method at conditions where the atomization already occurs hydrodynamically.

Two major challenges were faced with the decrease in the orifice size. One of the issues was the clogging of the orifice with the increase in the injection velocity. This problem was solved with the installation of 2 μm swage lock filters just before the atomizer inlet. This increased the system resistance significantly; however, critical velocity conditions were still achievable under operating conditions. Second

challenge was to maintain the alignment of the injector electrode to the orifice. In order to solve this issue, a series of reinforcements were done inside the atomizer to minimize the deflection of the injector needle at high pressure and electrode gap ratio, L/d, was set to a lower value of 1.

The variation of spray current as a function of the applied electrode voltage is shown in Figure 6.8 for 75 μm orifice disk. As seen from Figure 6.8, a higher amount of electric charge could be injected into the liquid at the higher axial orifice velocity of 25 m/s compared to the 15 m/s case as in agreement with previous studies. Higher injection velocity was allowing higher amount of electric charge to be carried away from the inter-electrode gap prior to leaking to the ground through the atomizer body. A maximum spray current of 0.35 μA was obtained for u=15 m/s, and for u=25m/s maximum measured current contained in the spray was around 0.65 μA. Electrode voltage is an important parameter in the initiation and development of charge injection. Injection of the charge starts earlier at these conditions around 3 kV due to the lower inter-electrode gap ratio (L/d) of 1.

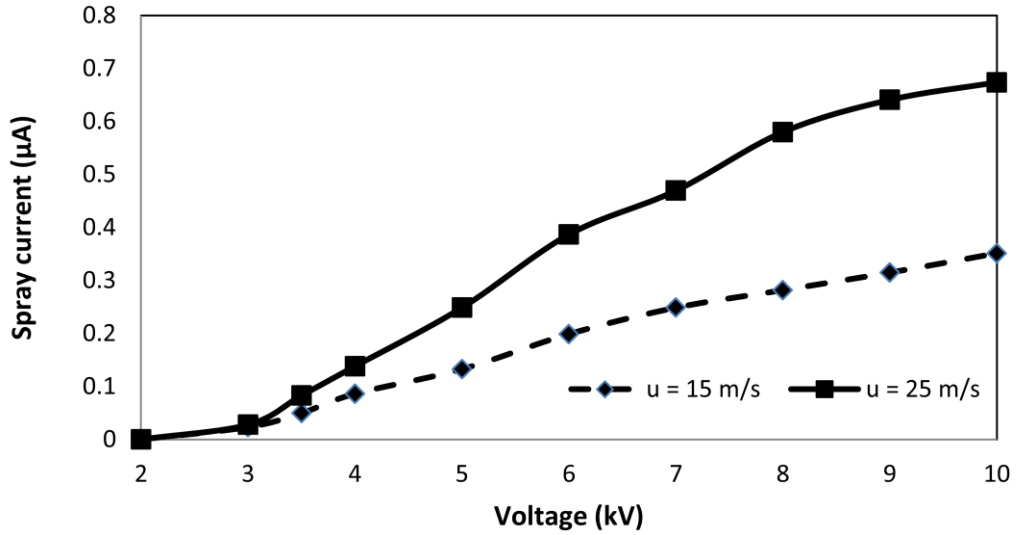

Figure 6.8 Spray current as a function of the applied voltage for u=15 m/s and u=25m/s, for d = 75 µm

The positive effect of the high hydrodynamic pressure and thus the injection velocity on the maximum spray specific charge was shown in the previous sections. The trend was similar with the 75 µm orifice disk as illustrated in Figure 6.9. A greater amount of specific charge could be achieved at the higher axial orifice velocity of 25 m/s with respect to the 15 m/s case at operating voltages above 4 kV. A specific charge level of 6 C/m^3 could be achieved at the maximum stable operating voltage of 10 kV. The value of charge density at the injecting electrode indicates the strength of the charge injection at this configuration.

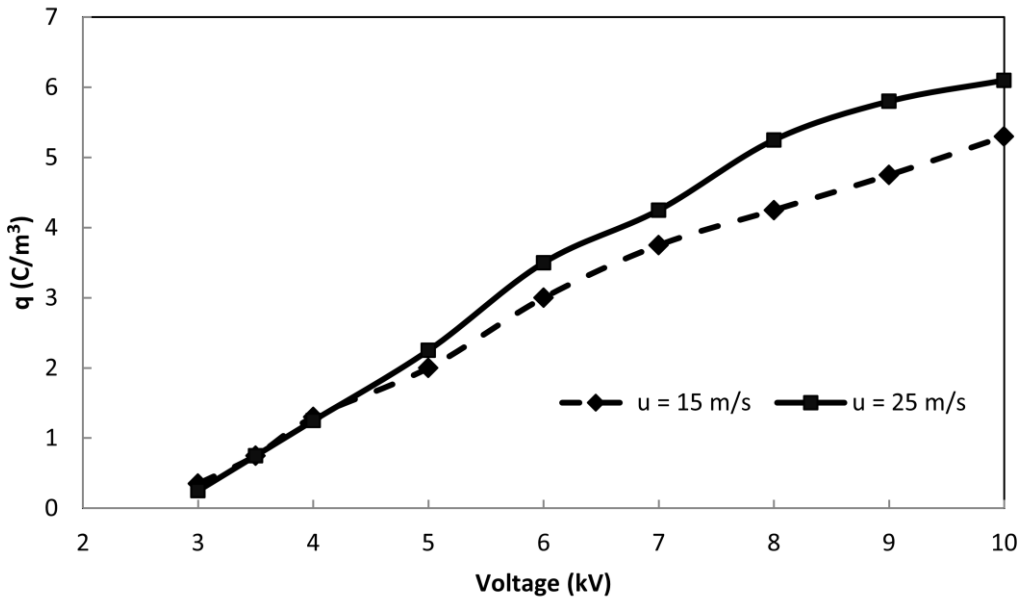

Figure 6.9 Spray specific charge density as a function of applied voltage for u=15 m/s and u=25m/s

6.5.2 **Effective surface tension**

At high specific charge levels, the concept of `effective surface tension' becomes important and is worth mentioning before moving onto the imaging study with the d=75 μm orifice disk. Effective surface tension was originally presented by Laoonual [95] to explain secondary atomization by modifying both the droplet We and Oh numbers with the corresponding specific charge levels. The space charge present in the liquid jet promotes the ligamentation and subsequent atomization of the jet via an effective surface tension reduction as the surface tension and Coulomb force on a droplet surface will oppose each other. This effective decrease in the surface tension will be analyzed in two scales as drop and the liquid jet. Drop scale will help to explain the process of the secondary atomization of the large drops into smaller

drops. On the other side, jet stream scale will explain the initiation of the ligamentation in the jet stream for the orifice sizes used at this testing for different specific charge levels. The effective surface tension term in terms of the specific charge on a droplet surface can be shown as [47]:

$$\sigma^{*} = \sigma - \frac{q^2 D^3}{288\varepsilon} \qquad (6.1)$$

where D is the size of the individual droplet.

The effective surface tension values are tabulated in Table 6.2 for the experimental values of $\sigma = 0.025$ N/m, $0 < q < 5$ C/m^3 and 20 μm < D < 100 μm. As seen from the table, breaking up process of the large drops into smaller drops is a much easier process than breaking up of small drops into further smaller drops. A drop of 200 μm in diameter experiences a very sharp decrease in the effective surface tension with the increase in specific charge. At a specific charge level of 4 C/m^3, the surface tension goes to zero which is indicative of the non-existence of such large drops in sprays at such high specific charge levels. This is in close agreement with the drop size testing results conducted in previous section that in the measurable zone, q> 0.5 C/m^3, the statistical volumetric data, $D_v0.9$, was found smaller than 200 μm for all testing conditions. For drops smaller than 50 μm, even a high specific charge level of 5 C/m^3 is not enough to lower the surface tension to break it up into further smaller drops.

q (C/m3)	D (μm)				
	10	20	50	100	200
1	0.025	0.025	0.025	0.025	0.024
2	0.025	0.025	0.025	0.024	0.019
3	0.025	0.025	0.025	0.023	0.012
4	0.025	0.025	0.025	0.022	0.002
5	0.025	0.025	0.024	0.021	

Table 6.2 Effective surface tension (N/m) for several sizes of droplets at different specific charge levels

The effective surface tension for jet-stream scale can be computed as follows using the Rayleigh limit for cylindrical configuration [47]:

$$\sigma^* = \sigma - \frac{q^2 d^3}{48\varepsilon} \qquad (6.2)$$

where d is the thickness of the jet that can be approximated as the orifice size.

Table 6.3 shows the effective surface tension term for the orifice disk used in this study ($75 < d < 250$ μm). The table is in agreement with the maximum specific charge levels that could be obtained with the corresponding orifice sizes. A specific charge level of 2 C/m^3 could be achieved with 200 and 250 μm orifice disks where the effective surface tension drops to zero as observed from Table 6.3. For 100 μm case, a specific charge level of 5 C/m^3 could be achieved where the effective surface tension goes to zero. For the orifice size of 75 μm, a significantly higher specific charge level is required to effectively reduce the surface tension. In the electrical performance experiments, a specific charge level of 6 C/m^3 could be achieved; however, there seems to be a better potential with this orifice size by observing Table 6.3. This potential could be observed by introducing a higher hydrodynamic pressure

hence higher injection velocity; however, the maximum operating pressure imposes a limit. One can conclude that a larger specific charge level is required to observe the effect of electrostatic charge injection method in atomization for smaller orifice sizes. A similar experimental investigation was conducted by Guildenbecher et. al.[96] into the secondary atomization of charged droplets using conductive and dielectric liquids. Their results showed that the effects of aerodynamic forces are dominant over electrostatic forces on breakup morphology and breakup time.

q	d (μm)			
(C/m3)	75	100	200	250
1	0.025	0.024	0.016	0.008
2	0.023	0.021	0.001	~0.000
3	0.021	0.015		
4	0.018	0.008		
5	0.014	0.002		

Table 6.3 Effective surface tension (N/m) for jets at different orifice disks at different specific charge levels

6.5.3 **Imaging at above critical velocity conditions**

From the findings of the effective surface tension term, an imaging study was undertaken to observe the development of the jet with the 75 μm as a function of the increasing specific charge. As seen from Figure 6.10(a), this condition is above the critical velocity that could generate a pure hydrodynamic spray at zero applied voltage. As the applied voltage was increased further, no noticeable changes were observed with naked eye in Figure 6.10(b) and (c). This is in agreement with the

findings in effective surface tension study which indicated a minimal drop in the surface tension with the increase in specific charge at small orifice sizes.

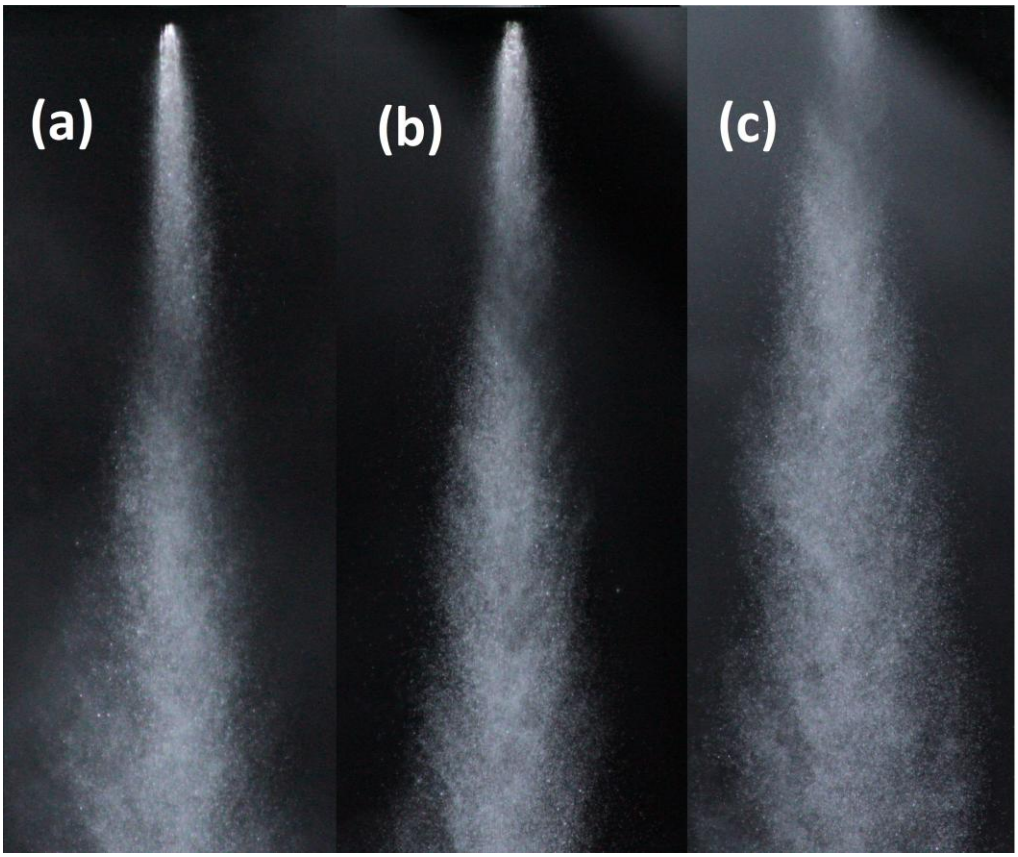

Figure 6.10 Stages of spray development with increasing voltage at 75 micron disk and u= 25 m/s, (a) V=0 kV (b) V=-6 kV (c) V=-9 kV

6.5.4 **Normalized droplet size at above critical velocity conditions**

After the visual studies, drop size measurements were conducted to see if the electrostatic charge injection technique has an effect on reducing the volume median diameter. The results are tabulated as a normalized ratio of the drop sizes with respect to the volume median diameter of the pure hydraulic spray (q = 0) which is about 26 μm for the injection velocity of 15 m/s and 22 μm for u = 25 m/s. As seen from the

figure, some drop in the volume median diameter size is observed about 15%, which is about 3 μm . The misting created inside the testing chamber might have contributed to this minor decrease in VMD.

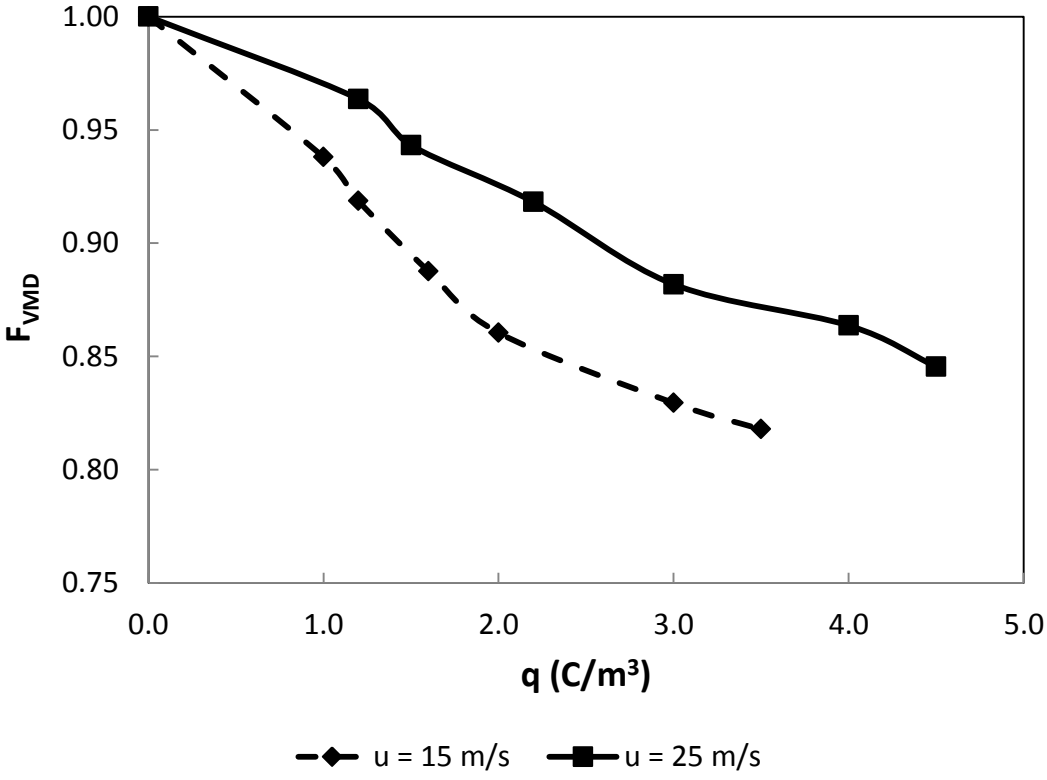

Figure 6.11 Normalized VMD values as a function of specific charge density for u=15 m/s and u=25 m/s

7 CONCLUSIONS AND FUTURE WORK

7.1 Conclusions

The present research has expanded the knowledge on electrostatic atomization technique and resulted in different atomizer designs serving several purposes. The experimental results of the electrostatic charge injection atomization show that:

- The quiescent dielectric liquid results show that a higher amount of charge can be injected using a blade type injector when compared to a point-plane injector. Using a larger number of blades increases the injected charge with efficiency dependent on the number of blades, applied voltage, and type of fluid.
- Previous experimental charge injection laws have been observed with Diesel fuel.
- The investigation of viscous oils of biological origin demonstrated reliable performance with blade-plane type charge injectors. Threshold voltage values at which the charge injection begins were observed to be proportional to the liquid viscosity.
- Our studies confirmed the three previously observed regimes between the applied voltage and the injected current.
- It was proved that electrostatic atomization with a separated nozzle is a feasible method for producing wide range of sprays. Initial tests that were conducted with a wide angle hollow cone nozzle showed the increase in dispersion and spray angle with the increase in specific charge present in the spray.

- The causes of possible charge losses were investigated. The existence of static charge accumulation inside the tubing wall due to the wall friction effects, was presented and studied in detail.
- The electrostatic charge atomization technique is shown to be a viable method to obtain finer sprays at up to 40 bar by means of electrical measurements, spray imaging and laser diffraction spectrometry (LDS) droplet size testing.
- High hydrodynamic pressure allows for a higher amount of charge injection to the liquid. A specific charge level of approximately 5 C/m^3 could be reached with the d=100 μm orifice disk. This aids in increasing the atomization quality at higher flow rates by forming fairly small droplet diameters down to a VMD of 0.16d.
- Statistical drop size data parameters are compared at two different downstream positions from the orifice. A small decrease in maximum drop size is noticed; however, the change in volume median diameter (VMD) is found to be negligible.
- The stages in the spray development as a function of applied voltage are shown by means of an imaging technique.
- High pressure assisted electrostatic atomization technique has been further investigated by analyzing the effect of critical jet velocity, which is defined as the case where pure hydrodynamic atomization occurs at zero applied voltage. Although visual observations didn't show a significant change in the spray plume, droplet size measurements showed that very high specific charge levels should be obtained to have 15% smaller droplets. These findings are assisted with effective surface tension study.

- Both electrostatic effect and hydrodynamic effect are enhanced with the increase of injection velocity. However, the enhancement in hydrodynamic effect seems to be more pronounced especially at the conditions above the critical injection velocity.

7.2 Recommendations for Further Study

Some possibilities for further work can be listed as:

- Combustion of the resulting electrostatic sprays can be investigated. Electrostatic atomizer can be retrofitted to a small test engine to observe the contribution in power and torque output.
- Different nozzles, including external air-mixing nozzles, can be used as a separated nozzle to observe different spray patterns.
- Higher hydrodynamic pressures can be utilized to analyze the effect of turbulent flow inside the orifice channel on the spray pattern and the drop size profile.
- In order to analyze number density and velocity distribution of the droplets along the radial direction across the spray plume, phase Doppler anemometry (PDPA) measurements may be conducted. A comparison may be prepared between volume flux and spatial drop size measurement techniques.
- The third generation electrostatic atomizer could be optimized to be used to spray coolants or oil-based paints to enhance the applications of this technique.
- A heating system can be added to the rig to work with more viscous oils (> 1000 cP).

References

[1] A. C. Pinto, L. N. Guarieiro, M. J. C. Rezende, N. M. Ribeiro, E. A. Torres, W. A. Lopes, P. A. de Pereira, J. B. de Andrade, "Biodiesel: An overview", J. Braz. Chem. Soc., Vol. 16, pp. 1313-1330, 2005.

[2] R. C. Altin¸ S. Etinkaya and H.S. Yücesu, "The potential of using vegetable oil fuels as fuel for Diesel engines", Energy Conversion Management, Vol. 42, pp. 529–38, 2001.

[3] A. R. H. Rigit. and J. S. Shrimpton, "Spray characteristics of charge-injection electrostatic atomizers with small-orifice diameters", Atomization and Sprays, Vol. 16, pp. 421–442, 2006.

[4] J. S. Shrimpton and A. J. Yule, "Atomization, combustion and control of charged hydrocarbon sprays", Atomization and Sprays, Vol. 11, pp. 365–396, 2001.

[5] A. R. H. Rigit. and J. S. Shrimpton, "Electrical performance of charge- injection electrostatic atomizers", Atomization and Sprays, Vol. 16, pp. 401–419, 2006

[6] L. Rayleigh, "Investigation of the character of the equilibrium of an incompressible heavy fluid of variable density". Proceedings of the London Mathematical Society, pp. 170–177, 1883

[7] J. Zeleny, "The role of the surface instability of electrified drops", J. Franklyn Institute, Vol. 219, pp. 659-675, 1935.

[8] J. Zeleny, "Instability of electrified liquid surfaces.", Physical Review, pp. 1–6, 1917.

[9] J. S. Shrimpton and A. J. Yule, "Atomization, combustion and control of charged hydrocarbon sprays", Atomization and Sprays, Vol. 11, pp. 365–396, 2001.

[10] W. Balachandran, W. Machowski, M. Halimic, L. Morgan, C. Gray, and C. Wilson. “Development of an electrostatic nozzle for gas turbine applications.” Proceedings of ILASS, Toulouse, France, 1999.

[11] John David Jackson, Classical Electrodynamics, John Wiley & Sons, 1998.

[12] J. Zeleny, "The electrical discharge from liquid points, and a hydrostatic method of measuring the electric intensity at their surfaces".Physical Review , pp. 69–91, 1914.

[13] G. Taylor, "Disintegration of Water Droplets in an Electric Field". Proc. Roy. Soc. London. Ser. A, pp. 383, 1964.

[14] H. Stone, J. JLister, M. Brenner, “Drops with conical ends in electric and magnetic fields”, Proc. Roy.Soc. Lond. A, pp. 329-347, 1999.

[15] Fernandes De La Mora, “On the Outcome of the Columbic Fission of a Charged Isolated Drop”, J. Colloid Interface Sci., pp. 109-218, 1996.

[16] A. Gomez, K. Tang, "Charge and fission of droplets in electrostatic sprays.". Physics of Fluids, pp. 404–414, 1994.

[17] J.B. Fenn, " Electrospray Wings for Molecular Elephants (Nobel Lecture)", Angewandte Chemie, Vol. 42, pp. 3871–3894, 2003.

.

[18] R. Luther, "Electrostatic atomization of No.2 heating oil", Proceedings of the API Research conference on distillate fuel combustion, API Publication 1701, Paper CP62-3, 1962.

[19] Bellan J & Harstad K, "Mechanical and electrostatic dispersion of a polydisperse cluster of drops for soot control", Proceedings of ICLASS-97, 1, 617, August 18-22 1997.

[20] D. C. Kyritsis, S. Roychoudhury, C. McEnally, Pfefferle, A. Gomez, “Mesoscale combustion: a first step towards liquid fuelled batteries”, Experimental Thermal and Fluid Science, pp. 763-770, 2004.

[21] D. C. Kyritsis, B. Coriton, F. Faure, S. Roychoudhury, A. Gomez, “Optimization of a catalytic combustor using electrosprayed liquid hydrocarbons for mesoscale power generation”, Combustion and Flame, pp. 77-89, 2004.

[22] K. Kim and J. Turnbull, "Generation of charged drops of insulating liquids by electrostatic spraying", Journal of Applied Physics, Vol. 47, 5, 1964.

[23] K. S. Robinson, J. Turnbull, and K. Kim, “Electrostatic Spraying of Liquid Insulators,” Trans. IEEE Ind. App. Sys. 16: pp. 308-317, 1980.

[24] A. J. Kelly, “Electrostatic Atomizing Device,” United States Patent 4,255,777, March 10, 1981.

[25] A. Jaworek, W. Balachandran, A. Krupta, J. Kulon and W. Machowski, “Electrohydrodynamic Atomization of Viscous Liquids,” Inst. Phys. Conf., Edinburgh, UK, March 2003.

[26] J. S. Shrimpton, “Electrostatic Atomization and Combustion of Hydrocarbon Oils,” Ph.D. thesis, University of Manchester Institute of Science and Technology, Manchester, UK, 1995.

[27] M. Jido, “Study of Electrostatic Charged Droplets: Part 1,” J. Jpn. Soc. Chem. Eng., pp. 24-33, 1986.

[28] Al-Ahmad, J. S. Shrimpton, E. L. Ergene, and F. Mashayek, " Electrical performance of a charge-injection atomizer using viscous organic oils", Atomization and Sprays, Vol.19, pp. 547-566, 2009.

[29] A.J. Kelly. Charge injection electrostatic atomizer modelling. Aerosol Science Technology, 12, pp. 526-537, 1990.

[30] J. Allen, P. Ravenhill, and J. S. Shrimpton. Spray characteristics of a novel multi orice electrostatic atomizer. Proceedings of the 20th ILASS Europe Meeting, pp. 373-377, 2005.

[31] G. Malkawi, Point-to-plane and plane-to-plane electrostatic charge atomization for insulating liquids, University of Illinois at Chicago (UIC), 2010.

[32] A. Castellanos, Electrohydrodynamics, International Centre for Mechanical Sciences, 1998.

[33] Darrigol, Olivier, “Electrodynamics from Ampère to Einstein” Oxford, [England]: Oxford University Press, pp. 9-25, 2000.

[34] A.R.H. Rigit and J.S. Shrimpton, “Estimation of the diameter-charge distribution in polydisperse electrically charged sprays of electrically insulating liquids”, Experiments in Fluids, 46: pp. 1159-1171, 2009.

[35] A, V. Getling, Rayleigh–Bénard Convection: Structures and Dynamics., 1998.

[36] A. Castellanos, P. Atten and M. G. Velarde, "Oscillatory and steady convection in dielectric liquid layers subjected to unipolar injection and temperature gradient", Physics of Fluids, Vol. 27, pp. 1607-1615, 1984.

[37] R. Tobazéon, “Electrohydrodynamic Instabilities and Electroconvection in the Transient and A. C. Regime of Unipolar Injection in Insulating Liquids: A Review”, Journal of Electrostatics, Vol. 15, pp. 359-384, 1984.

[38] V. V. Gogosov, V. A. Polyanskii, I. P. Semenova and A. E. Yakubenko, “EHD flows at large electric Reynolds numbers”, Journal of applied mechanics and technical physics, pp. 1-7, 1969.

[39] Michelson, Electrostatic Atomization, Adam Hilger NY, 1990.

[40] J.C. Lacroix, P. Atten and E. Hopfinger, “ Electro-convection in a dielectric liquid layer subjected to unipolar injection.” , Journal of Fluid Mechanics, 69: pp. 539-564, 1975.

[41] H. Hamann, A. Hamnett, W.Vielstich, Electrochemistry, 1998

[42] J. S. Shrimpton, Charge Injection Systems: Physical Principles, Experimental and Theoretical Work, 2009.

[43] Goldston and Rutherford, Introduction to Plasma Physics, Institute of Physics Publishing, 1997.

[44] J. S. Shrimpton and A. J. Yule, “Electrohydrodynamics of Charge Injection Atomization: Regimes and Fundamental Limits,” Atomization and Spray, Vol. 13, pp. 173-190, 2003.

[45] N. Bonifaci, A. Denat and V.M. Atrazhev, “Work Functions for a HV Cathode in Nonpolar Liquids”, Trans. IEEE Die. and Elect. Ins. Vol. 1, pp. 657-662, 1994.

[46] P. Atten, “Electrohydrodynamic Instability and Motion Induced by Injected Space Charge in Insulating Liquids”, IEEE Transactions on Dielectrics and Electrical Insulation, Vol. 3, pp. 1-17, 1996.

[47] J. S. Shrimpton, “Electrostatic Atomization and Combustion of Hydrocarbon Oils,” Ph.D. thesis, University of Manchester Institute of Science and Technology, Manchester, UK, 1995.

[48] A. Rigit and J. S. Shrimpton, “Electrical Performance of Charge-Injection Electrostatic Atomizers,” Atomization and Sprays 16: pp. 401–419, 2006.

[49] J. S. Shrimpton and A. G. Yule, “Atomization, Combustion and Control of Charged Hydrocarbon Sprays,” Atomization and Sprays 11: pp. 365–396, 2001.

[50] D. Jin, “Electrophoresis of a Charged Droplet in a Dielectric Liquid for Droplet Actuation”, Anal. Chem., 2011.

[51] http://www.astm.org/Standards/E1620.htm

[52] P. Rosin and E. Rammler ,"The Laws Governing the Fineness of Powdered Coal", Journal of the Institute of Fuel, pp. 29–36, 1933.

[53] http://www.astm.org/DATABASE.CART/HISTORICAL/D2624-06.htm

[54] I. Adamczewski, “Conductivity and Breakdown in Dielectric Liquids,”, Taylor and Francis, London, 1969.

[55] R. C. Altın¸ S. Etinkaya and H.S. Yücesu, "The potential of using vegetable oil fuels as fuel for Diesel engines", Energy Conversion Management, Vol. 42, pp. 529–38, 2001.

[56] Web link for full text http://unfccc.int/resource/docs/convkp/kpeng.pdf

[57] E. L. Ergene, A. Kourmatzis, J. Komperda, R. Schick, J. Shrimpton, F. Mashayek, “Investigation of the Electrostatic Charge Injection Method at High Hydrodynamic Pressures”, ILASS Americas, 2011.

[58] Rigit, “Performance of a Charge-injection Electrostatic Atomizer and Spray Characteristics,” Ph.D. thesis, Imperial College, London, UK, 2005.

[59] G. Malkawi, J. Shrimpton, F. Mashayek, E. L. Ergene, “Electrostatic atomization of vegetable oils”, Proceedings of the 20th International Liquid Atomization and Spray Systems, ILASS, Chicago IL, 2007.

[60] F. M. McCluskey and A. T. Perez, "The electrohydrodynamic plume between a line source of ions and a flat plate-theory and experiment", IEEE Trans. Electr. lnsul., Vol. 27, pp. 334-341, 1992.

[61] T. Takashima, R. Hanaoka, Ishibashi, R. and Ohtsubo, A., "I-V characteristics and liquid motion in needle-to-plane and razor blade-to-plane configurations in transformer oil and liquid nitrogen", IEEE Trans. Electr. lnsul., Vol. 23, pp. 645-658, 1988.

[62] P. Atten and M. Haidara, "Electrical conduction and EHD motion of dielectric liquids in a knife-plane electrode assembly", IEEE Trans. Electr. lnsul., Vol. 20, pp. 187-198, 1985.

[63] J. S. Shrimpton and A. J. Yule, "Electrohydrodynamics of charge injection atomization: Regimes and fundamental limits", Atomization and Sprays, Vol. 13, pp. 173–190, 2003.

[64] R. A. Serway, Physics for Scientists and Engineers with Modern Physics, 4th edition. pp. 687., 1996.

[65] A. Denat, B. Gosse and J. P. Gosse, "Ion injections in hydrocarbons", J. Electrostatics, Vol. 7, pp. 205-225, 1979.

[66] A. Castellanos and F. Pontiga, "Generalized Thomson-Onsager model for charge injection into dielectric liquids", Conference on Electrical Insulation and Dielectric Phenomena Annual Report., pp. 616-620, 1995.

[67] L. Onsager, "Deviations from Ohm's law in weak electrolytes", J. Chem. Phys., Vol. 2, pp. 599-615, 1934.

[68] E. R. Neagu and C. J. Dias, "Charge injection/extraction at a metal-dielectric interface: experimental validation", IEEE Electr. Insul. Mag., Vol. 25, pp. 15-22, 2009.

[69] P. Atten and M. Haidara, "Electrical conduction and EHD motion of dielectric liquids in a knife-plane electrode assembly", IEEE Trans. Electr. lnsul., Vol. 20, pp. 187-198, 1985.

[70] D. J. Griffiths, Introduction to Electrohydrodynamics, Prentice Hall, Third edition, 1999.

[71] F. M. McCluskey and A. T. Perez, "The electrohydrodynamic plume between a line source of ions and a flat plate-theory and experiment", IEEE Trans. Electr. lnsul., Vol. 27, pp. 334-341, 1992.

[72] P. K. Watson. “Electrohydrodynamic stability of space-charge-limited currents in dielectric liquids. i. theoretical study”, Physics of Fluids, 13, pp. 194-1954, 1970.

[73] P. Atten, “Electrohydrodynamic Instability and Motion Induced by Injected Space Charge in Insulating Liquids”, IEEE Transactions on Dielectrics and Electrical Insulation, Vol. 3(1), pp. 1-17

[74] J. Seddon, E. Kooij, B. Poelsema, H.Zandvliet and D. Lohse, “Surface bubble nucleation stability”, American Physical Society, 2011.

[75] F. P. Incropera and D. DeWitt, Introduction to Heat Transfer, John Wiley & Sons Inc., 2002

[76] P. K. Watson, W. G. Chadband and M. Sadeghzadeh-Araghi, “The role of electrostatic and hydrodynamic forces in the negative-point breakdown of liquid dielectrics”, IEEE Trans. Electr. Insul., Vol.26, pp. 543-559, 1991.

[77] D. Palanker, I. Turovets, A. Lewis, “Dynamics of ArF excimer laser-induced cavitation bubbles in gel surrounded by a liquid medium”, Lasers in Surgery and Medicine, Volume 21, Issue 3, pp. 294–300, 1997.

[78] S. Oliveri, R. Kattan and A. Denat, “Numerical Study of Single Vapour Bubble Dynamics in Insulating Liquids Initiated by Electrical Current Pulses”, Journal of Applied Physics, Vol. 71(1), pp. 108-112, 1992.

[79] R. Kattan, A. Denat and N. Bonifaci, “Formation of Vapour Bubbles in Non-Polar Liquids Initiated by Current Pulses”, IEEE Transactions on Electrical Insulation, Vol. 26(4), pp. 656-662, 1991.

[80] A. J. Kelly, "The electrostatic atomization of hydrocarbons", J. Inst. Energy, Vol. 57, pp. 312–320, 1984

[81] web link: http://plastics.dupont.com/plastics/pdflit/americas/delrin/H76836.pdf?GXHC_locale=en_US

[82] G. Al-Ahmad, J. Shrimpton, F. Mashayek, E. L. Ergene, “Electrical Performance of a Charge-Injection Atomizer using Viscous Organic Oils”, Atomization and Sprays, 19(6), pp. 547-566, 2009

[83] R. L. Daugherty and J. B. Franzini, Fluid Mechanics, 6th ed. (New York: McGraw-Hill), pp. 338-349, 1965.

[84] A. Lichtarowicz, R. K. Duggins, E. Markland, “Discharge Coefficients for Incompressible Non-cavitating Flow Through Long Orifices”, J. Mech. Eng. Sci., 7 (2), pp. 210-219, 1965

[85] web link: http://fluorotherm.com/Properties-FEP.asp

[86] web link: http://www.ce-mag.com/archive/1999/novdec/mrstatic.html

[87] web link: http://www.machinerylubrication.com/Read/809/electrostatic-charge-hydraulic

[88] J. H. Kassebaum and R. A. Kocken, "Controlling static electricity in hazardous (classified) locations". Petroleum and Chemical Industry 42nd Annual Conference Papers, pp. 105–113, 1995.

[89] MIL-H-25579E, Military specification: hose assembly, polytetrafluoroethylene, high temperature, medium pressure, general specification for [s/s by MIL-DTL-25579F] , 1985.

[90] web link: http://www.everyspec.com/FED-STD/FED-STD-101C_21226/

[91] A. Kourmatzis, E. L. Ergene, J. S. Shrimpton, D. C. Kyritsis, F. Mashayek, M. Huo, ‘Electrostatic Primary Atomization of Dielectric Liquid Jets Containing High Specific Charge’, Experiments in Fluids, Submitted, 2011.

[92] J. S. Shrimpton and A. J. Yule, “Characterization of charged hydrocarbon sprays for application in combustion systems”, Experiments in fluids, Vol. 16, pp. 460-469, 1999.

[93] G. Al-Ahmad, J. S. Shrimpton, E. L. Ergene, and F. Mashayek, " Electrical performance of a charge-injection atomizer using viscous organic oils", Atomization and Sprays, Vol.19, pp. 547-566, 2009.

[94] R. L. Daugherty and J. B. Franzini, *Fluid Mechanics*, 6th ed. (New York: McGraw-Hill), pp. 338-349, 1965.

[95] Y. Laoonual, "Optical investigation of evaporating spray", PhD Thesis, Imperial College London, 2006.

[96] D. R. Guildenbecher and P. E. Sojka, “Secondary Atomization of Electrostatically Charged Drops”, ICLASS 2009, Colorado USA, 2009.

A List of Publications

1. G. Al-Ahmad, J. S. Shrimpton, F. Mashayek, E. L. Ergene, “Electrostatic atomization of vegetable oils”, ILASS Americas, 2007.
2. G. Al-Ahmad, J. S. Shrimpton, F. Mashayek, E. L. Ergene, “Atomization of High-viscosity Organic Oils using the Charge-injection Method,” , Volume of Extended Abstracts of the 21st Annual Conference on Liquid Atomization and Spray Systems, Orlando FL, 2008.
3. G. Al-Ahmad, J. Shrimpton, F. Mashayek, E. L. Ergene, “Electrical Performance of a Charge-Injection Atomizer using Viscous Organic Oils”, Atomization and Sprays, 19(6), pp. 547-566, 2009
4. E. L. Ergene, G. Malkawi, J. S. Shrimpton, F. Mashayek, ‘Charge Injection with Multiple Blade-Plane Configurations in a Quiescent Dielectric Liquid”, IEEE Dielectrics and Insulation, 2010.
5. E. L. Ergene, A. Kourmatzis, J. Komperda, R. J. Schick, J. S. Shrimpton, F. Mashayek, ‘Investigation of the Electrostatic Charge Injection Method at High Hydrodynamic Pressures’, ILASS Americas, 2011
6. A. Kourmatzis, E. L. Ergene, J. S. Shrimpton, D. C. Kyritsis, F. Mashayek, M. Huo, ‘Electrostatic Primary Atomization of Dielectric Liquid Jets Containing High Specific Charge’, Experiments in Fluids, Submitted, 2011.

B Experimental rig

Zenith HPB5704-2 pump was utilized for the high pressure studies. For viscosity measurements, Brookfield DV-II+Pro viscometer and Keithley 6485 Picoammeter are used. The verification of the results is done with the precise digital conductivity meter “Model 1152”.

The experimental rig consisted of these components: pressure vessel, fuel filters, flowmeter, analogue pressure gauge, and tubing. A 7-gallon pressure tank was used to pressurize the fuel up to 6 bar. Transparent tubing with 3 mm inner diameter was connected to check the tank fuel level. A ball valve was connected to control the flow output from the tank.

A 7 µm particle size filter made by Swagelok was used to filter the solid particles from the Diesel fuel. For the high pressure runs on 75 µm orifice size, 2 µm filter was installed just before the atomizer inlet. The aim of the filters was not only to clean the fuel from particles but also to avoid air bubble formation.

For high flow rate studies, a digital gauge made by GPI was used. This gauge was already calibrated for Diesel fuel and mostly used by gas stations to calibrate their fuel pump gauges. This digital pressure gauge was placed at the atomizer inlet. The gauge can measure up to 15 bar within %0.1 error.

C Labview

The software package, LabView was used to collect multiple current data and average it over the number of readings. The interface is shown in Figure C.1.

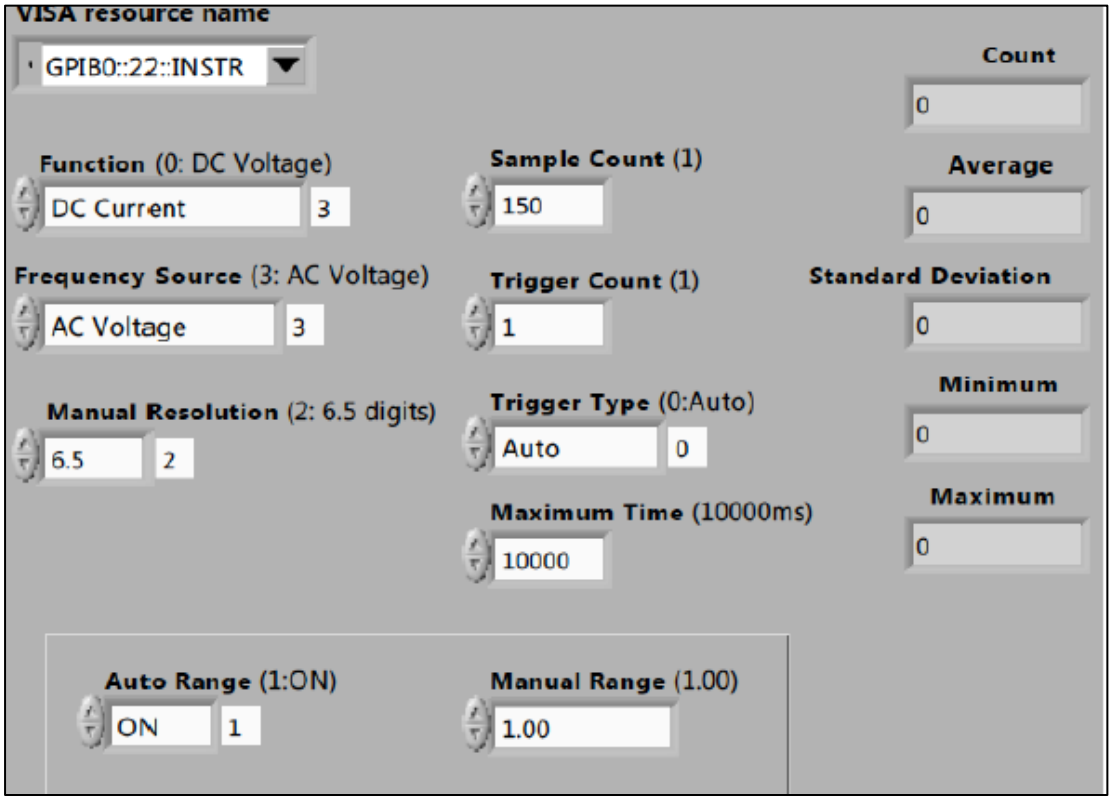

Figure C.1 LabView interface

D Technical Drawings for Blade to Plane Charge Injector

This section briefly explains the procedure followed to decide the minimum thickness for PTFE which is selected as the insulating material regarding its properties like permittivity; non-conductivity and ease of machining. We carried out a two dielectrics (PTFE and air) model. The inner dielectric is PTFE and the outer is surrounding air. As there is no electric charge source in the dielectrics region, from the gauss law [64]:

$$\varepsilon_{PTFE} E_{PTFE} = \varepsilon_{air} E_{air} \quad \text{(D.1)}$$

Dielectric permittivities are:

$$\varepsilon_{PTFE} = 1.771x10^{-11} F/m \text{ and } \varepsilon_{air} = 8.854x10^{-12} F/m \quad \text{(D.2)}$$

Operating applied voltage conditions are:

$$E(x) = -\frac{\delta V}{\delta x} \text{ and } V(x=0) = V_{\max} = 24kV \quad \text{(D.3)}$$

Boundary conditions are:

$$V(x = r_{PTFE}) = V_{breakdown} = 14kV \text{ and } V(x = L_{out}) = 0kV \quad \text{(D.4)}$$

$$L_{out} = r_{PTFE} + r_{air} \quad \text{(D.5)}$$

Evaluating $E(x)$:

$$E(x \le r_{PTFE}) = \frac{V_{\max} - V_{breakdown}}{r_{PTFE}} \quad \text{(D.6)}$$

$$E(r_{PTFE} \le x \le L) = \frac{V_{breakdown} - 0}{L - r_{PTFE}} \quad \text{(D.7)}$$

Assuming an L and calculating the r_{PTFE} from the previous equations.

$$\frac{\varepsilon_{PTFE}(V_{\max} - V_{breakdown})}{r_{PTFE}} = \frac{\varepsilon_{air}(V_{breakdown} - 0)}{L - r_{PTFE}} \qquad \text{(D.8)}$$

Rearranging;

$$r_{PTFE} = \frac{\frac{L(\varepsilon_{PTFE}(V_{\max} - V_{breakdown}))}{\varepsilon_{air} V_{breakdown}}}{\frac{(\varepsilon_{PTFE}(V_{\max} - V_{breakdown}))}{\varepsilon_{air} V_{breakdown}} + 1} \qquad \text{(D.9)}$$

Assumed that $L = 10mm$; corresponding thickness and electric field becomes $r_{PTFE} = 5.8mm$ and $E_{air} = 3.4kV/mm$. As the electric field was found to be larger than the goal, $E_{air} > 3kV/mm$, we increased the L and so the r_{PTFE} to have a smaller electric field region in air side. From trial and error calculations with a safety factor of 2; 25 mm thickness is found to be safe. This means that there is 25 mm of PTFE around the sides and top of each piece so that they can face each other with only the fluid medium in between. As a result of these iterations; a charge injector design with outer dimensions of 80x80x30 mm (W/H/D) is decided.

For the charge injector design, several steps were undertaken as follows. First a decision was given on the necessary number of blades. Odd number of plates was foreseen to be more efficient due to symmetry. Later on, appropriate distance was decided to be in different amounts such as 0.0625", 0.125" and 0.25". The next decision was about the blade height.

Moreover, a charge receiver plate was designed to collect the injected charge into the quiescent fluid as shown in Figure D.2. Rather than having a flat plate, a reasonable amount of radius was initially proposed to increase the charging efficiency of the charge injector. We got the radius by defining three points where the first and

third plate a distance is taken nearly equal to the gap and about 80% of that distance is drawn from the middle plate.

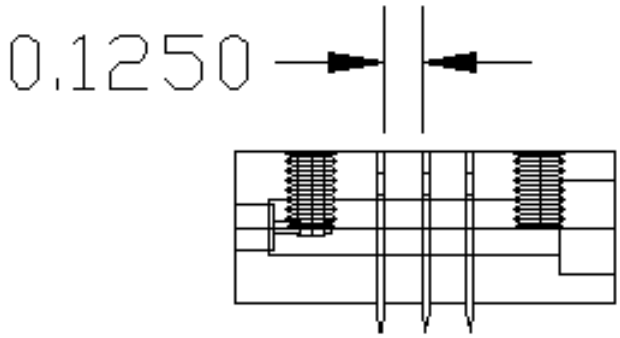

Figure D.1 Injector multi-blade assembly

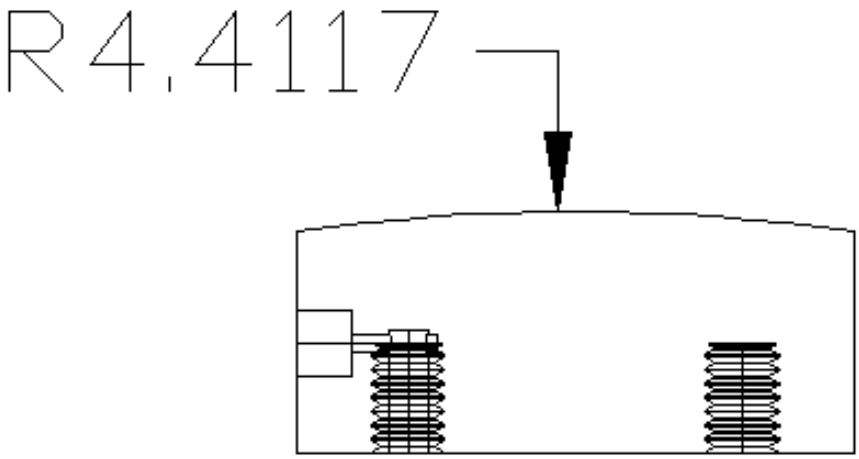

Figure D.2 Charge collector radius

The connection for the high voltage cable was made possible by a groove between two half circles on the contact point of the PTFE blocks to have the maximum insulation and to avoid corona effect. Diameter for the HV cable is 0.15”. Plastic screws were selected due to their electrically insulating properties and low cost to tighten PTFE blocks and main setup. We selected plastic machine screw from

www.mcmaster.com. Black Nylon Flathead Slotted Machine Screw 8-32 Thread, 1-1/4" Length, Packs of 100 Part Number: 95133A401. A total of 22 screws are needed as sixteen (2*8) will be used to attach outer and inner part of PTFE block and three of each will be used to attach the PTFE block to the main setup and charge receiver. For maximum accuracy; 2D drawing supplied from the company is used to rotate from axis to be formed a 3D solid object and assembled in the drawing. Set-screws are used to lock leakage cable stable to the brass injector body as shown in Figure D.3.

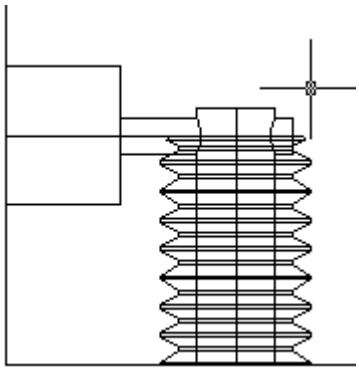

Figure D.3 HV cable connection

One last but not the least decision was made about the adjustment of gap between the blade and receiver. First, it was planned to manufacture blades at different heights and replace them but later on as the design process went on; it was realized that replacing blades were rather difficult due to design limitations. In order to prevent misalignment, large holes drilled to four corners in PTFE blocks where cylinder rods were placed in these drills and fixed from both edges.

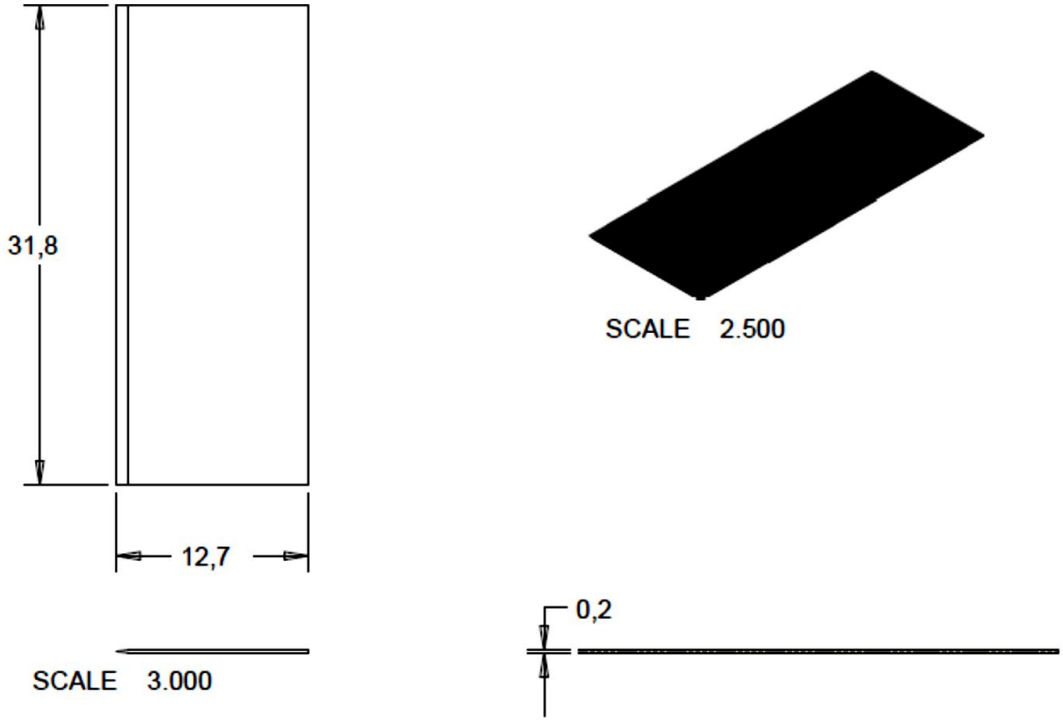

Figure D.4 Blades used as emitter electrode

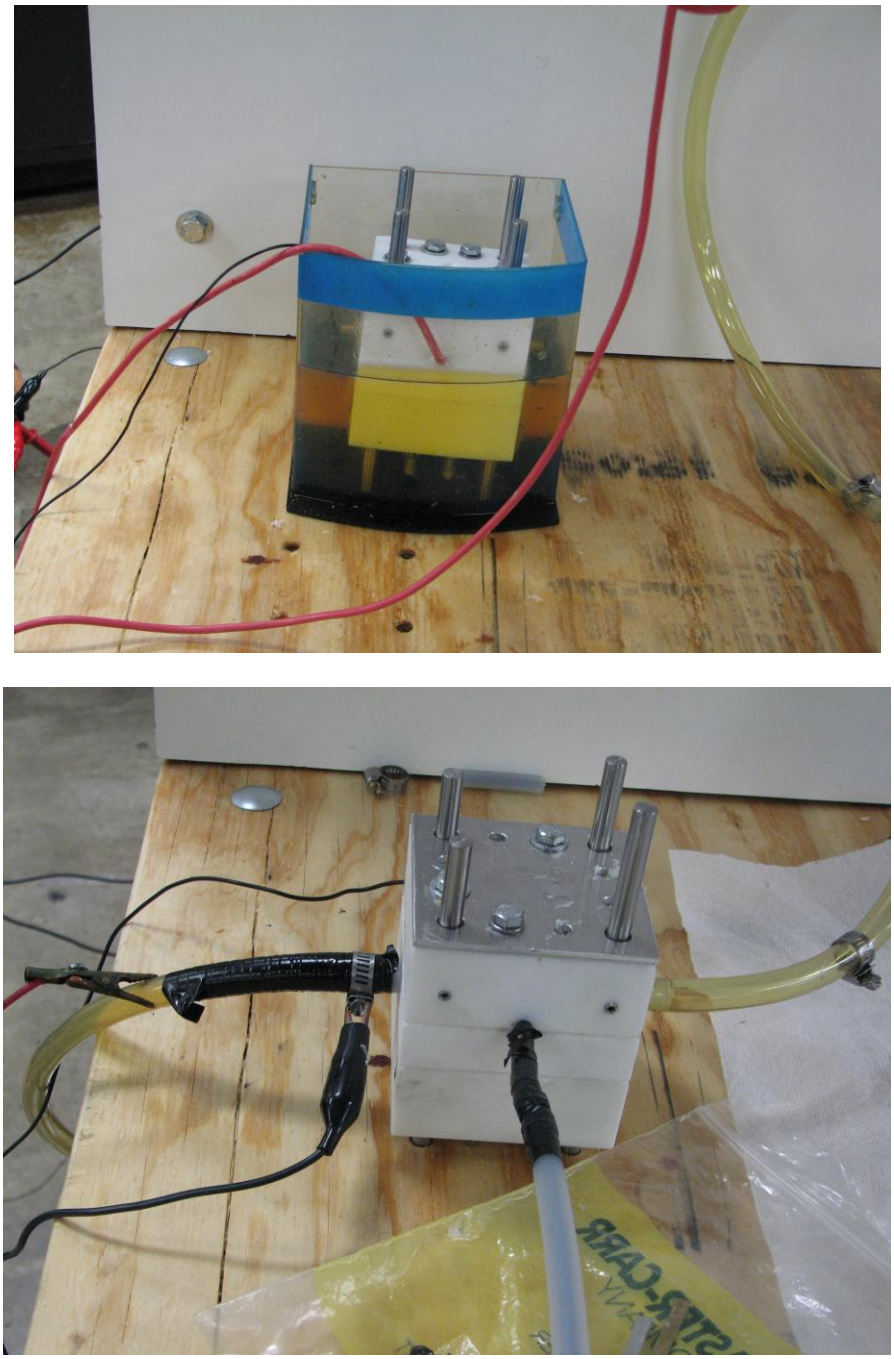

Figure D.5 Blade type charge injector – (a) no flow (b) high flow rate

–

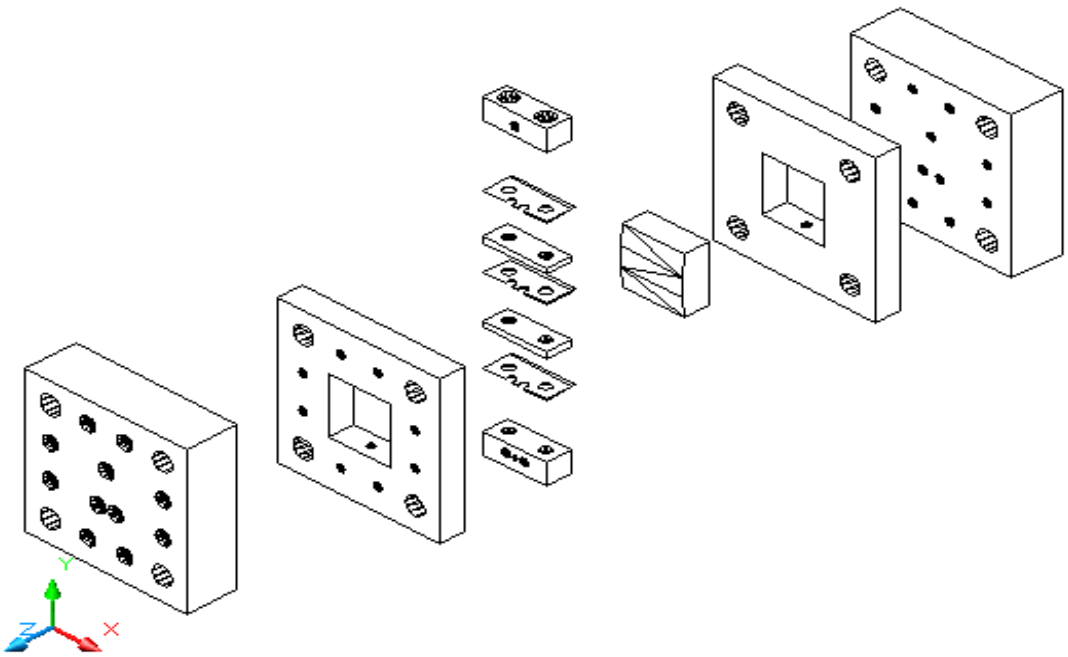

Figure D.6 Blade type charge injector – whole assembly

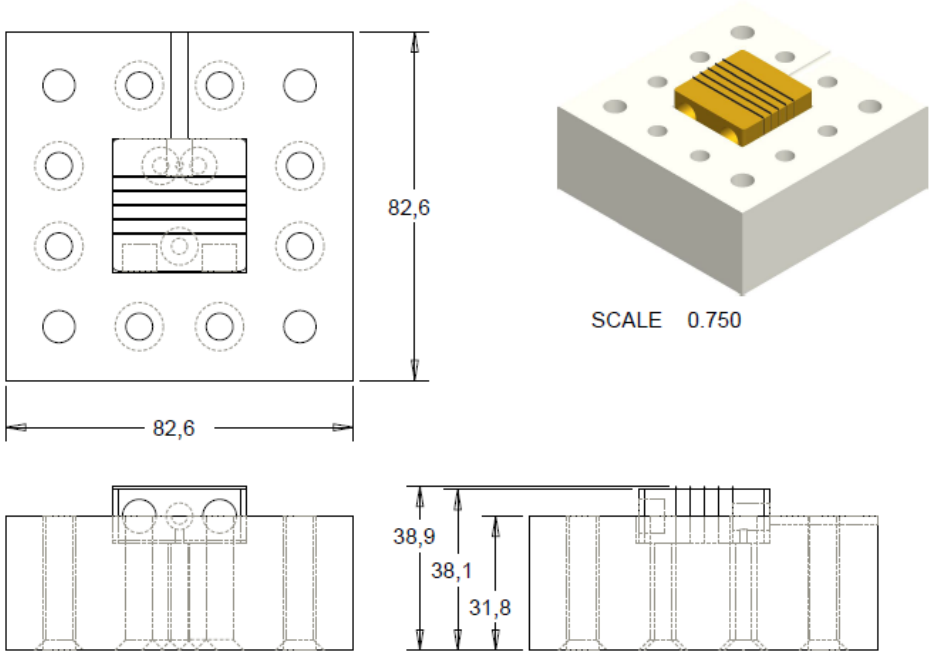

Figure D.7 Blade type charge injector – charger PTFE

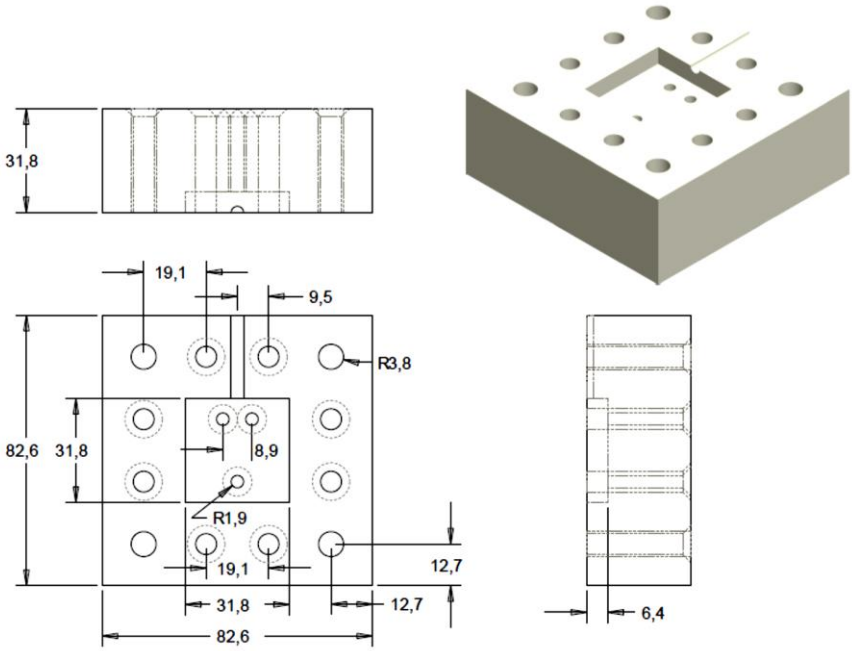

Figure D.8 Blade type charge injector – receiver PTFE

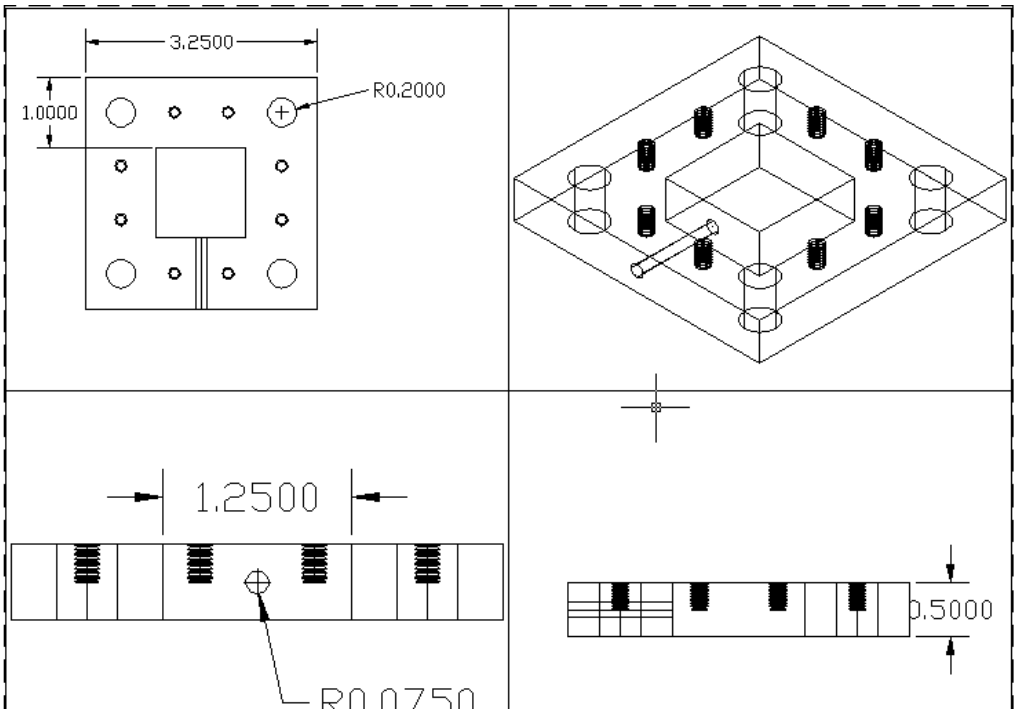

Figure D.9 Blade type charge injector – intermediate PTFE

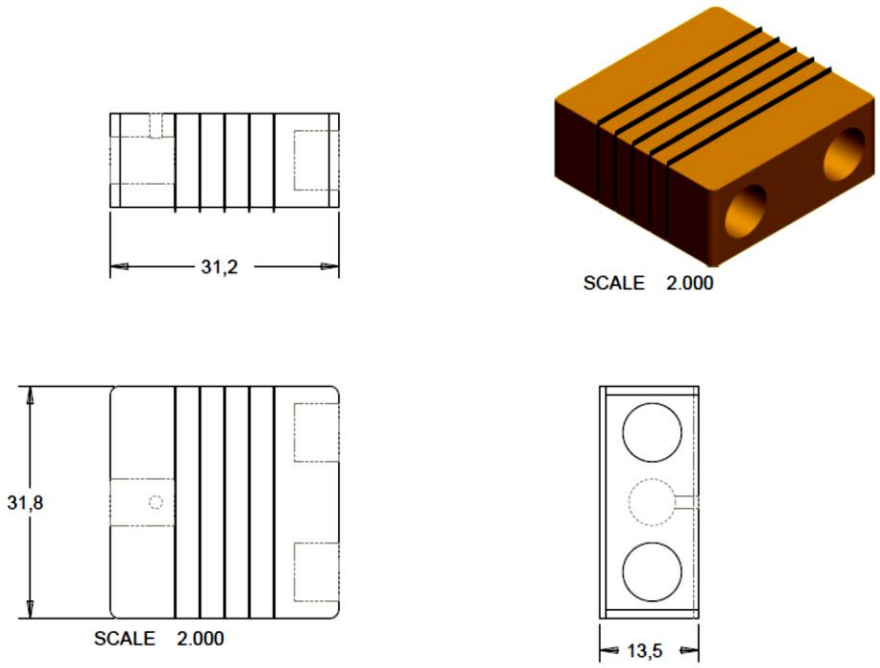

Figure D.10 Blade type charge injector – charger blade assembly

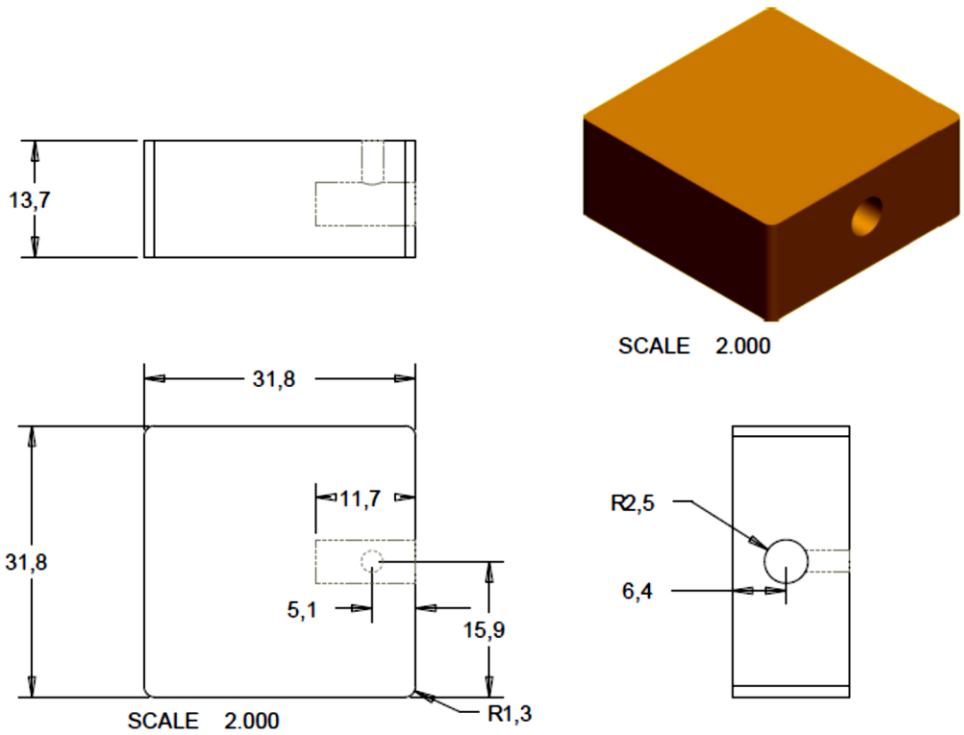

Figure D.11 Blade type charge injector – charge collector

E Computational Fluid Dynamics (CFD) analysis for blade to plane atomizer internal flow with no electric charge

The objective of this study is to find the velocity and pressure distributions inside the blade type atomizer for Diesel fuel mainly around the blade tip and orifice inlet and exit. The type of the flow is axisymmetric, incompressible and single phase.

The programs chosen for this study are CFX 11 for CFD and PROE WF3 for CAD. Applied boundary conditions are as follows: Inlet flow equals 29.5 mL/min; outlet pressure is atmospheric; and velocity is axisymmetric on symmetric faces and no slip condition on all walls. Meshing is shown in Figure E.1. Finer meshes were added near the wall to observe the boundary effects.

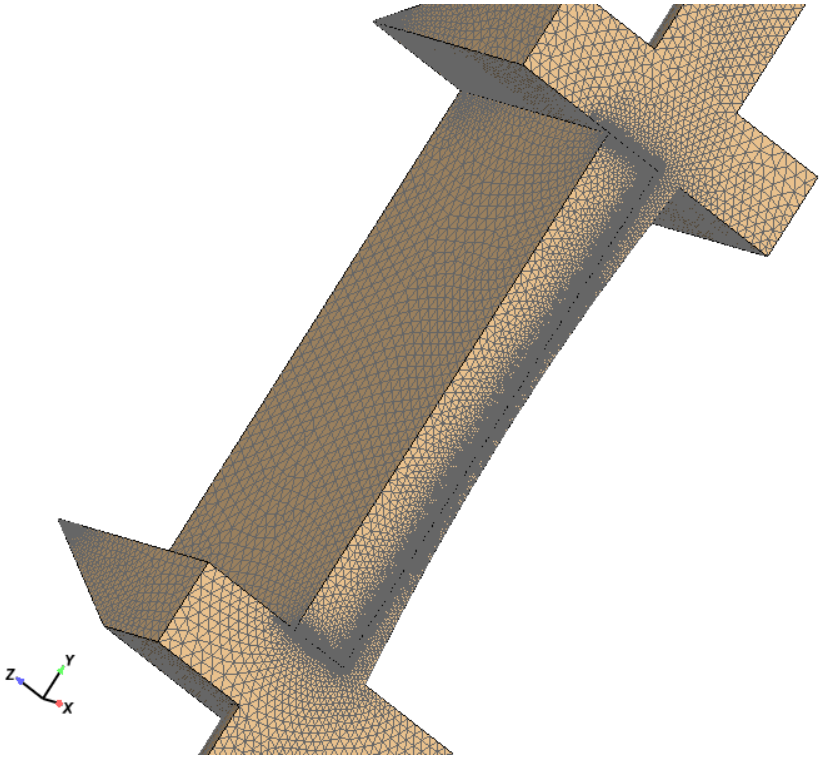

Figure E.1 Blade type charge injector – mesh

The velocity of the internal volume is shown in Figure E.2. An undesired flow recirculation was observed inside the atomizer. This recirculation increases the time the charge liquid is exposed to the earthed ground electrode. This results in a sharp drop in the charge contained in the exiting fluid and hence less efficient operation.

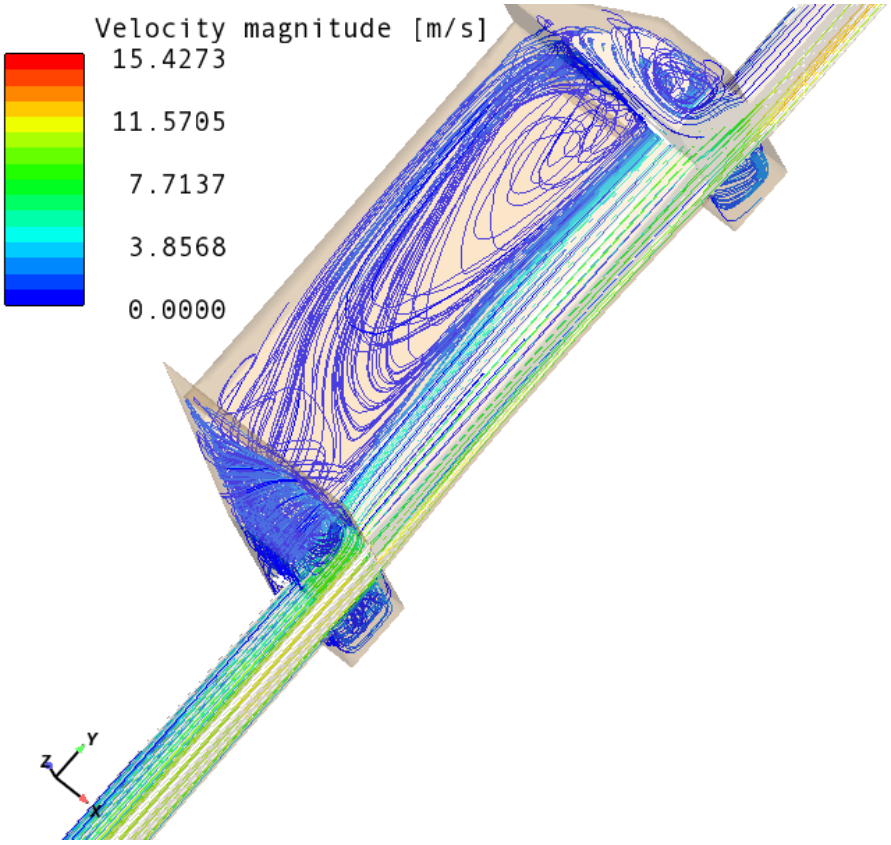

Figure E.2 Blade type charge injector – velocity of the internal volume

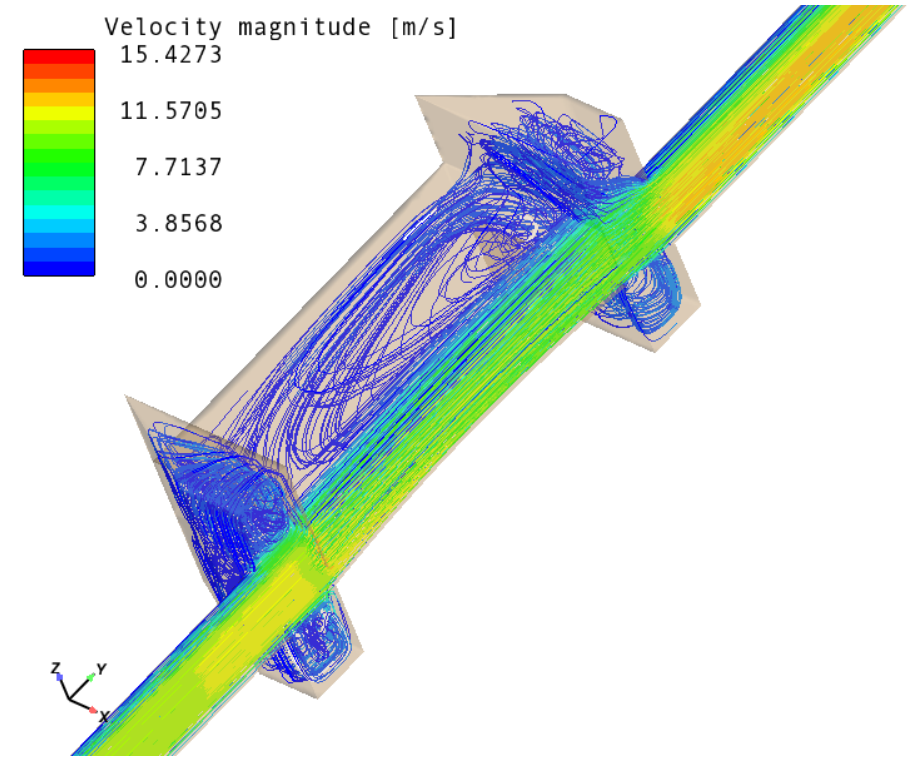

Figure E.3 Blade type charge injector – velocity of the symmetry plane

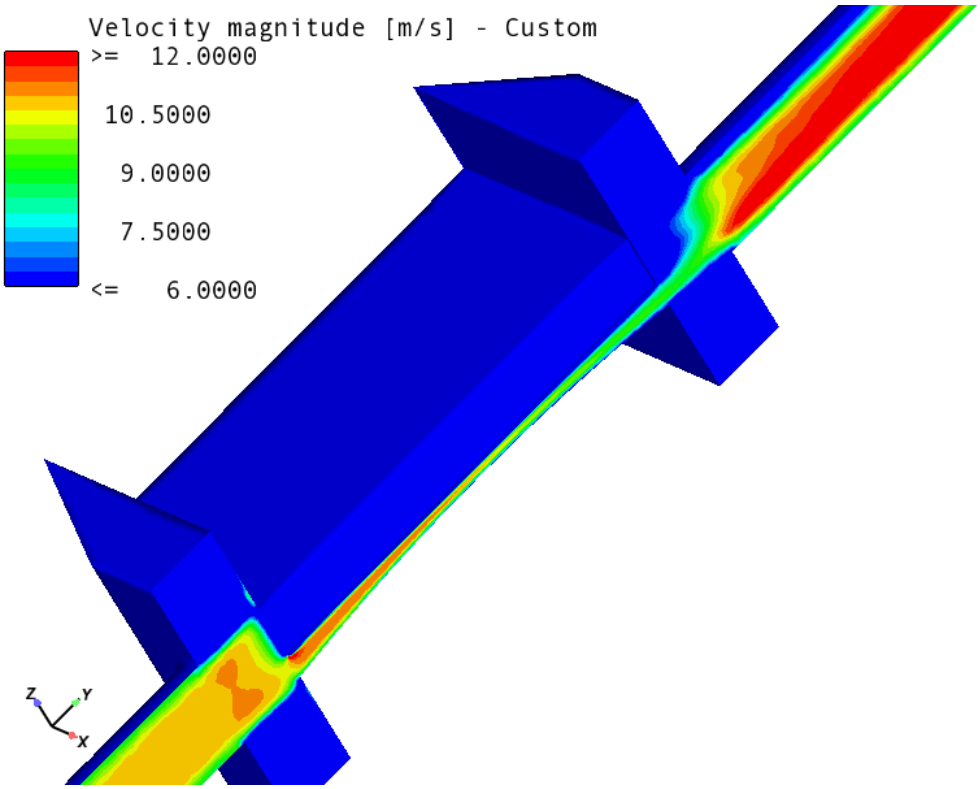

Figure E.4 Blade type charge injector – velocity contour at the blade tip

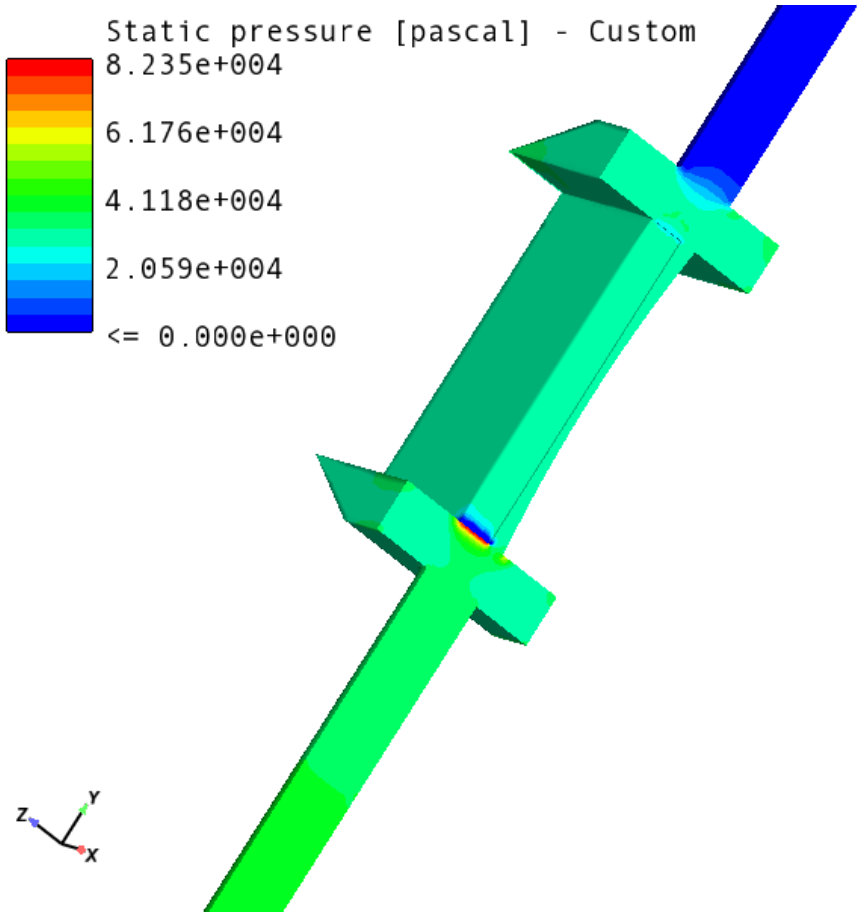

Figure E.5 Blade type charge injector – pressure drop

F Technical drawings for separated spray design

This appendix contains the detailed parts and assembly drawings for the separated atomizer in chapter 5. Figure F.1 shows the overall assembly with the Delrin® add-on piece and the secondary nozzle.

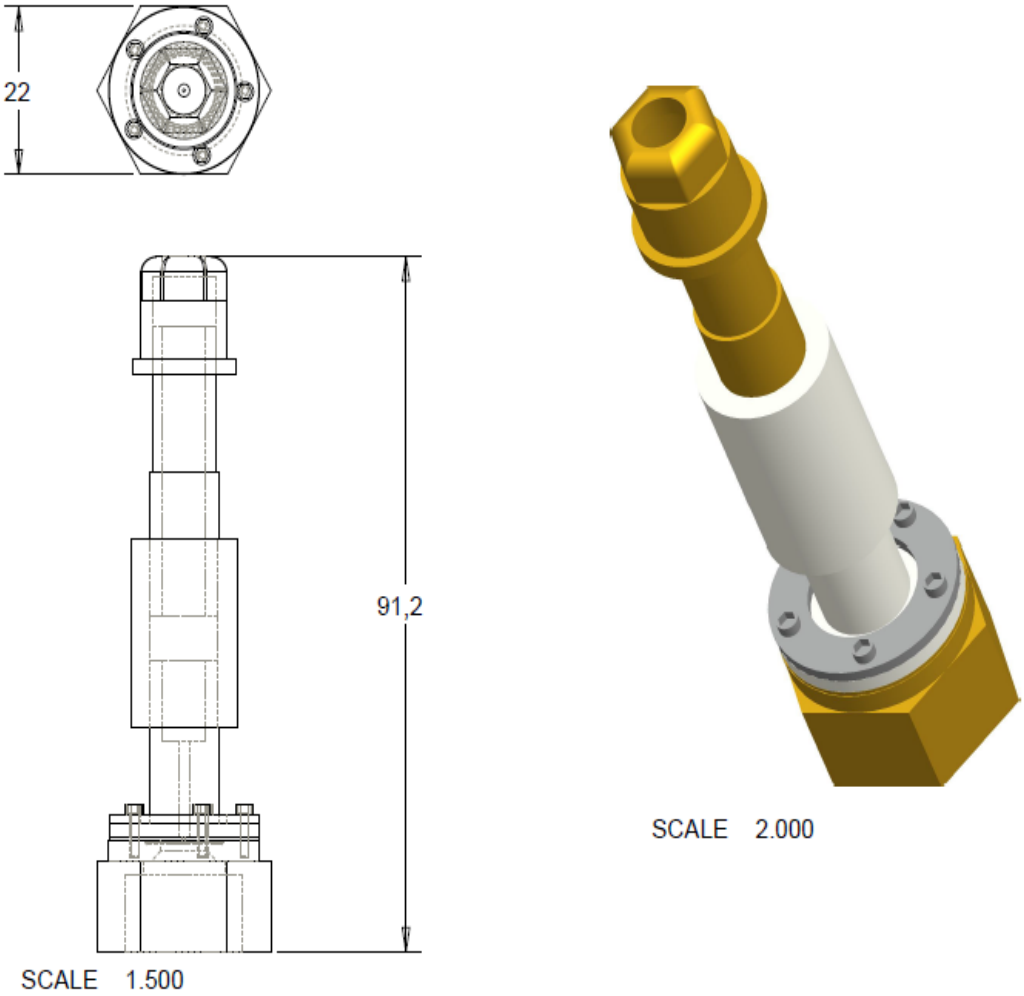

Figure F.1 Separated nozzle assembly

Figure F.2 shows the quick connect adaptor and tubing configuration. Figure F.3 shows the detailed drawing of the secondary nozzle body.

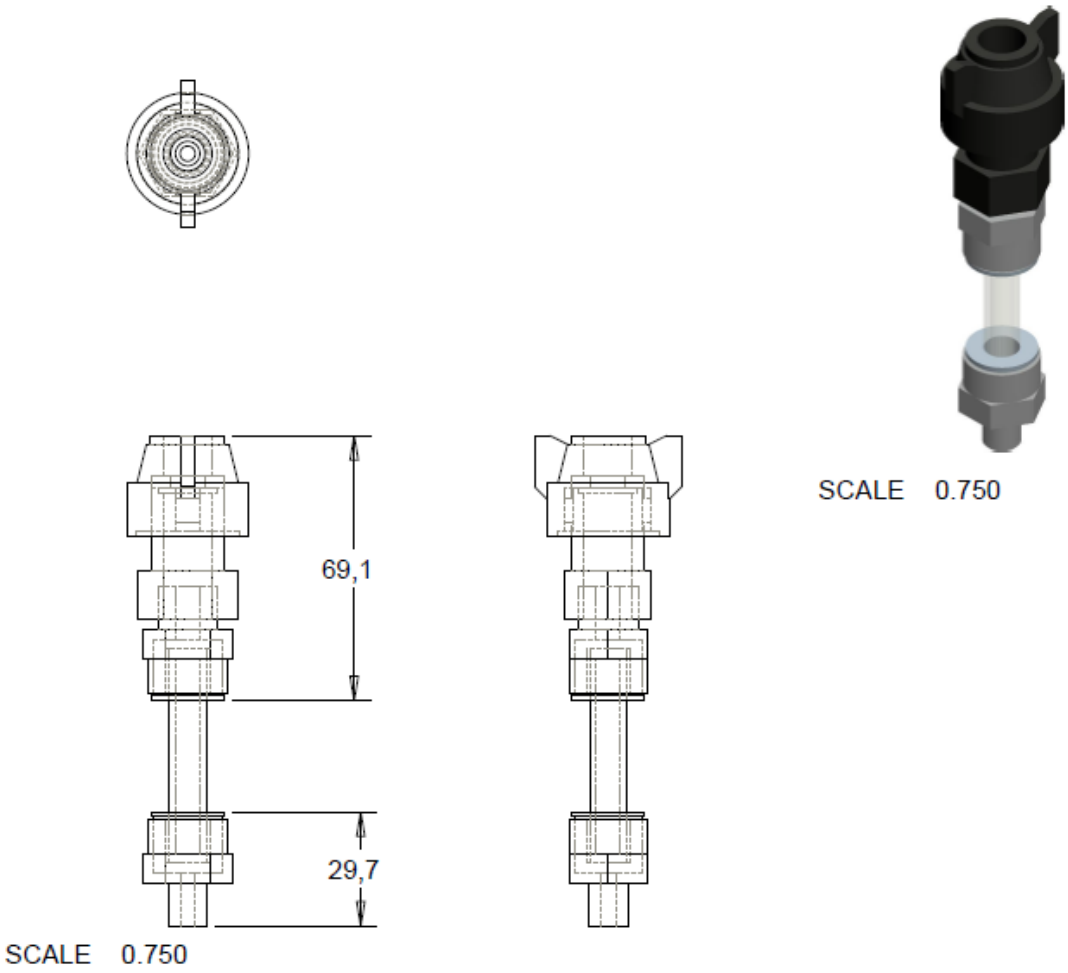

Figure F.2 Tubing - quick connect assembly

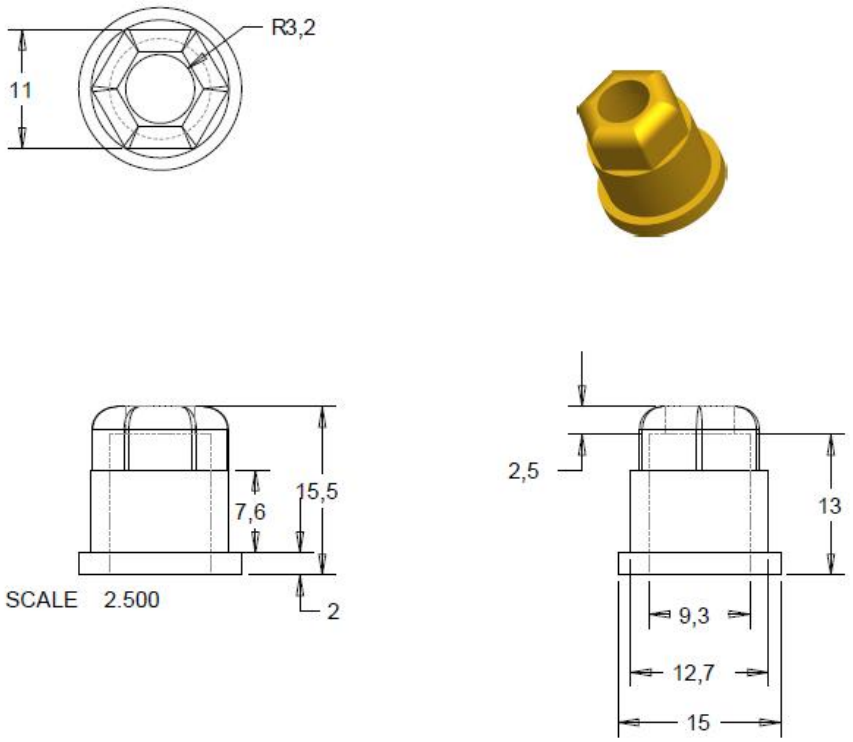

Figure F.3 Separated nozzle

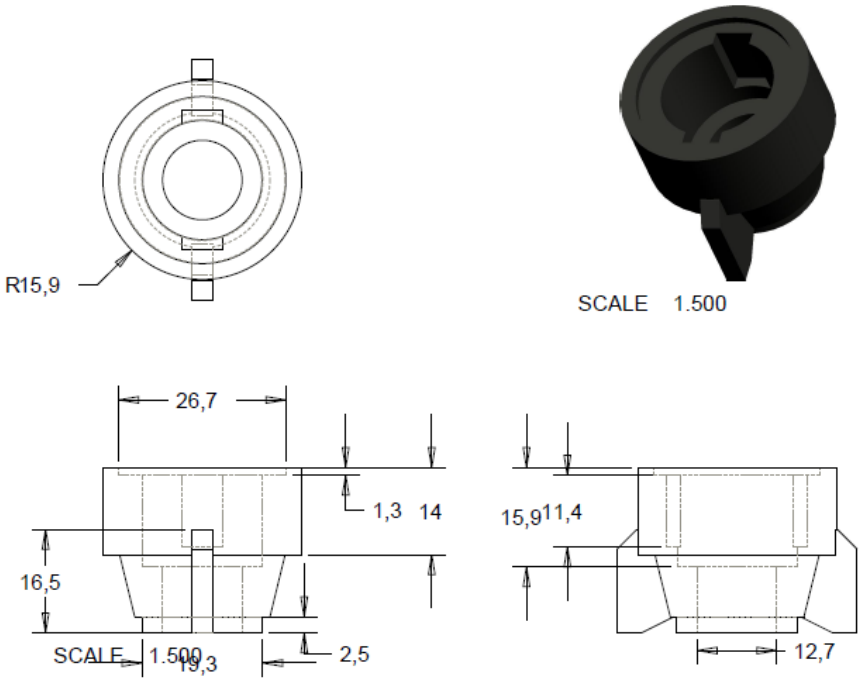

Figure F.4 Quick connect adaptor - female

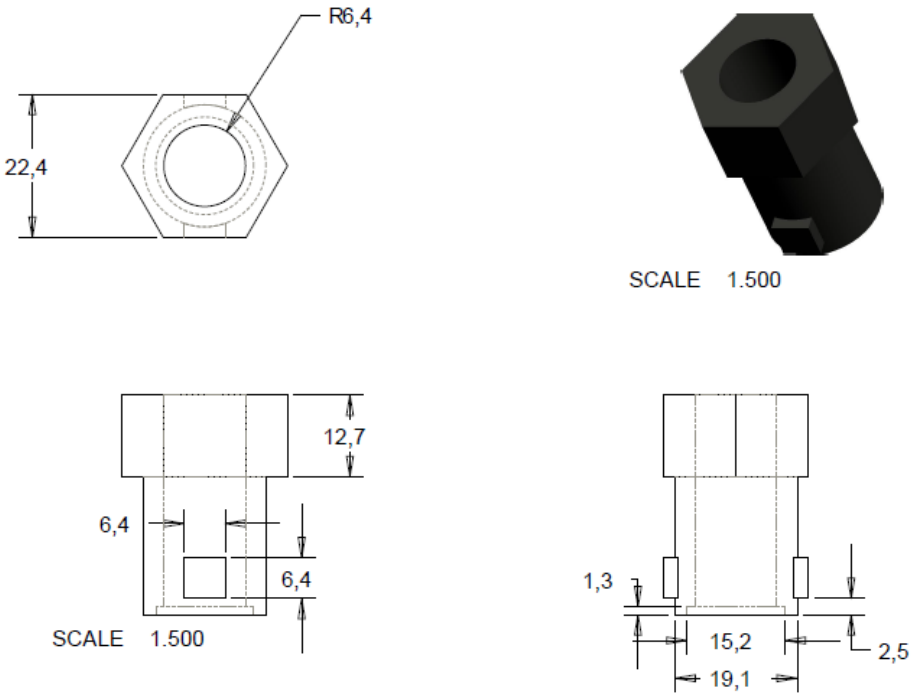

Figure F.5 Quick connect adaptor - male

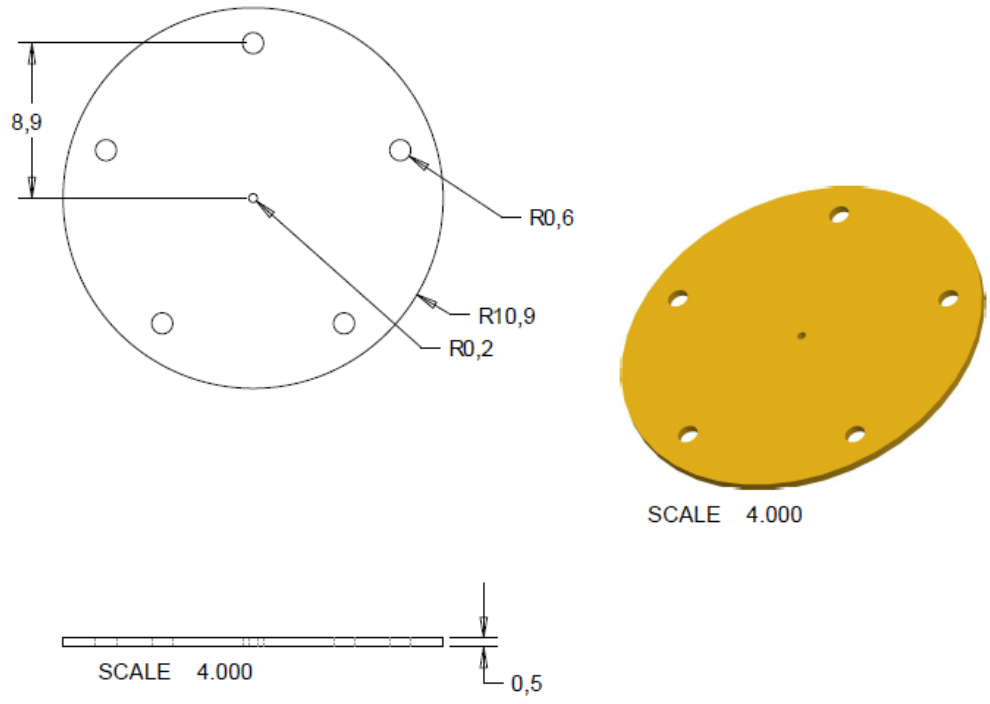

Figure F.6 Orifice plate

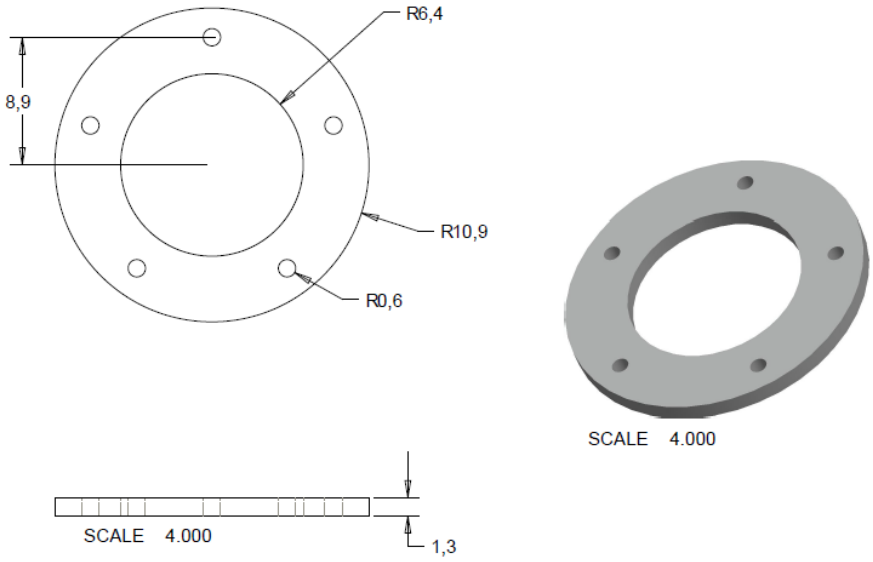

Figure F.7 Alignment ring

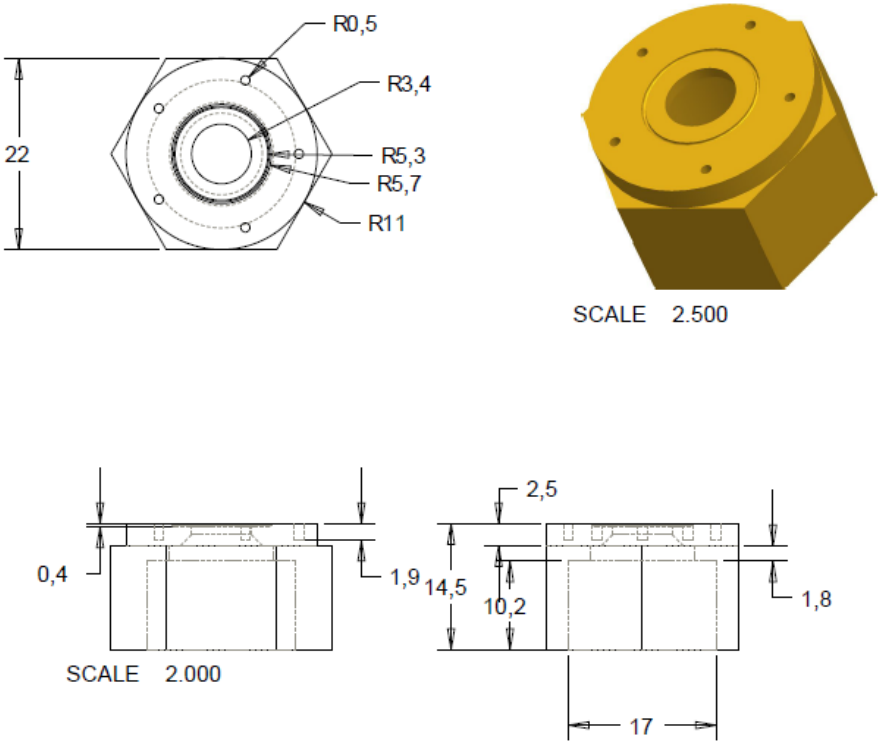

Figure F.8 Threaded nozzle adapter

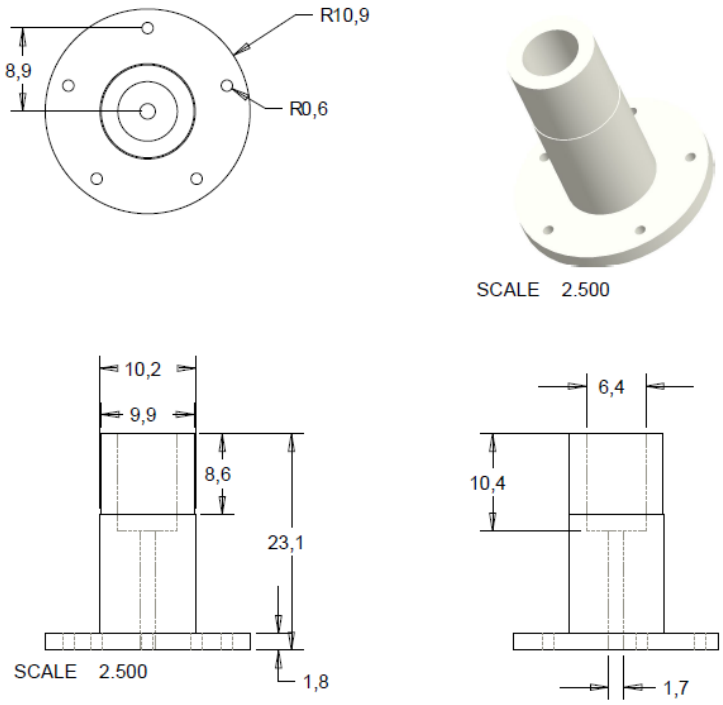

Figure F.9 Delrin® add-on piece

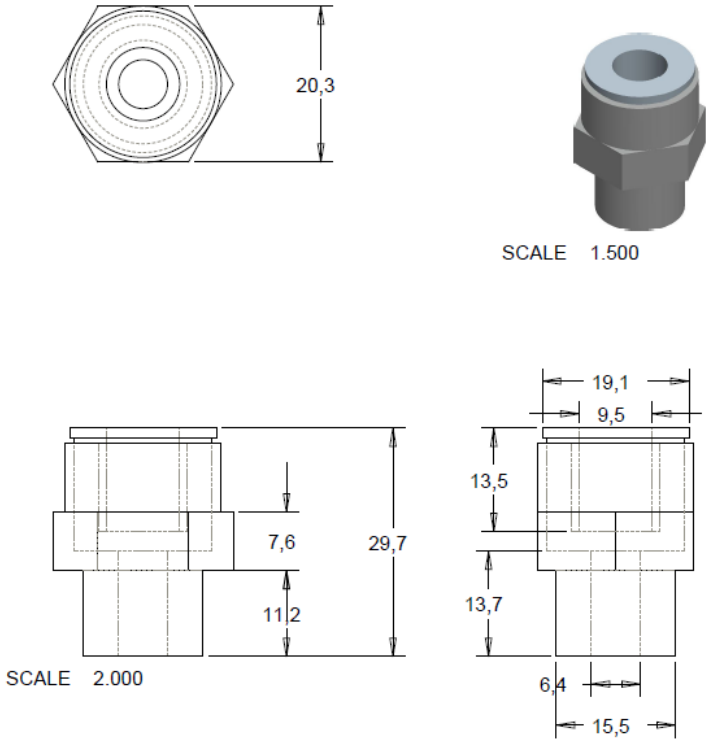

Figure F.10 Easy connect tubing fitting

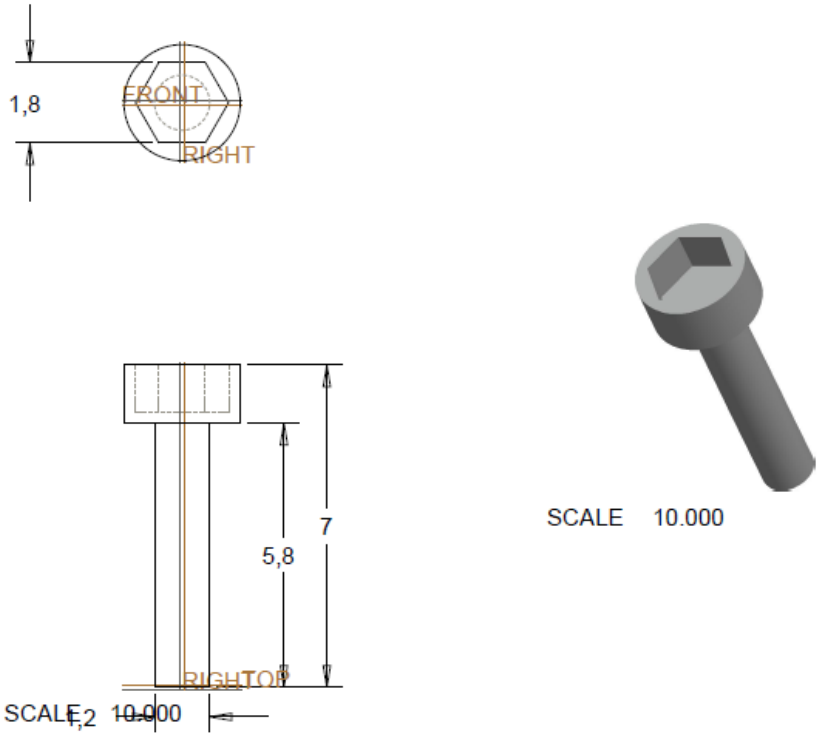

Figure H.11 Screws holding nozzle assembly

G Viscosity Measurement for UIC Biodiesel Fuel

University of Illinois at Chicago (UIC) Spray and Atomization Laboratory needed viscosity measurements for the first sample of Biodiesel fuel prepared by Whitney Young Magnet High School (WYHS) students as a collaborative effort with the UIC Department of Mechanical and Industrial Engineering (MIE).

Viscosity measurements will give an understanding whether the first sample meets the ASTM viscosity standards. Moreover, it has long been known that viscosity is one of the major parameters in the development of spray atomization. The viscosity data as a function of shear rate and temperature will be analyzed by UIC MIE and WYHS to define the most suitable composition for their Biodiesel fuel.

Viscosity was measured with the Brookfield® DV-II+ Viscometer as shown in Figure G.1.

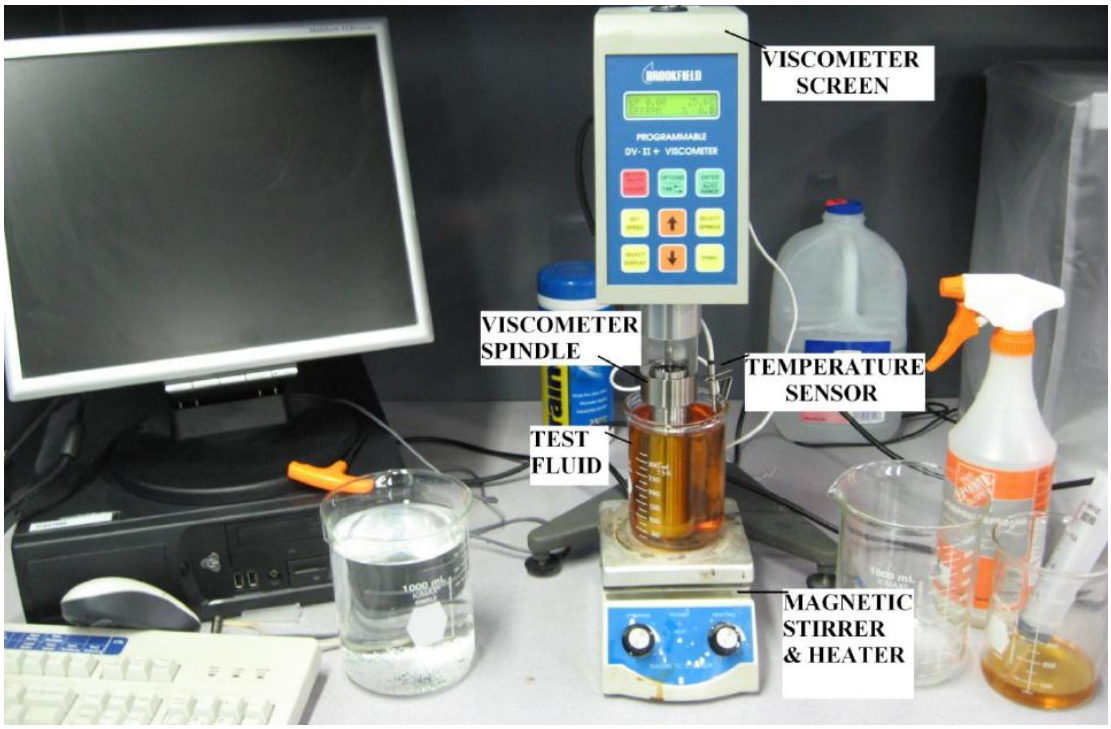

Figure G.1 Test setup

G.1 **Test Results**

First set of experiments were performed at varying shear rate by changing the rotational speed of the viscometer spindle. No significant variations are observed in the viscosity with the increase in shear rate. Figure G.2 shows the viscosity profile with respect to shear rate. All shear rate testing was performed at laboratory conditions of 20 °C.

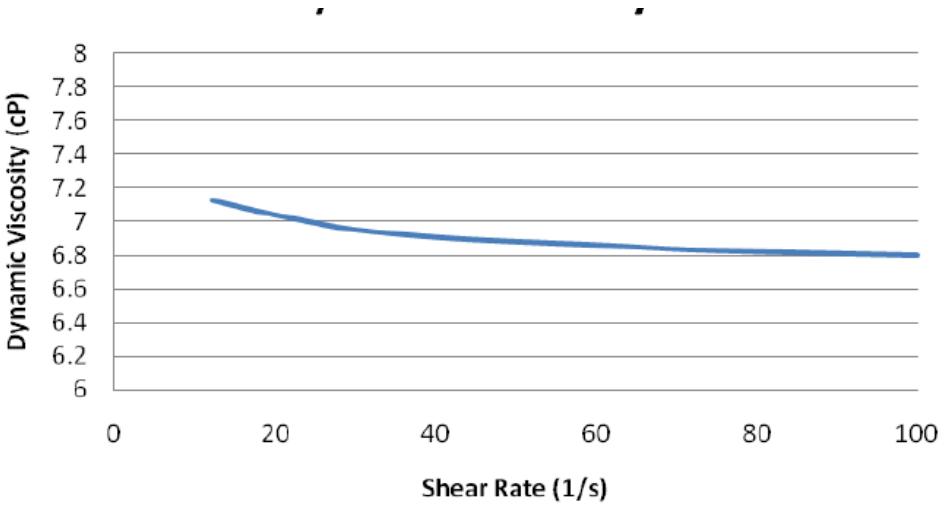

Figure G.2 Dynamic viscosity

Second set of experiments were done to observe the variation of dynamic viscosity at varying temperatures. This was crucial to see if the viscosity meets the ASTM standards. According to ASTM D6751, the acceptable viscosity range of BioDiesel fuel is 1.9 to 6 cP at 40 °C. On the other side, room temperature viscosity is important for UIC electrostatic atomizer testing. Figure G.3 shows the variation of dynamic viscosity with respect to fluid temperature. As expected, viscosity goes down the increase in temperature.

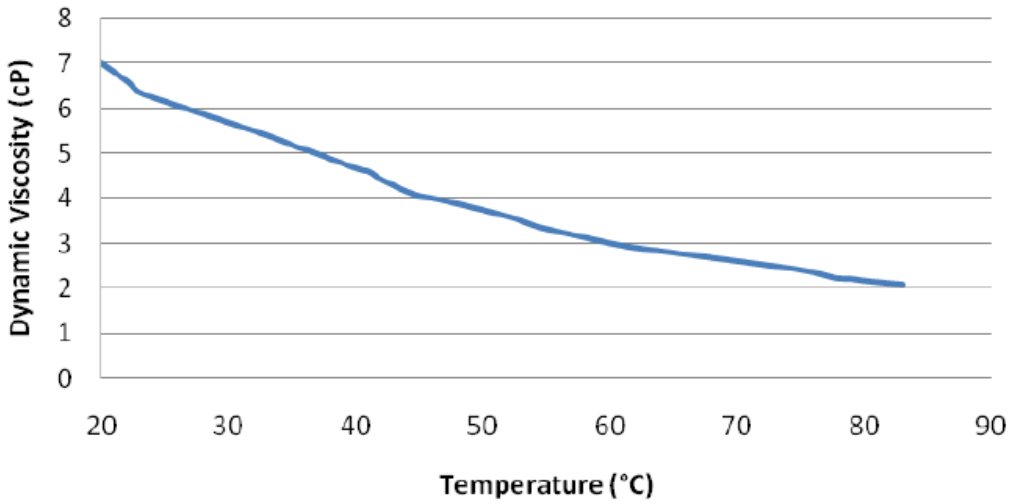

Figure G.3 Dynamic viscosity with varying temperature

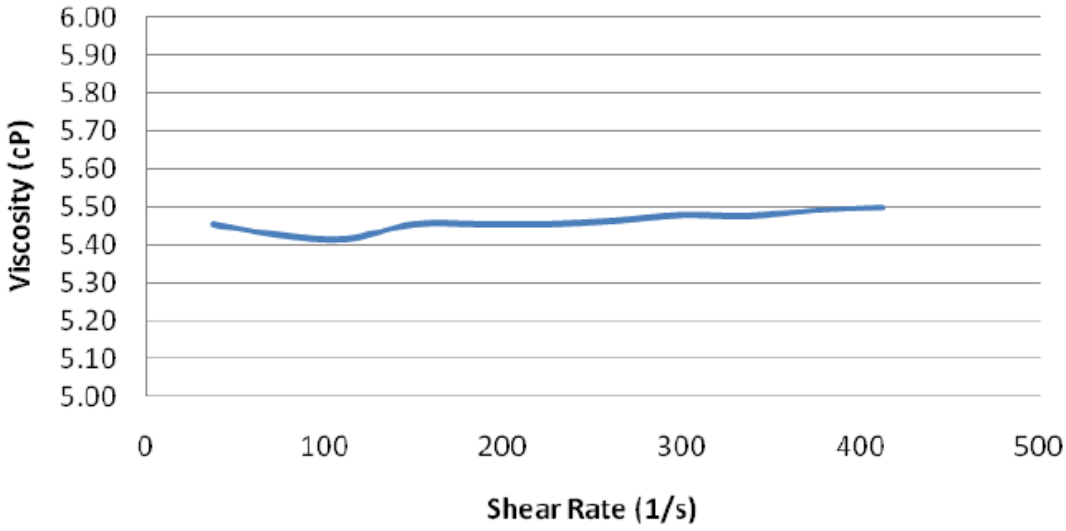

Figure G.4. Biodiesel fuel data collected by Egemen Ergene & Ghazi Malkawi on 5/21/2009.

G.2 **Conclusion**

The results presented here acquired with the Brookfield® DV-II+ Viscometer provides viscosity characterization of the Biodiesel fuel prepared at UIC MIE. These measurement results provide clear results with the Biodiesel fuel tested. Test results can be compared to the data given in appendices section.

Biodiesel fuel tested for this study is found to be within the ASTM viscosity standards; however, it is a bit thicker than the Biodiesel fuel provided by Dr. Baranescu in 2009.

VITA

Education

Ph.D. in Mechanical Engineering **08/2006 to 01/2012**
University of Illinois at Chicago (UIC)
4.00/4.00 GPA

B.Sc. in Mechanical Engineering **09/2001 to 05/2006**
Middle East Technical University (METU) / Ankara – TURKEY
3.70/4.00 GPA, (Top 5%),
High Honor Student (Dean's list), 2003-2006

Professional Experience

Spraying Systems Co. Headquarters, **12/2009 to 08/2011**
Research Engineer

- Provided professional consulting services to small and mid-sized corporations; developing and implementing recommendations that focus on improving the efficiency and controlling the cost in areas encompassing general spray operations.
- Performed over 50 customer projects at Special Projects Department Manage the customer testing process by preparing the quote, building experiment rigs, conducting drop size testing using PDI, PDPA, and Malvern instruments with several nozzle products and prepare the report showing the final test results.
- Conducted tests with various liquids including Diesel and bio-fuel spray while utilizing laser sheet imaging techniques using LaVision instruments to optimize spray pattern uniformity.
- Evaluated existing design and manufacturing methodologies, including assembly and inspection.
- Troubleshoot; identify actual and potential problem areas, and implement solutions to ensure maximum effectiveness.
- Served as a technical advisor and instructor to the lab technicians.
- Received Award and Recognition for quality workmanship and customer satisfaction.
- Submitted a technical paper on Diesel fuel injection and presented the company at ILASS 2011 conference.

University of Illinois at Chicago (UIC) **08/2006 to Present**
UIC, Teaching Assistant of Fluid Mechanics (ME211) and Experimental Methods (ME341)

- Lectured lab sessions, graded experiment reports and exams.

UIC, Research Assistant at Computational Multiphase Transport and Alternative Energy Laboratory:

- Organized a new laboratory, which is now known to be one of the best-equipped experimental divisions of UIC.
- Designed new experimental rigs for electrostatic fuel injection atomization systems using AutoCAD and PRO/E Software for several purposes (High flow rate, High pressure etc.). Machined parts at the UIC machining shop. Built

various experiments in the lab including hydraulic circuit, atomizers and electrostatic charge injection units.

- Gained testing engine assembly experience while retrofitting the prototype fuel injectors.
- Implemented electrostatic charge atomization technique for high viscosity bio-fuels. Studied the electrostatic spray characteristics experimentally by measuring electric charges densities in sprays. Worked on optimizing the spray performance in an attempt to extend the application of the method to internal combustion engines.
- By using advanced imaging techniques, conducted spray analysis about the effect of charge injection on droplet sizes, distributions and conical angles using different nozzle geometries.
- Analyzed fluid flow inside the rig by correlating CFD results with experimental data using Fluent Software.

METU, Student Assistant of: **09/2005 to 05/2006**

- Applied Mathematics for Mechanical Engineers (ME210) and Numerical Methods (ME310)
- Versed in both digital and analog electronics with specific emphasis on computer software/hardware.
- Special expertise in system and component evaluation.

FORD MOTOR COMPANY, Istanbul, Turkey **Summer 2005**

Research and Development Engineer

- Created CFD Models for Ford automatic transmission to avoid heat failures.
- Performed stress analysis and final drawings for variable speed transmission.
- Analyzed returned parts and organized part recalls.
- Attended educational courses for the Ford service technicians.

ARCELIK Multi-Purpose Power Plant, Istanbul **06/2004 to 01/2005**

Research and Development Engineering Intern

- Worked on the CAD design and CFD analysis of several electric motors using I-DEAS to improve motor operating efficiency. Correlated CFD results with dynamometer results.

Computer skills

- **CAD software:** PRO/E, AutoCAD, Cadkey and I-DEAS
- **FEA/CFD software:** ANSYS, FLUENT/GAMBIT, Workbench, CFX, ICEMCFD
- **Operating systems:** Windows Server NT, UNIX (Linux)
- **Programming language:** FORTRAN 90/95, C++
- **OTHER:** Microsoft Office, Matlab, MathCAD, Mathematica, Maple, Tecplot, Photoshop, Labview